EPRI
Electric Power
Research Institute

Topics:
Void fraction
Drift-flux modeling
CCFL
Two-phase flow
Reactor safety
Thermal hydraulics models

EPRI NP-3989-SR
Revision 1
Special Report
September 1986

A Full-Range Drift-Flux Correlation for Vertical Flows (Revision 1)

Prepared by
Electric Power Research Institute
Palo Alto, California

REPORT SUMMARY

SUBJECTS	Safety analysis / Analysis and testing / Code development	
TOPICS	Void fraction Drift-flux modeling CCFL	Two-phase flow Reactor safety Thermal hydraulics models
AUDIENCE	Safety engineers / R&D analysts	

A Full-Range Drift-Flux Correlation for Vertical Flows (Revision 1)

The drift-flux correlation described in this report is applicable to the full range of pressures and flows in LWRs. This revision corrects an error involving countercurrent flows. The error did not affect upward cocurrent flows. The impact on cocurrent downflow was minimal.

BACKGROUND Utilities must be able to predict the thermal-hydraulic behavior of LWRs during normal operation and during accidents. Such predictions require determining the void fractions of steam-water mixtures in primary and secondary coolant systems. Void fractions are usually expressed through a relationship that depends on mixture flow regimes. It is difficult, however, to calculate such regimes.

OBJECTIVE To devise a drift-flux model for predicting void fractions in LWR primary and secondary coolant systems without knowing steam and liquid flow regimes.

APPROACH The research team developed an empirical drift-flux correlation expressing velocity fields as a mixture of center-of-mass velocity and the drift velocity of the vapor phase. The researchers then qualified the correlation against such steady-state steam-water test data as (1) high-pressure high flows, (2) high-pressure low flows, (3) low-pressure low flows, (4) countercurrent flooding limitation, (5) natural circulation flows, and (6) cocurrent downflows. The correlation was applied to geometries representative of PWR and BWR fuel assemblies and to pipes up to 18 in. in diameter.

RESULTS The correlation was successful for all geometries in the full range of pressures, flows, and void fractions for vertical flow conditions. The comparisons ranged from good to excellent.

EPRI PERSPECTIVE Drift-flux modeling is extensively used in the nuclear industry because of its simplicity and its applicability to a wide range of two-phase flow problems. The correlation described in this study eliminates needing to know flow regimes before predicting void fractions. As the correlation is continuous throughout the full range of LWR operating conditions and is applicable to a wide range of geometries, it should improve computational efficiency when incorporated in thermal-hydraulic computer codes such as RETRAN.

PROJECT EPRI Project Managers: B. Chexal; G. Lellouche
Nuclear Power Division

For further information on EPRI research programs, call EPRI Technical Information Specialists (415) 855-2411.

A Full-Range Drift-Flux Correlation for Vertical Flows (Revision 1)

NP-3989-SR, Revision 1

Special Report, September 1986

Prepared by

B. Chexal
G. Lellouche

Generic Safety Analysis Program
Analytical Methods and Verification Program
Nuclear Power Division

Electric Power Research Institute
3412 Hillview Avenue
Palo Alto, California 94304

ORDERING INFORMATION

Requests for copies of this report should be directed to Research Reports Center (RRC), Box 50490, Palo Alto, CA 94303, (415) 965-4081. There is no charge for reports requested by EPRI member utilities and affiliates, U.S. utility associations, U.S. government agencies (federal, state, and local), media, and foreign organizations with which EPRI has an information exchange agreement. On request, RRC will send a catalog of EPRI reports.

NOTICE

ABSTRACT

An empirical drift flux correlation has been developed that eliminates the need to know the flow regime before void fraction predictions can be made. This correlation covers the full range of pressures, flows, and void fractions and has been qualified against several sets of steady state test data covering wide range of initial conditions and geometries (PWR and BWR fuel assemblies as well as large pipes up to 18 inches in diameter). The correlation is based on the drift flux model described in EPRI report NP-2246-SR [1].

This correlation should be of great value to code developers and code users in determining the drift-flux parameters (C_0 and V_{gj}) for both co-current and counter-current two-phase flows for a full range of pressures, flows and void fractions including counter current flooding limitation (CCFL) and natural circulation. The correlation is continuous throughout the full range and does not depend on flow regime maps or spline fitting.

ACKNOWLEDGMENTS

The authors wish to note the important contributions of Jeff Horowitz, consultant and Jim Healzer, S. Levy, Inc. The support provided by Mrs. Joy Hughes in typing the manuscript is greatly appreciated.

CONTENTS

Section		Page
1	INTRODUCTION AND SUMMARY	1-1
2	DRIFT FLUX RELATIONSHIPS	2-1
3	EPRI FULL RANGE DRIFT FLUX CORRELATION PARAMETERS	3-1
4	COMPARISON WITH HIGH PRESSURE-HIGH FLOW DATA	4-1
	4.1 Comparison with FRÖJA FRIGG and CISE Data [5-9]	4-1
	4.2 Comparison with Kasai et al Data [22]	4-1
5	COMPARISON WITH HIGH PRESSURE-LOW FLOW DATA	5-1
	5.1 Comparison with ORNL Data [8]	5-1
	5.2 Comparison with TLTA Data [9]	5-3
6	COMPARISON WITH LOW PRESSURE-LOW FLOW DATA	6-1
	6.1 Comparison with Hall et al Data [10]	6-1
	6.2 Comparison with Wong et al Data [11]	6-2
	6.3 Comparison with JOWITT Data [12]	6-3
7	COMPARISON WITH COUNTERCURRENT FLOW LIMITATION DATA	7-1
	7.1 Development of Calculational Procedure for Predicting CCFL	7-1
	7.2 Comparison with TLTA CCFL Data [13]	7-3
	7.3 Comparison with ORNL CCFL Data [14]	7-4
8	COMPARISON WITH NATURAL CIRCULATION FLOW DATA	8-1
9	CO-CURRENT DOWN FLOWS	9-1
10	APPLICATION TO LARGE DIAMETER PIPES	10-1
11	REFERENCES	11-1
APPENDIX A:	SAMPLE PROBLEMS	A-1

ILLUSTRATIONS

Figure		Page
4-1	Comparison with FRIGG, FROJA, CISE, High Press.-High Flow Bundle Data	4-5
4-2	Comparison with FRIGG, High Press.-High Flow Bundle Data: Test FT-36B 413-140	4-6
4-3	Comparison with FRIGG, High Press.-High Flow Bundle Data: Test FT-36B 413-141	4-7
4-4	Comparison with FRIGG, High Press.-High Flow Bundle Data: Test FT-36C 631-118	4-8
4-5	Comparison with FRIGG, High Press.-High Flow Bundle Data: Test FT-36B 413-117	4-9
4-6	Comparison with FRIGG, High Press.-High Flow Bundle Data: Test FT-36C 613-123	4-10
4-7	Comparison with FRIGG, High Press.-High Flow Bundle Data: Test FT-36B 413-149	4-11
4-8	Comparison with Kasai et al High Press.-High Flow Pipe Data	4-12
5-1	Comparison with Anklam et al High Pres.-Low Flow Bundle Uncovering Data: Test 3.09.10I	5-1
5-2	Comparison with Anklam et al High Press.-Low Flow Bundle Uncovering Data: Test 3.09.10J	5-2
5-3	Comparison with Anklam et al High Press.-Low Flow Bundle Uncovering Data: Test 3.09.10K	5-3
5-4	Comparison with Anklam et al High Press.-Low Flow Bundle Uncovering Data: Test 3.09.10L	5-4
5-5	Comparison with Anklam et al High Press.-Low Flow Bundle Uncovering Data: Test 3.09.10M	5-5
5-6	Comparison with Anklam et al High Press.-Low Flow Bundle Uncovering Data: Test 3.09.10N	5-6
5-7	Comparison with Anklam et al High Press.-Low Flow Bundle Uncovering Data: Test 3.09 10AA	5-7
5-8	Comparison with Anklam et al High Press.-Low Flow Bundle Uncovering Data: Test 3.09.10BB	5-8
5-9	Comparison with Anklam et al High Press.-Low Flow Bundle Uncovering Data: Test 3.09.10CC	5-9
5-10	Comparison with Anklam et al High Press.-Low Flow Bundle Uncovering Data: Test 3.09.10DD	5-10

Figure		Page
5-11	Comparison with Anklam et al High Press.-Low Flow Bundle Uncovering Data: Test 3.09.10EE	5-11
5-12	Comparison with Anklam et al High Press.-Low Flow Bundle Uncovering Data: Test 3.09.10FF	5-12
5-13	Comparison with TLTA BWR High Press.-Low Flow Bundle Uncovery Data: Test Run 3	5-13
5-14	Comparison with TLTA BWR High Press.-Low Flow Bundle Uncovery Data: Test Run 5	5-14
5-15	Comparison with TLTA BWR High Press.-Low Flow Bundle Uncovery Data: Test Run 6	5-15
5-16	Comparison with TLTA BWR High Press.-Low Flow Bundle Uncovery Data: Test Run 7	5-16
6-1	Comparison with Hall Data in a Heated Bundle at 1,2,3,4 Bars	6-5
6-2	Comparison with Hall Data in a 105 MM Pipe at 1,2,3,4 Bars	6-6
6-3	Comparison with FLECHT SEASET Low Pres.-Low Bundle Uncovering Data: Test Run 35557	6-7
6-4	Comparison with FLECHT SEASET Low Press.-Low Flow Bundle Uncovering Data: Test Run 35658	6-8
6-5	Comparison with FLECHT SEASET Low Press.-Low Flow Bundle Uncovering Data: Test Run 35759	6-9
6-6	Comparison with JOWITT Data in a Heated Bundle at 2,5,10,20,40 Bars	6-10
7-1	Comparison with TLTA Steam-Water CCFL Data for a 2.43 In Orifice at 1 ATM	7-4
7-2	Comparison with TLTA Steam-Water CCFL Data for a 1.48 In Orifice at 1 ATM	7-5
7-3	Comparison with TLTA Steam-Water CCFL Data for a 1.257 In Orifice at 1 ATM	7-6
7-4	Comparison with ORNL Steam-Water CCFL Data - PWR Upper Tie Plate at 65 psia (Hydraulic Diameter=0.0344 ft)	7-8
7-5	Comparison with ORNL Steam-Water CCFL Data-PWR Upper Tie Plate at 100 psia (Hydraulic Diameter=0.0344 ft)	7-9
8-1	Comparison with FIST Natural Circulation Data at Various Downcomer Levels	8-3
9-1	Comparison with Petrick Data in a 2 Inch Pipe at 600 psia-Co-Current Down Flow	9-2
9-2	Comparison with Petrick Data in a 2 Inch Pipe at 1000 psia-Co-Current Down Flow	9-3
9-3	Comparison with Petrick Data in a 2 inch Pipe at 1500 psia-Co-current Down Flow	9-4
10-1	Comparison with B&W Data in a 6.625 Inch Pipe at 1200, 1400 1800 and 2400 psia	10-2
10-2	Comparison with Carrier Data in a 456 mm Pipe at 600, 800, 1000,1200, 1400 and 2000 psia	10-4

TABLES

Table		Page
4-1	Summary of FRÖJA, FRIGG & CISE, Rod Bundle Experiments	4-2
4-2	Rod Bundle Experiments, Model Vs Data Statistical Analysis	4-3
4-3	Rod Bundle Experiments, Model vs Data Error Distribution	4-4
5-1	Summary of Mixture-Level Swell Test Conditions for ORNL Data	5-2
5-2	Summary of TLTA Test Conditions	5-17
6-1	Summary of Boil-Off Test Conditions for FLECHT-SEASET Data	6-3
6-2	Summary of Test Conditions for JOWITT Data	6-10

Section 1

INTRODUCTION AND SUMMARY

The ability to predict accurately the thermal hydraulic behavior of light water reactors during normal operation or during an accident requires correct simulation of steam and liquid phases in the primary and secondary coolant systems. Since in two-phase flows there is always some relative motion of one phase with respect to the other, such flow problems should be formulated in terms of two velocity fields. A general transient two-phase flow problem can be formulated by using a two-fluid model [2] or a drift flux model [3, 4] depending on the degree of the dynamic coupling between the phases.

In the two-fluid model, each phase is considered separately, hence the model is formulated in terms of two sets of conservation equations governing the balance of mass, momentum, and energy of each phase. However, the introduction of two momentum equations in a two-fluid model presents considerable difficulties because of mathematical complications and of uncertainties in specifying interaction terms between the two phases. Numerical instabilities caused by improper choice of interaction terms in the phase momentum equations are quite common, and therefore very careful studies on the phase interaction equations are required in the two-fluid model formulation.

In the drift flux model the difficulties associated with a two-fluid model can be reduced significantly by representing the motion of the whole mixture by a mixture momentum equation and the relative motion between phases by a kinematic equation. Therefore, the basic concept of the drift flux model is to consider the mixture as a whole, rather than as two separated phases. It is evident that the drift flux model formulation based on the mixture balance equation is simpler than the two-fluid model based on the separate balance equations for each phase. The most important assumption associated with the drift flux model is that the dynamics of two phases can be expressed by the mixture momentum equation with the kinematic equation specifying the relative motion between phases. The use of the drift flux model is appropriate when the motions of two phases are strongly coupled.

In the drift flux model, the velocity fields are expressed in terms of the mixture center-of-mass velocity and the drift velocity of the vapor phase (V_{gj}), which is the vapor velocity with respect to the volume center of the mixture. In order to close the system of equations, it is necessary to specify this vapor drift velocity by a constitutive equation. Since in the drift flux model, the motion of the fluid is expressed by the mixture momentum equation alone, it can be said that the drift flux model is an approximate formulation in comparison with the more rigorous two-fluid formulation. However, because of its simplicity and applicability to a wide range of two-phase flow problems of practical interest, the drift flux model is of considerable importance. In particular, the model is useful for transient thermo-hydraulic and accident analyses of LWRs.

Since the rate of momentum transfer at the interface depends on the structure of two-phase flows, the drift velocity (V_{gj}) historically has been defined as a function of flow regimes. These flow regimes, however, are difficult to predict accurately.

This report describes an empirical drift flux correlation that eliminates the need to know the flow regime before void fraction predictions can be made. The correlation covers the full range of pressures, flows and void fractions for co-current or counter-current vertical flow conditions, and has been validated successfully against the following types of data:

- High pressure - High flows: **(Comparison with FRIGG, CISE and FROJA data shows excellent agreement. Similar agreement was also obtained with Kasai et al data. The statistics are better than reported in the earlier model [1] for this range. See Figures 4-1 through 4-8 for data comparison and Tables 4-1 and 4-2 for statistical analysis.** These conditions are typical of a BWR at normal operation and steam generators in a PWR at normal operation. The ability to model these conditions correctly helps provide the accurate system response for normal operational transients.

- <u>High pressure - Low flows</u>: **(Comparison with ORNL and TLTA data shows excellent agreement. See Figures 5-1 through 5-12 for ORNL and 5-13 through 5-16 for TLTA.)**

  These conditions are typical of a small break LOCA. During such transients, it is important to predict the extent of core uncovering that may occur. The extent of core uncovering is dependent upon both the liquid inventory in the core and on the core void fraction distribution (mixture swell). These conditions also occur during BWR Anticipated Transient Without Scram (ATWS) analyses if downcomer water level is lowered to the top of the active fuel to reduce reactor power.

- <u>Low pressure - Low flows</u>: **(Comparisons are made with Hall, Wong and Jowitt's data. The results are good. See Figures 6-1 through 6-6. Data comparisons cover within and above the heated assemblies.)**

  These conditions are typical of a large break LOCA accident and are expected to occur during core uncovering or reflood conditions.

- <u>Counter-current Flooding Limitation</u>: **(Comparisons are made with TLTA side entry orifice data and ORNL upper tie plate/upper plenum data with excellent agreement predicting both pressure and diameter effects accurately. See Figures 7-1 through 7-5.)**

  These conditions occur during a LOCA at the upper tie-plates and bottom side-entry orifices in a BWR and are important for determining the heat transfer in the core. These conditions are also expected to occur in a PWR at the core/upper plenum interface and in the downcomer.

- Natural Circulation Flows:
  (Comparison with FIST natural circulation data at various downcomer water levels shows excellent agreement. See Figure 8-1.)

  These conditions are typical of low-power reactor operation and also of system behavior during certain small break LOCA transients.

- Co-Current Down Flows:
  (Comparison with Petrick data is quite good. See Figures 9-1, 9-2 and 9-3.)

  These conditions are typical of a PWR with upper plenum or upper head injection during a reflood in a large LOCA or in a BWR downcomer.

- Large Diameter Pipes:
  (Comparison with Hughes data in a 6.625 inch pipe and Carrier data in an 18 inch pipe is quite good. See Figures 10-1 and 10-2.)

  These are typical of primary coolant system outside the core region and of the steam generator secondary above the tube bundle region.

It has been shown that the present correlation for the drift flux parameters (C_o, V_{gj}) agrees well with the available data.

Section 2

DRIFT FLUX RELATIONSHIPS

The drift flux model, in its most general form, has five field equations (2 mass, 2 energy, and 1 mixture momentum) with a kinematic equation specifying the relative motion between two phases.

The most widely used four field equations drift flux model results from the elimination of one energy and one momentum equation from the original six field equations of the two-fluid model. Therefore, the relative motion and energy difference should be expressed by additional constitutive equations. These two effects inherent to the two-phase flows are taken into account by using a continuity equation for one of the phases and supplementing it with kinematic and phase-change constitutive equations.

The cross-sectional area averaging is very useful for complicated engineering problems involving fluid flow and heat transfer, since field equations can be reduced to quasi-one-dimensional forms. By area averaging, the information on changes of variables in the direction normal to the main flow within a channel is basically lost, therefore, the transfer of momentum and energy between the wall and the fluid should be expressed by empirical correlations or by simplified models. The rational approach to obtain a one-dimensional model is to integrate the three-dimensional model over a cross-sectional area then to introduce proper mean values.

A simple area average of any local parameter $\overline{F}$ over the cross-sectional area A is defined by

$$F \equiv \langle F \rangle \equiv \frac{1}{A} \int_A \overline{F} dA$$

The void fraction weighted values for drift flux parameters, C_0 and V_{gj} are given by

$$C_o = \frac{<\bar{\alpha}\cdot\bar{j}>}{<\bar{\alpha}><\bar{j}>}$$

$$V_{gj} = \frac{<\bar{\alpha}\cdot\bar{V}_{gj}>}{<\bar{\alpha}>}$$

If $V_{gj} = 0$ and $C_o = 1$, drift flux relationships describe homogeneous flow. If $V_{gj} = 0$, but $C_o \neq 1$, drift flux relationships yield the so called slip equations. It can be shown that $C_o < 1$ when the void concentration at the wall is greater than at the center, and $C_o > 1$ for the reverse condition. Thus for a channel which experiences the entire range of boiling regimes, C_o should vary as $C_o < 1 \rightarrow C_o > 1 \rightarrow C_o = 1$. In the early stages of subcooled boiling, the voids exist primarily near the wall, whereas in fully developed boiling the preponderance of voids are in the center of the channel. In the limit when $\alpha \rightarrow 1$, C_o approaches 1 and V_{gj} approaches 0.

The drift flux relationship is given by: $V_g = \frac{j_g}{\alpha} = C_o j + V_{gj}$

where j = Total volumetric flux or average superficial velocity

$= j_f + j_g$

j_g = Volumetric vapor flux or superficial vapor velocity

$= \alpha\ (C_o j + V_{gj}) = <\bar{\alpha}\ \bar{V}_g> = \frac{Q_g}{A}$

j_f = Volumetric liquid flux or superficial liquid velocity

$= (1-\alpha\ C_o)j - \alpha V_{gj} = <(1-\bar{\alpha})\ \bar{V}_f> = \frac{Q_f}{A}$

$\bar{V}_g$ = Local vapor velocity

$\bar{V}_f$ = Local liquid velocity

Q_g = Volumetric vapor flow rate

Q_f = Volumetric liquid flow rate

A = Total flow area

V_{gj} = void weighted "drift velocity" of the vapor phase with respect to the average superficial velocity j

C_o = void weighted "distribution parameter" to account for non-uniform distribution of voids and velocities across a channel.

$<\bar{\alpha}>$ = Void fraction

The general drift-flux formulation for void fraction is thus given by:

$$\alpha \equiv <\bar{\alpha}> \equiv \frac{j_g}{C_o\ (j_f + j_g) + V_{gj}}$$

The drift flux parameters C_o and V_{gj} are defined in Section 3.

The relationships for vapor velocity, V_g, liquid velocity, V_f, and the slip velocity, V_g-V_f, in terms of drift flux parameters and total mass flow velocity, G_o, can be derived using the following two equations:

drift flux relationship: $$\frac{j_g}{\alpha} = C_o j_g + C_o\ j_f + V_{gj} \qquad (2\text{-}1)$$

mass conservation: $$G_o A = \rho_f\ j_f\ A + \rho_g\ j_g\ A \qquad (2\text{-}2)$$

where α = void fraction

j_g, j_f = superficial gas, vapor velocities

A = total flow area

G_o = total mass flow velocity

C_o, V_{gj} = drift flux distribution parameter, drift velocity.

From eq. 2-2, $$j_f = \frac{G_o - \rho_g j_g}{\rho_f};\ j_g = \frac{G_o - \rho_f j_f}{\rho_g} \qquad (2\text{-}3)$$

To calculate V_g, local vapor velocity, the j_f from equation (2-3) can be substituted in equation (2-1) to give

$$\frac{j_g}{\alpha} = C_o j_g + C_o \left(\frac{G_o - \rho_g j_g}{\rho_f}\right) + V_{gj} = V_g$$

or

$$V_g = \frac{\frac{C_o G_o}{\rho_f} + V_{gj}}{1 - \alpha C_o \left(1 - \frac{\rho_g}{\rho_f}\right)} \tag{2-4}$$

Similarly, substituting j_g from equation (2-3) into eq. (2-1) yields

$$\left(\frac{G_o - \rho_f j_f}{\rho_g}\right)(1 - \alpha C_o) = \alpha C_o\, j_f + \alpha V_{gj}$$

$$\therefore\ V_f = \frac{j_f}{1-\alpha} = \frac{(1-\alpha C_o)\left[G_o - \frac{\alpha \rho_g V_{gj}}{1-\alpha C_o}\right]}{\rho_f (1-\alpha)\left[1 - \alpha C_o \left(1 - \frac{\rho_g}{\rho_f}\right)\right]} \tag{2-5}$$

The expression for slip velocity, $V_g - V_f$ can be obtained by taking difference of equation (2-4) and (2-5) and is given by

$$V_g - V_f = \frac{V_{gj}\left[1 - \alpha\left(1 - \frac{\rho_g}{\rho_f}\right)\right] - \frac{G_o (1 - C_o)}{\rho_f}}{1 - \alpha\, C_o \left[1 - \frac{\rho_g}{\rho_f}\right] (1-\alpha)} \tag{2-6}$$

where $G_o = \frac{W}{A}$

W = Total mass flow rate

A = Total flow area

The value of void fraction at the two phase/single phase interface (the "level"), α^*, can be obtained at steady state by equating V_f to zero in equation 2-5.

$$\alpha^* = \frac{G_o}{\rho_g V_{gj} + G_o C_o} \tag{2-7}$$

Section 3

EPRI FULL RANGE DRIFT FLUX CORRELATION PARAMETERS

To predict void fraction using Chexal-Lellouche void model requires the knowledge of the system pressure, p, the hydraulic diameter, D_h, and the superficial liquid and vapor velocities. The positive flow direction is assumed to be up.

The bubble concentration parameter, C_o, for the Chexal-Lellouche void model is given by:

$$C_o = L(\alpha,p)/[K_o + (1-K_o)\alpha^r]$$

$$L(\alpha,p) = \frac{1 - \exp(-C_1\alpha)}{1 - \exp(-C_1)}$$

$$C_1 = 4p_{crit}^2/[p(p_{crit} - p)]$$

p = pressure, psia

p_{crit} = critical pressure, psia

$$K_o = B_1 + (1 - B_1)(\rho_g/\rho_f)^{1/4}$$

$$B_1 = \min(0.8, A_1)$$

$$A_1 = 1/[1 + \exp(-Re/60{,}000)]$$

$Re = Re_g$ if $Re_g > Re_f$ or $Re_g < 0.0$

$Re = Re_f$ if $Re_g \le Re_f$

Re_f = Local <u>Liquid</u> superficial Reynolds number

$$= \frac{W_f \cdot D_H}{\mu_f \cdot A}$$

Re_g = Local <u>Gas</u> superficial Reynolds number

$$= \frac{W_g \cdot D_H}{\mu_g \cdot A}$$

It should be noted that the sign convention for all Reynolds numbers, Re, Re_f, and Re_g is the same as the sign convention for the individual flows.

r = $(1 + 1.57\ \rho_g/\rho_f)/(1 - B_1)$

ρ_g, ρ_f = Saturated vapor & liquid densities, lbm/ft^3

W_g, W_f = Local vapor and liquid mass flow rates, lbm/sec

μ_g, μ_f = Saturated vapor and liquid viscosities, $\frac{lbm}{ft \cdot Sec}$

A = Flow area, ft^2

D_h = hydraulic diameter, ft

The drift velocity, V_{gj}, for the Chexal-Lellouche correlation is given by:

$$V_{gj} = 1.41 \left[\frac{(\rho_f - \rho_g)\sigma\ g\ g_c}{\rho_f^2}\right]^{1/4} \cdot (1-\alpha)^{K_1} C_2 \cdot C_3 \cdot C_4 \text{ ft/sec}$$

σ = surface tension, lbf/ft

K_1 = B_1 if $Re_g \geq 0.0$

= $\min\ [0.65,\ 0.5 \exp\ \{|Re_g|/4000\}]$ if $Re_g < 0.0$

C_2 = 1 if $C_5 \geq 1$

$$= \frac{1}{1 - \exp(-C_6)} \text{ if } C_5 < 1$$

$$C_5 = \sqrt{150 \cdot (\rho_g/\rho_f)}$$

$$C_6 = \frac{C_5}{1 - C_5}$$

The parameter, C_3, is determined based on the directions of the gas and liquid flows. It is continuous as the two directional boundaries are crossed. The values of C_3 for the three types of flows (co-current upflow, co-current downflows, and countercurrent flows) are given by:

Upflow (both j_f and j_g are positive):

$$C_3 = \max\left[0.50,\ 2 \exp\left\{ - |Re_f|/60{,}000\right\}\right]$$

Downflows (both j_f and j_g are negative):

$$C_3 = C_3'$$

$$C_3' = 2 \exp \left\{|Re_f|/350{,}000\right\}^{0.4} - 1.75 \left(|Re_f|\right)^{0.03} \exp \left\{\frac{-|Re_f|}{50000} \cdot \left(\frac{D_1}{D_h}\right)^2 \right\} + \left(\frac{D_1}{D_h}\right)^{0.25} \cdot |Re_f|^{0.001}$$

Countercurrent flows (j_g is positive and j_f is negative):

For clarity, this procedure is described in two parts - one relating to prediction of the countercurrent flooding limit (CCFL) and the other relating to below the CCFL line, i.e., countercurrent flow.

CCFL Line

$$C_3 = C_3'$$

Countercurrent Flow Below the CCFL Line

In the limited region of countercurrent flow, there are two solutions for void fraction (α_1 and α_2) at every point. These are first obtained assuming $C_3 = C_3'$. The desired void fraction, α_{des}, known a priori from pressure drop or other information is then used in selecting the appropriate C_3 as follows:

$$C_3 = C_3' \text{ if } \alpha_{des} = \max(\alpha_1, \alpha_2)$$

$$C_3 = C_3' \left(\frac{j_f}{j_f^*}\right) + \left(1 - \frac{j_f}{j_f^*}\right)\left(1 + \frac{|Re_f|}{60{,}000}\right) \text{ if } \alpha_{des} = \min(\alpha_1, \alpha_2)$$

Where j_f^* is the value on the CCFL line corresponding to j_g and is calculated using $C_3 = C_3'$.

D_1 = Normalizing diameter = 0.125 ft

$$C_4 = 1 \text{ if } C_7 \geq 1$$

$$= \frac{1}{1 - \exp(-C_8)} \text{ if } C_7 < 1$$

$$C_7 = \left(\frac{D_2}{D}\right)^{0.6}$$

$$C_8 = \frac{C_7}{1 - C_7}$$

D_2 = Normalizing diameter, 0.3 ft

The model is numerically identical in SI units. C_o has no units. V_{gj} in British units is in Ft/sec. In SI units, it will be in corresponding meters/sec. If one programs the correlation in SI units, one should run the sample problems in Appendix A to ensure that it is giving correct answers.

Section 4

COMPARISON WITH HIGH PRESSURE-HIGH FLOW DATA

These conditions are typical of a BWR at normal operation and steam generators in a PWR at normal operation. The ability to model these conditions correctly helps provide the accurate system response for normal operation transients.

In this section, the empirical drift flux correlation void fraction predictions are compared with FRÖJA loop project [5] and FRIGG loop project [6, 7, 8] data taken at the nuclear power laboratories of ASEA in Sweden, and CISE [9] data taken in Italy. In addition, comparison is made using Kasai et al data [22] in a vertical tube with inside diameter that corresponds to the hydraulic diameter of a typical subchannel in a BWR fuel assembly. In general, the predicted void fractions agree closely with the test measurements.

4.1 COMPARISON WITH FRÖJA , FRIGG AND CISE DATA

A summary of test conditions is provided in Table 4-1. The test conditions span a wide range of pressures, flows, and inlet subcoolings. Figure 4-1 compares the calculated void fraction with measured void fraction. Figures 4-2 through 4-7 show the void fraction comparison with data at various elevations for six selected tests spanning the range of pressures and flows.

Tables 4-2 and 4-3 show the statistical analysis performed to establish the model bias for similar conditions. The bias is very small and the results in general show that the empirical drift flux correlation predicts the void fractions very well under high pressure-high flow conditions.

4.2 COMPARISON WITH KASAI ET AL DATA [22]

Several tests were conducted by Kasai et al in a vertical boiling channel with 1.5 cm inside diameter in forced convection under typical BWR operational conditions. The range of steady state experimental conditions were as follows: pressure: 6.87 MPa; flow rate: 1-6 $MKg/m^2/hr.$; quality: 0-0.4; and axial power shape: uniform, middle and bottom peak. Figure 4-8 compares the calculated void fraction with measured void fraction. In general, the comparison is quite good.

Table 4-1

SUMMARY OF FRÖJA, FRIGG & CISE
ROD BUNDLE EXPERIMENTS

Number of heated rods	6	36	36	36	36	19
Type of rod array	Circular[1]	Circular[2]	Circular[2]	Circular[2]	Square[3]	Circular[4]
Rod diameter (ft)	.0456[5]	.0453	.0453	.0453		.0656
Heated length (ft)	14.50	14.35	14.32	14.32		13.18
Flow Area (ft^2)	.03298[6]	.1538	.1538	.1538		.0312
Hydraulic diameter[7] (ft)	.1535[8]	.1201	.1201	.1201		.0318
Axial heat distribution	Uniform	Uniform	Uniform	Non-uniform[9]	Uniform	Uniform
Radial heat distribution	Uniform	Uniform	Non-uniform[10]	Non-uniform[11]	Uniform	Non-uniform[12]
Measurement technique	γ-ray	γ-ray	γ-ray	γ-ray	γ-ray	Valves
Average pressure (psia)	585	723	800	725	929	661
Average flow rate $\frac{MLB}{hr\text{-}ft^2}$	0.980	0.798	0.789	0.705	1.105	1.366
Average heat flux $\frac{MBTU}{hr\text{-}ft^2}$	0.167	0.123	0.157	0.191	0.154	0.128

Notes:

1. One central heated rod with five surrounding rods
2. One central unheated rod surrounded by three rings of rods containing 6, 12 and 18 rods respectively
3. A 6 by 6 square array of rods
4. A central heated rod surrounded by two rings of 6 and 12 rods respectively
5. 0.0453 feet for FRIGG FT-6A case
6. 0.03299 ft^2 for FRIGG FT-6A case
7. Hydraulic diameter defined as 4 x (Flow Area in ft^2)/(Total Surface Area per foot)
8. 0.1545 feet for FRIGG FT-6A case
9. Peak to Average = 1.18
10. Peak to Average = 1.180
11. Peak to Average = 1.097
12. Peak to Average = 1.141

Table 4-2

ROD BUNDLE EXPERIMENTS
MODEL VS DATA STATISTICAL ANALYSIS

Range of Measured void Fraction (α_m)	Average Error ε	RMS Error σ	Sample Size N
$0.0 < \alpha_m \leq 0.1$	-.0004	.035	74
$0.1 < \alpha_m \leq 0.2$	.0087	.028	67
$0.2 < \alpha_m \leq 0.3$	.0075	.038	86
$0.3 < \alpha_m \leq 0.4$	.0038	.028	87
$0.4 < \alpha_m \leq 0.5$	.0059	.026	110
$0.5 < \alpha_m \leq 0.6$	.0025	.024	119
$0.6 < \alpha_m \leq 0.7$	-.0018	.026	104
$0.7 < \alpha_m \leq 0.8$	-.0041	.025	81
$0.8 < \alpha_m \leq 0.9$	-.0060	.022	30
$0.9 < \alpha_m \leq 1.0$	-.034	.022	5
All α_m*	.0024	.029	784

Model Bias = 0.0024 ± .0010

*includes $\alpha_m \leq 0.0$ values

Table 4-3

ROD BUNDLE EXPERIMENTS
MODEL VS DATA ERROR DISTRIBUTION

$\alpha_c - \alpha_m$*	Fraction in Range
< -0.15	0.0
-0.15 to -.10	0.001
-0.10 to -0.05	0.025
-0.05 to 0.00	0.469
0.00 to 0.05	0.454
0.05 to 0.10	0.047
0.10 to 0.15	0.004
> 0.15	0.0

*α_c = calculated void fraction
α_m = measured void fraction

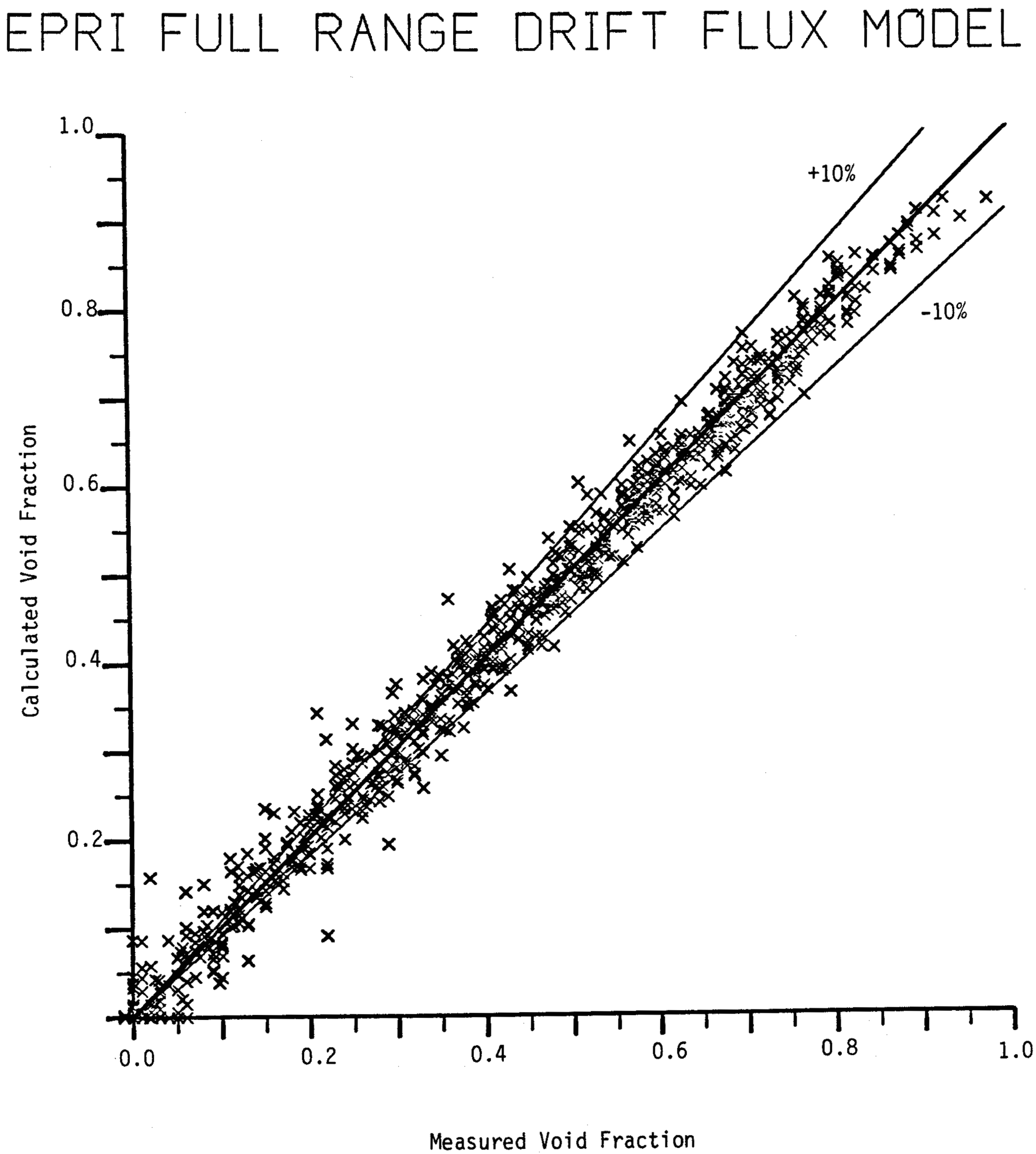

Figure 4-1. Comparison with FRIGG, FROJA, and CISE
High Press.-High Flow Bundle Data

EPRI FULL RANGE DRIFT FLUX MODEL

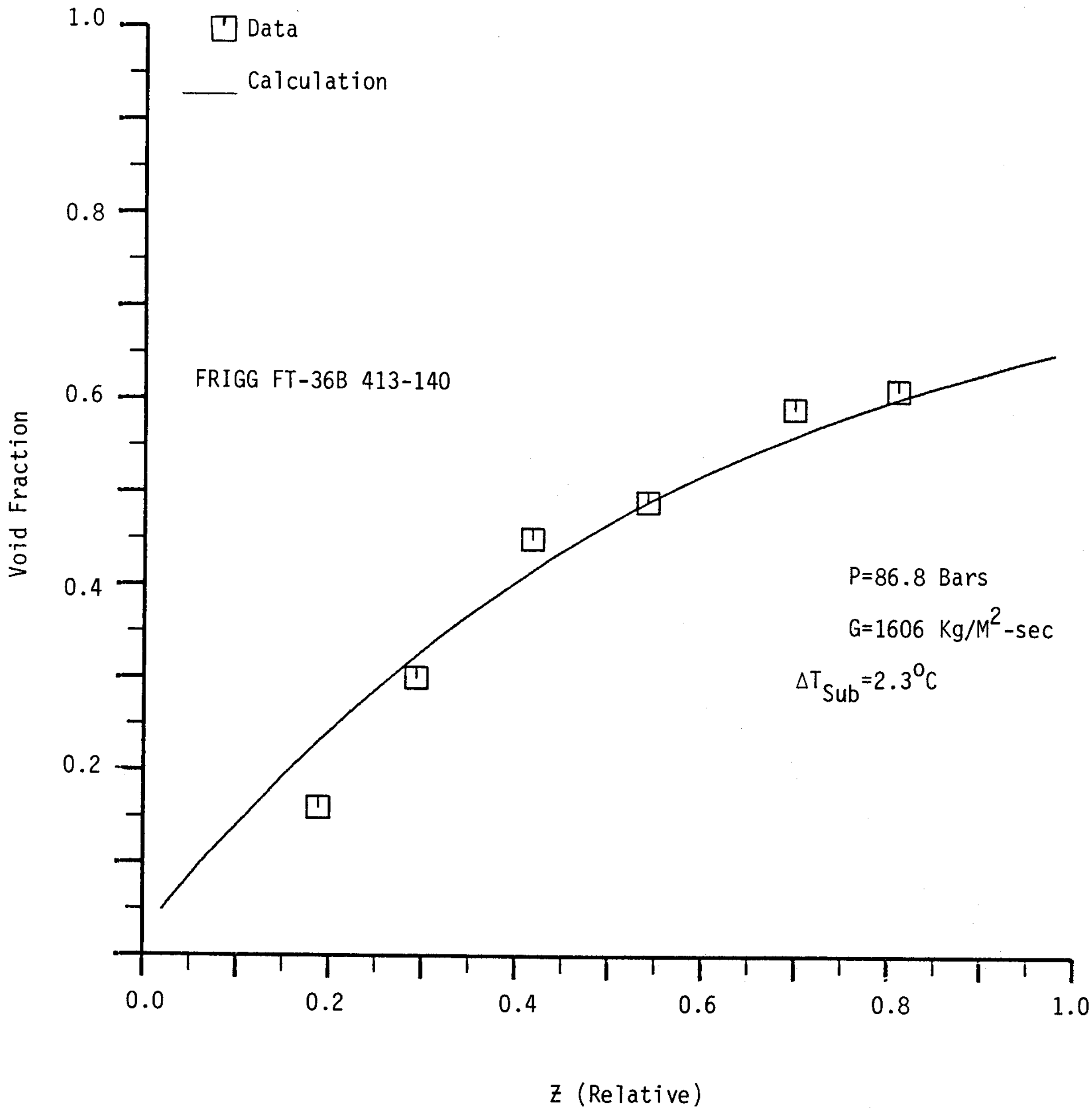

Figure 4-2. Comparison with FRIGG, High Press.-High Flow Bundle Data: Test FT-36B 413-140

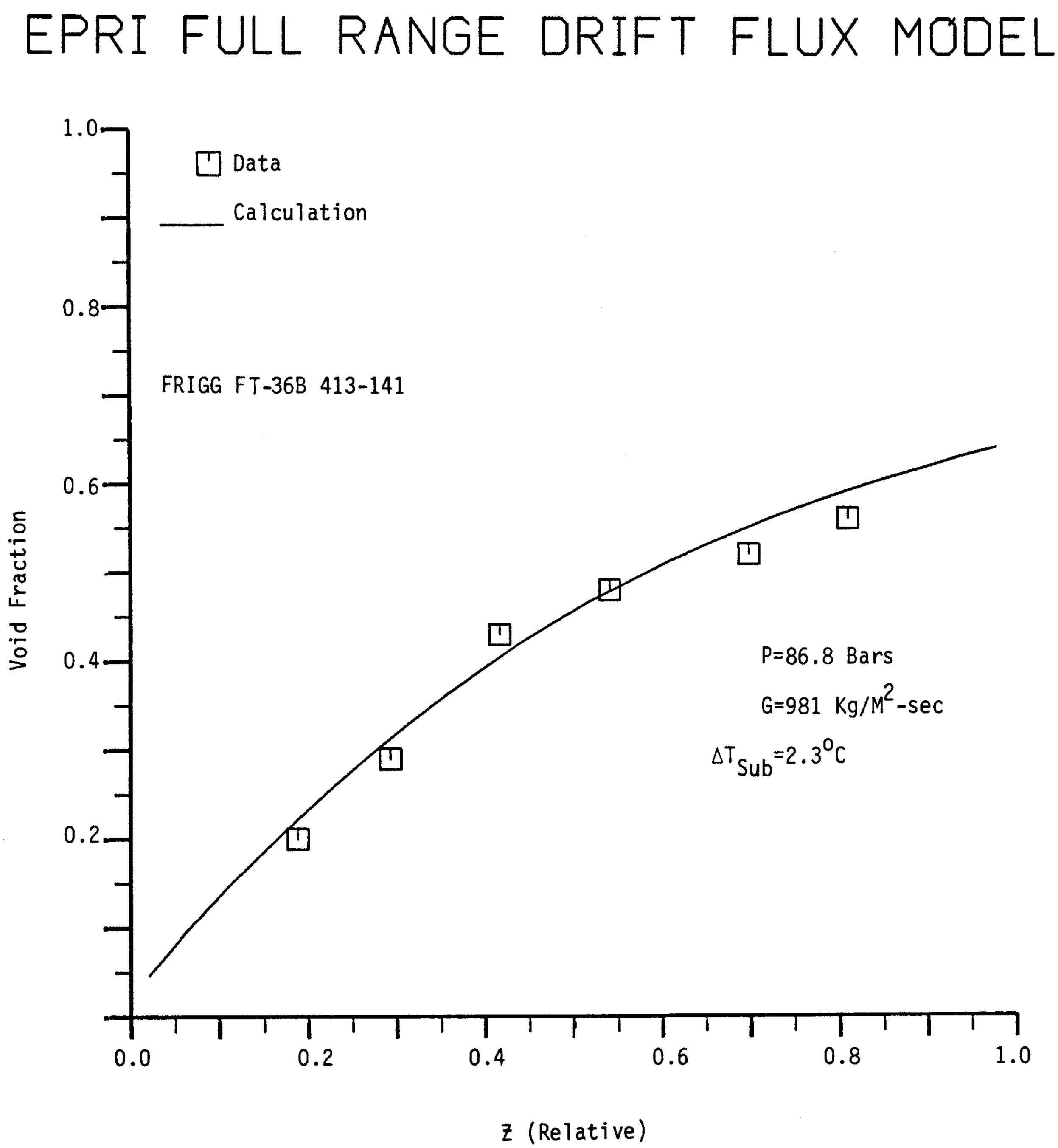

Figure 4-3. Comparison with FRIGG, High Press.-High Flow Bundle Data: Test FT-36B 413-141

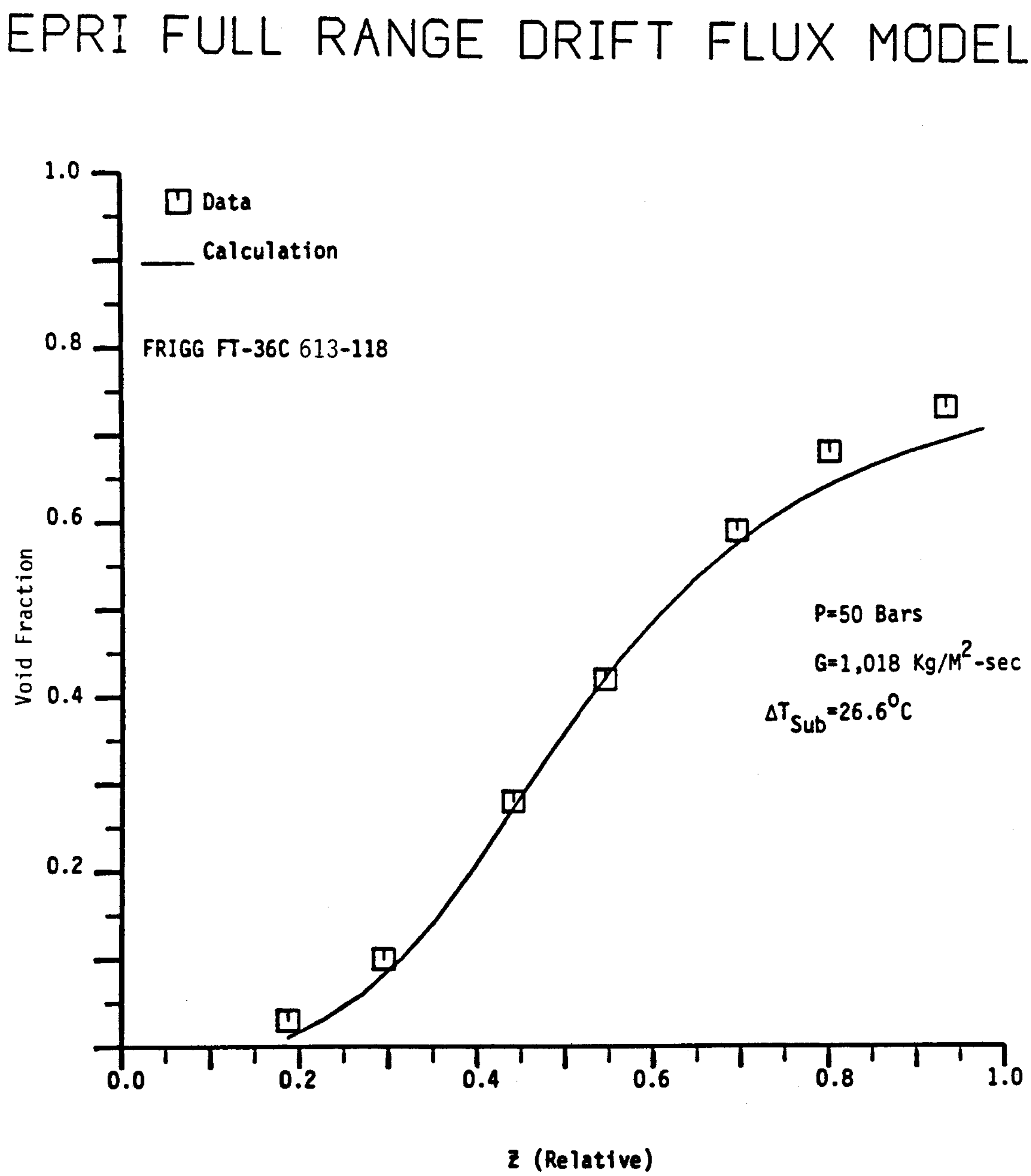

Figure 4-4. Comparison with FRIGG, High Press.-High Flow Bundle Data: Test FT-36C 631-118

EPRI FULL RANGE DRIFT FLUX MODEL

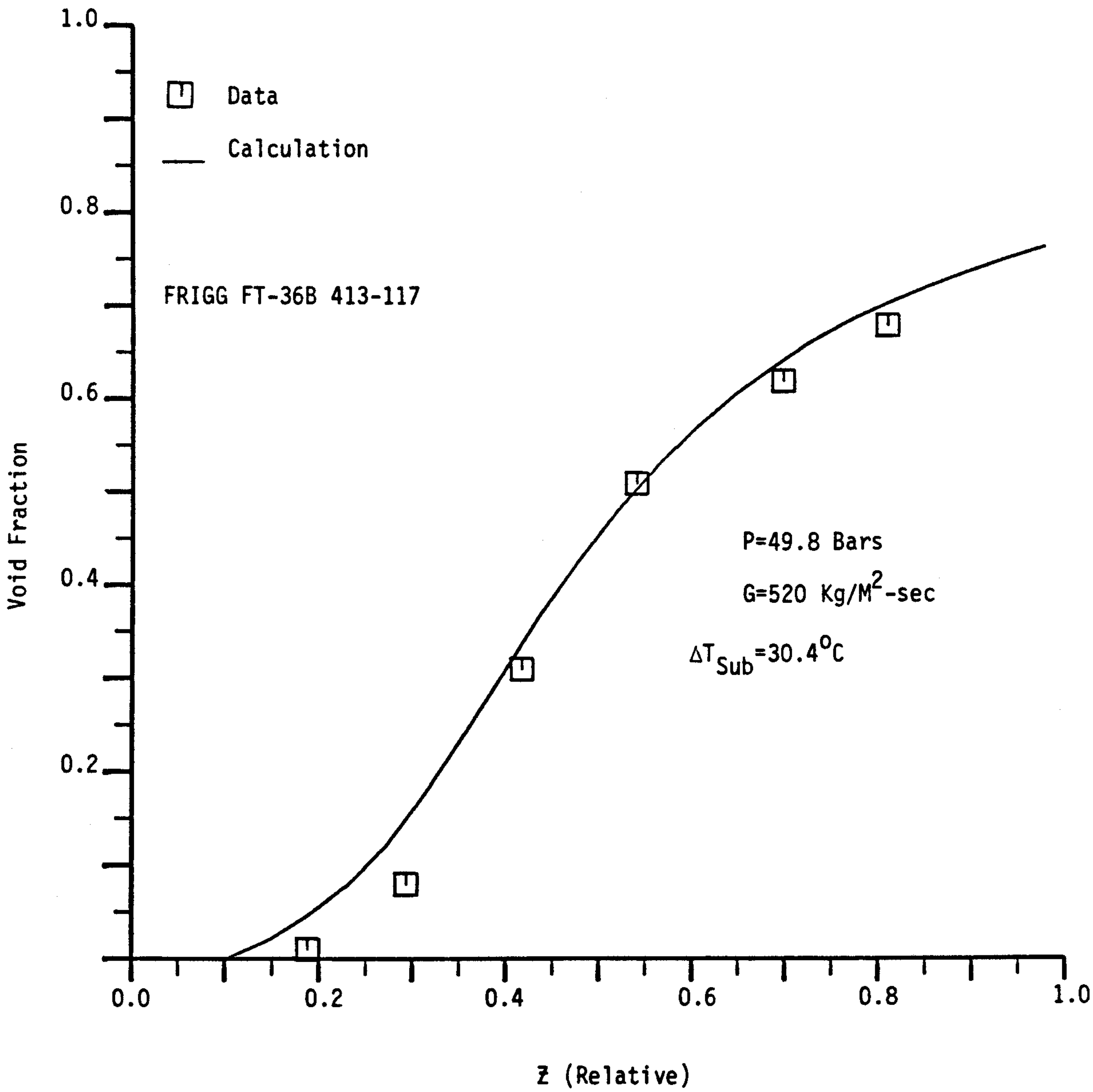

Figure 4-5. Comparison with FRIGG, High Press.-High Flow Bundle Data: Test FT-36B 413-117

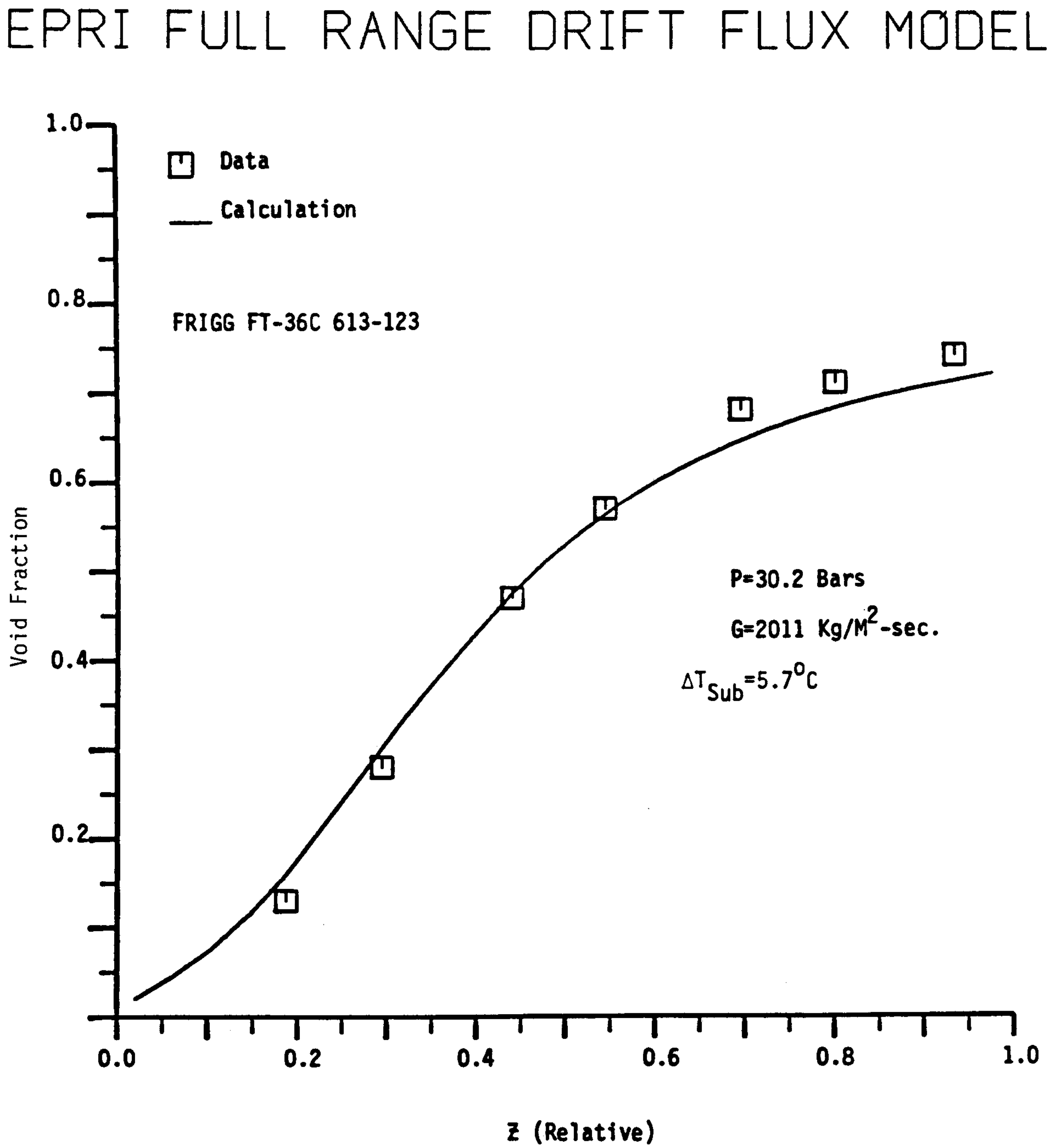

Figure 4-6. Comparison with FRIGG, High Press.-High Flow Bundle Data: Test FT-36C 613-123

EPRI FULL RANGE DRIFT FLUX MODEL

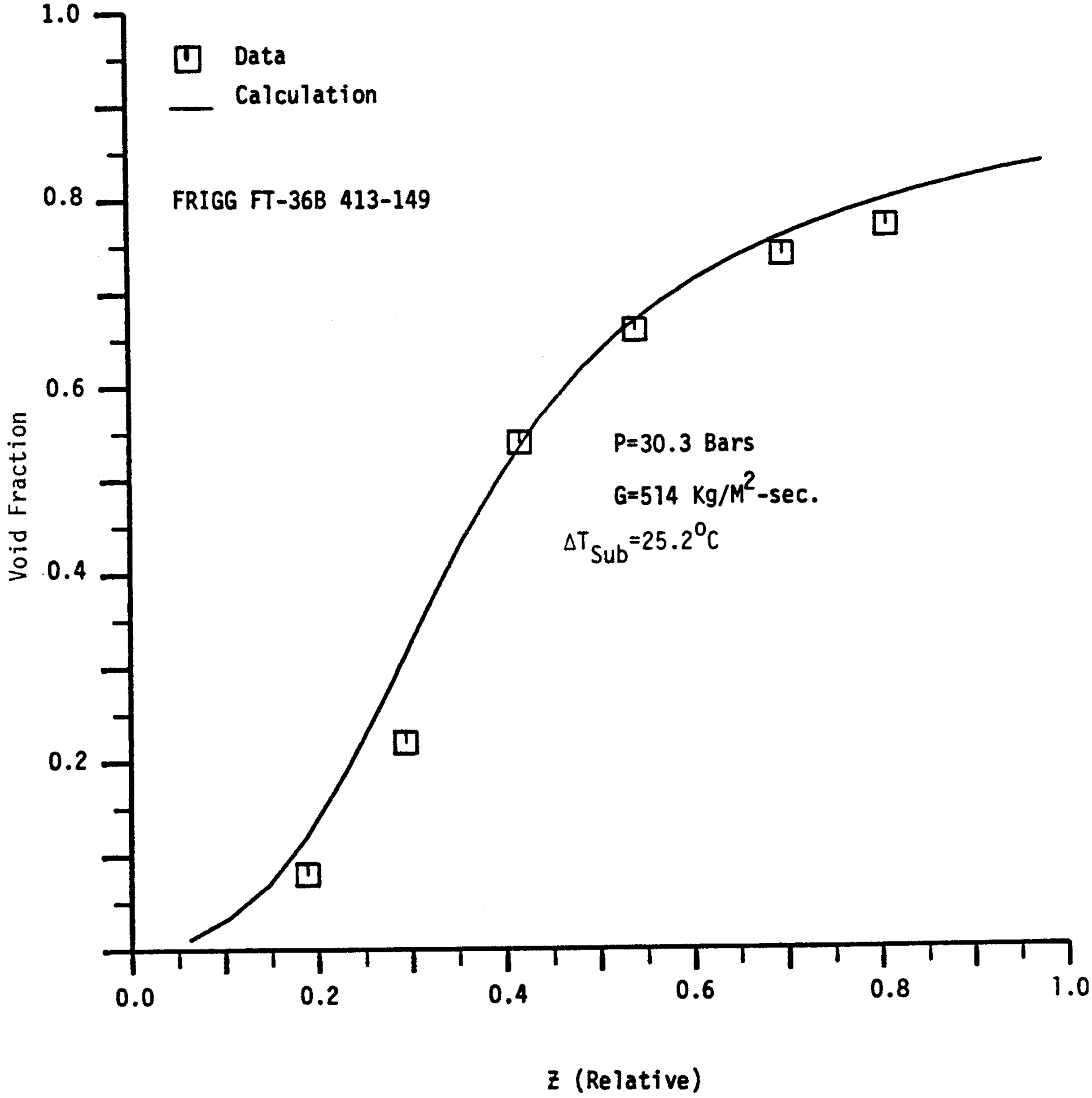

Figure 4-7. Comparison with FRIGG, High Press.-High Flow Bundle Data: Test FT-36B 413 149

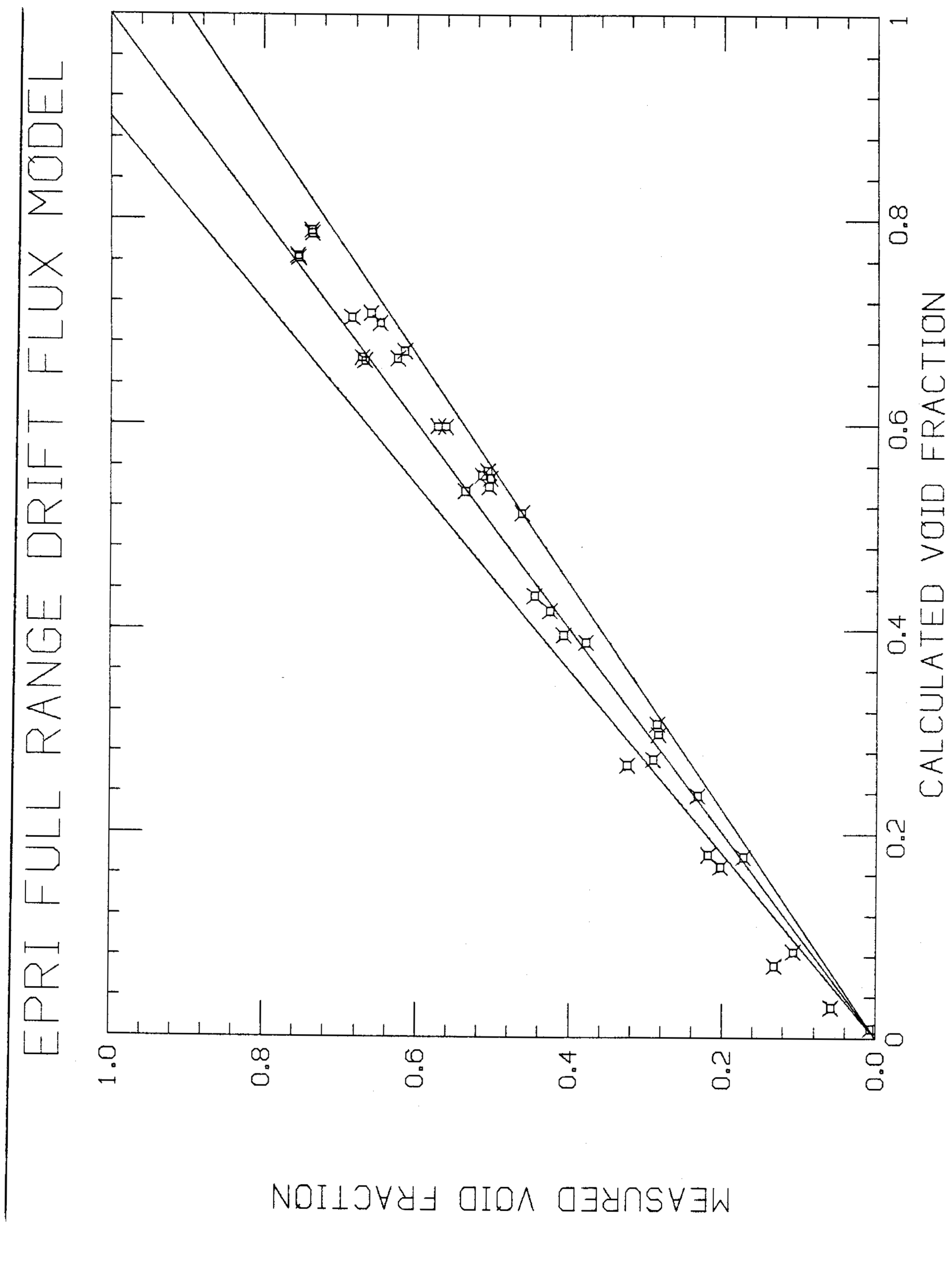

Figure 4-8. Comparison with Kasai et al High Press.-High Flow Pipe Data

Section 5

COMPARISON WITH HIGH PRESSURE-LOW FLOW DATA

These conditions are typical of a small break LOCA. During such transients, it is important to predict the extent of core uncovering that may occur. The extent of core uncovering is dependent upon both the liquid inventory in the core and on the core void fraction distribution (mixture swell). These conditions also occur during BWR Anticipated Transient Without Scram (ATWS) analyses if downcomer water level is lowered to the top of the active fuel to reduce reactor power.

In this section the empirical drift flux correlation void fraction predictions are compared with Anklam et al [10] data taken at Oak Ridge National Laboratory (ORNL) in the thermal hydraulic test facility (THTF) and Seedy et al [11] data taken at General Electric Company in the two-loop test apparatus (TLTA). In general, the predicted void fractions agree closely with the test measurements.

5.1 COMPARISON WITH ORNL DATA [10]

In November of 1980, Oak Ridge National Laboratory (ORNL) performed 12 high pressure mixture level swell tests using a 64 rod electrically heated bundle with internal dimensions typical of a 17 x 17 pressurized water reactor (PWR) fuel assembly. Summary of mixture level swell test conditions is given in Table 5-1. The conditions were typical of a small break accident in a PWR. Under these conditions, phase separation is governed primarily by buoyancy and drag forces; frictional effects are relatively unimportant. Two sets of experiments were run; the first to obtain both void fraction and uncovered core heat transfer data (Tests 3.09.10I-N) and the second to obtain only void fraction data (Tests 3.09.10AA-FF).

The heart of the THTF is a 64-rod bundle with a 12 ft. heated length. The bundle has an axially and radially uniform power profile and internally heated fuel rod simulators (FRSs). FRS temperature was monitored by internal sheath and centerline thermocouples at 25 elevations.

Table 5-1

SUMMARY OF MIXTURE-LEVEL SWELL TEST CONDITIONS FOR ORNL DATA

Test	System pressure (psia)	Linear power/rod (kW/ft)	Mixture level (ft)	Collapsed-liquid level (ft)	Beginning of boiling length (ft)
3.09.10I	650	0.68	8.60 ± 0.13	4.39 ± 0.1	1.18 ± 0.03
3.09.10J	610	0.33	8.10 ± 0.14	5.31 ± 0.1	0.89 ± 0.03
3.09.10K	580	0.10	6.98 ± 0.98	5.31 ± 0.1	0.92 ± 0.13
3.09.10L	1090	0.66	9.02 ± 0.29	5.77 ± 0.1	2.26 ± 0.07
3.09.10M	1010	0.31	8.60 ± 0.13	6.20 ± 0.1	1.80 ± 0.03
3.09.10N	1030	0.14	6.98 ± 0.98	6.10 ± 0.1	1.51 ± 0.23
3.09.10AA	590	0.39	11.23 ± 0.09	6.56 ± 0.1	1.84 ± 0.07
3.09.10BB	560	0.20	10.85 ± 0.12	7.61 ± 0.1	1.57 ± 0.07
3.09.10CC	520	0.10	11.80 ± 0.08	9.45 ± 0.1	1.34 ± 0.07
3.09.10DD	1170	0.39	10.61 ± 0.13	7.84 ± 0.1	2.95 ± 0.07
3.09.10EE	1120	0.19	11.40 ± 0.08	9.35 ± 0.1	3.02 ± 0.07
3.09.10FF	1090	0.98	10.61 ± 0.13	9.51 ± 0.1	2.82 ± 0.07

The differential pressure distribution was measured by a set of nine Rosemount Model 1151DP low range differential pressure (dP) cells. The dP cell tap separations varied from cell to cell (9 to 24 inches) with the smaller spacings in the upper half of the bundle. Smaller spacings in the upper bundle allowed better resolution of void fraction near the mixture level. test section inlet flow was measured by a low flow orifice meter and two 0.5 inch turbine meters. Outlet flow was measured by a set of orifice flow meters and a 2 inch turbine meter.

The experiment began by establishing the desired test section mass flux; this was done by adjusting the inlet flow control valve. Power was then applied and the bundle would uncover partially. In Tests 3.0910I-N, 30 to 40% of the bundle was uncovered to allow acquisition of heat transfer and void fraction data. In Tests 3.09.10AA-FF only 10 to 15% of the bundle was uncovered. This allowed more void fraction data to be acquired from the highly instrumented upper half of the bundle.

Excess volume that was generated during boildown was absorbed in the loop pressurizer which was initially filled with subcooled water and nitrogen; during testing, nitrogen was vented or added to maintain a constant loop pressure. When the mixture level had assumed its equilibrium position, data were taken. Finally, flow and power were slowly adjusted to the next test point.

The two-phase mixture level was calculated as the elevation midway between the highest instrumented bundle elevation indicating nucleate boiling and lowest elevation indicating FRS dryout. Under low flow conditions the axial pressure distribution is governed primarily by the hydrostatic head of the mixture. Therefore, void fraction can be calculated from measured differential pressure. A force balance on the dP cell shows that,

$$\underbrace{\rho_s g h_{meas}}_{\text{measured } \Delta P} = \underbrace{\rho_r g h_r}_{\text{reference leg } \Delta P} - \underbrace{\bar{\rho} g h_r}_{\text{Two-phase mixture } \Delta P}$$

where h_{meas} and h_r refer to the measured hydrostatic head and reference leg length, respectively. Now, from the definition of mixture density,

$$\bar{\alpha} = \frac{\rho_r - (h_{meas}/h_r)\rho_s - \rho_f}{(\rho_g - \rho_f)}$$

Figure 5-1 through 5-12 show the exprimentally derived void fraction data overlaid with predicted void profile computed by using empirical drift flux correlation

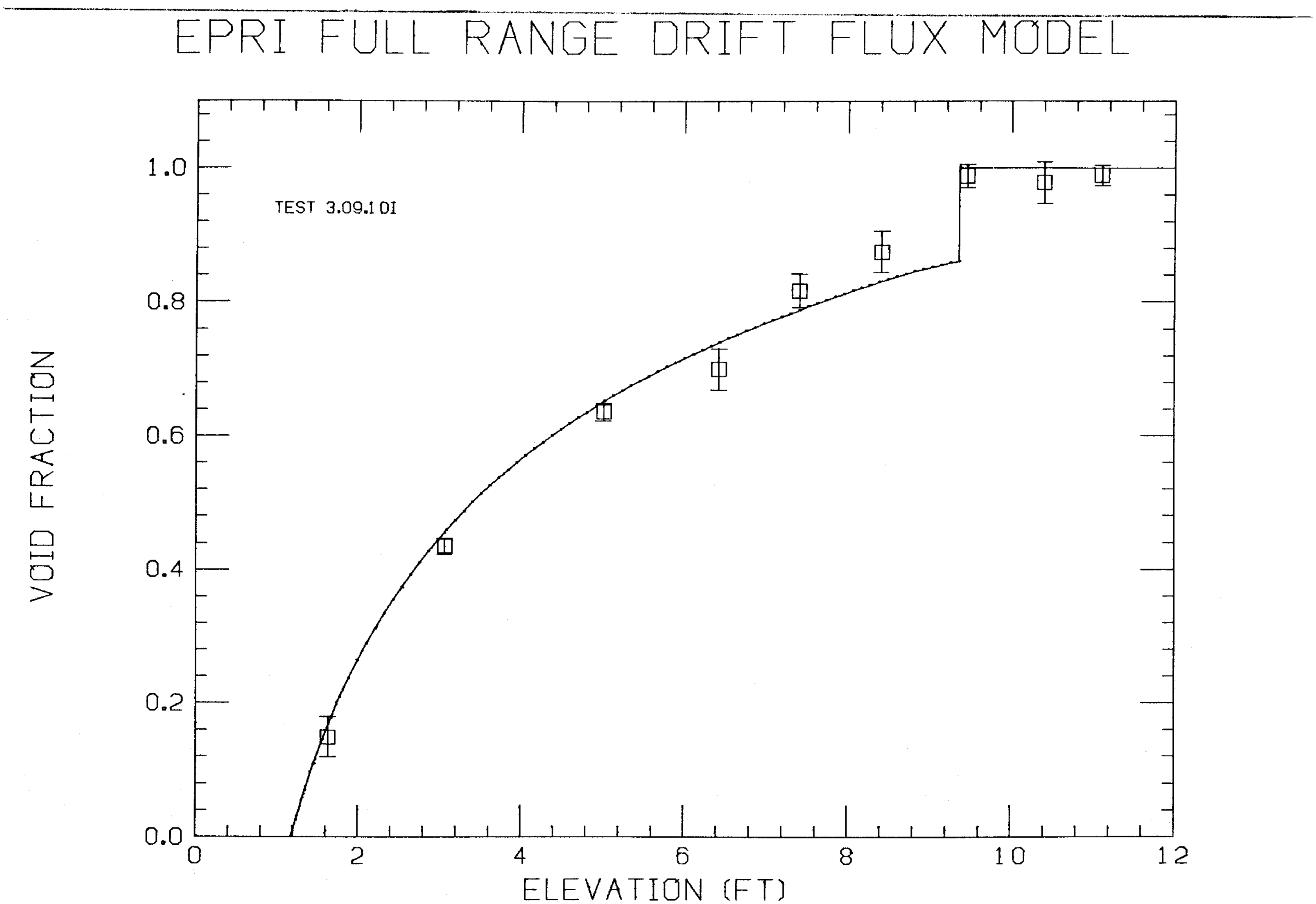

Figure 5-1. Comparison with Anklam et al High Press.-Low Bundle Uncovering Data: Test 3.09.10I

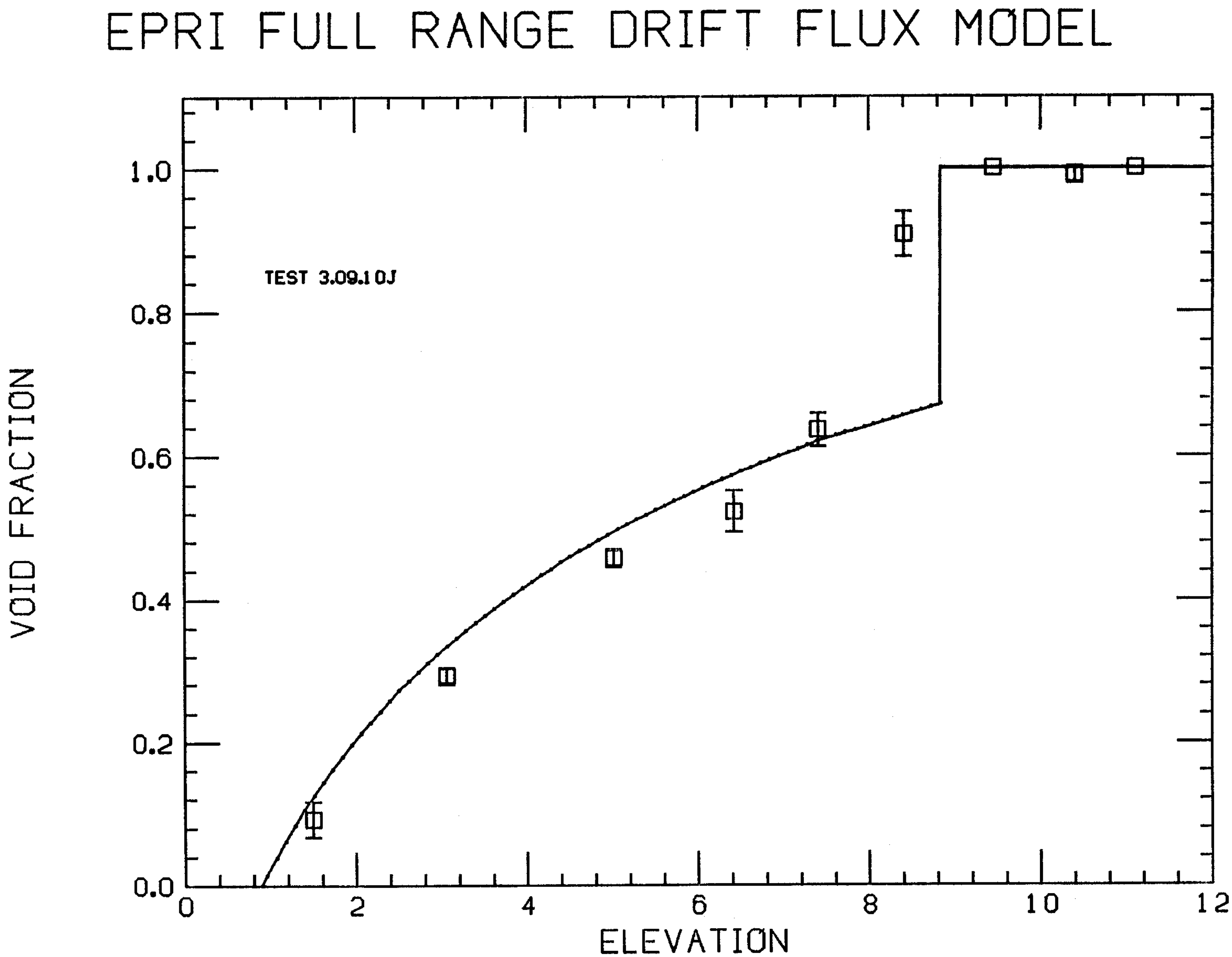

Figure 5-2. Comparison with Anklam et al High Press.-Low Flow Bundle Uncovering Data: Test 3.09.10J

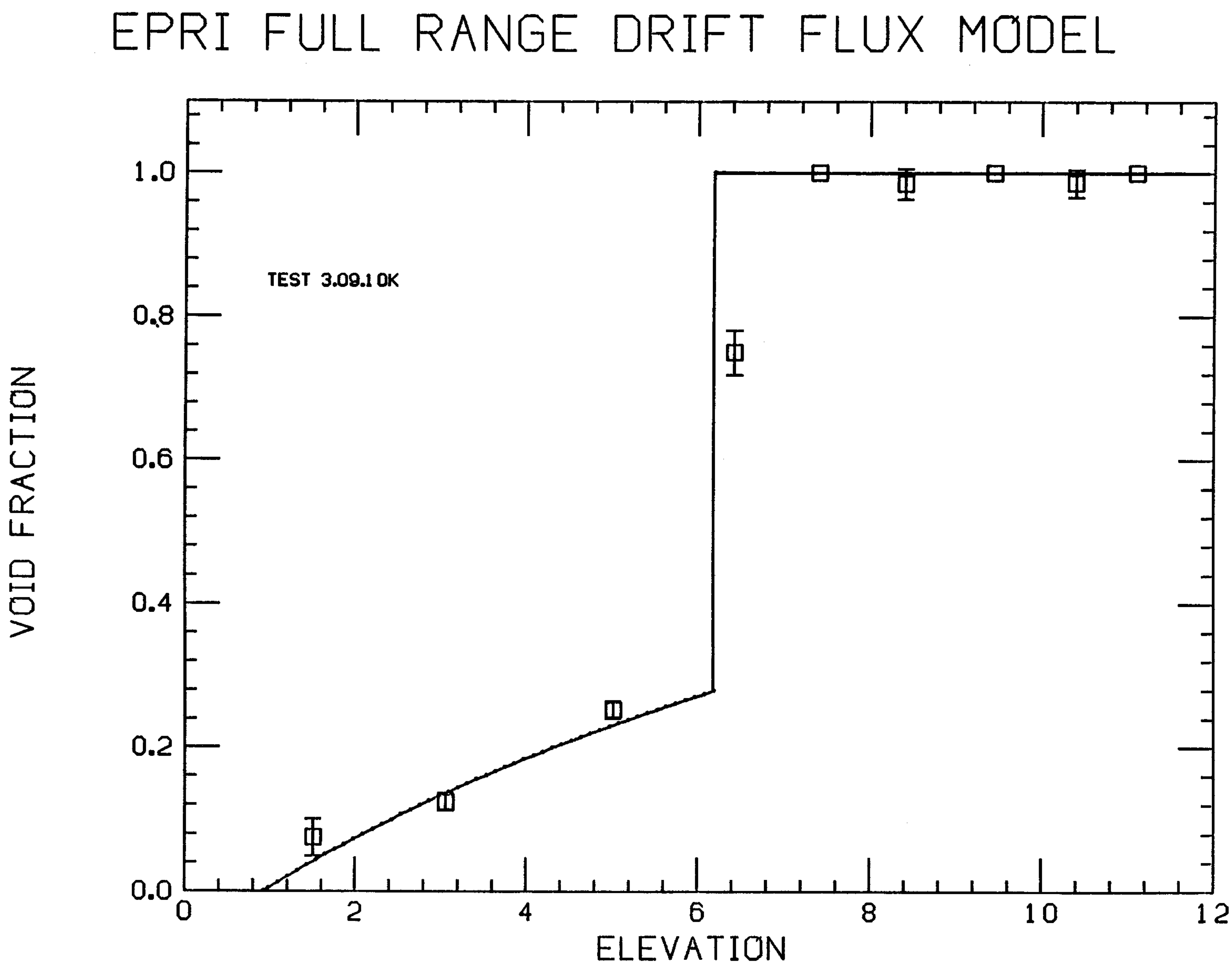

Figure 5-3. Comparison with Anklam et al High Press.-Low Flow Bundle Uncovering Data: Test 3.09.10K

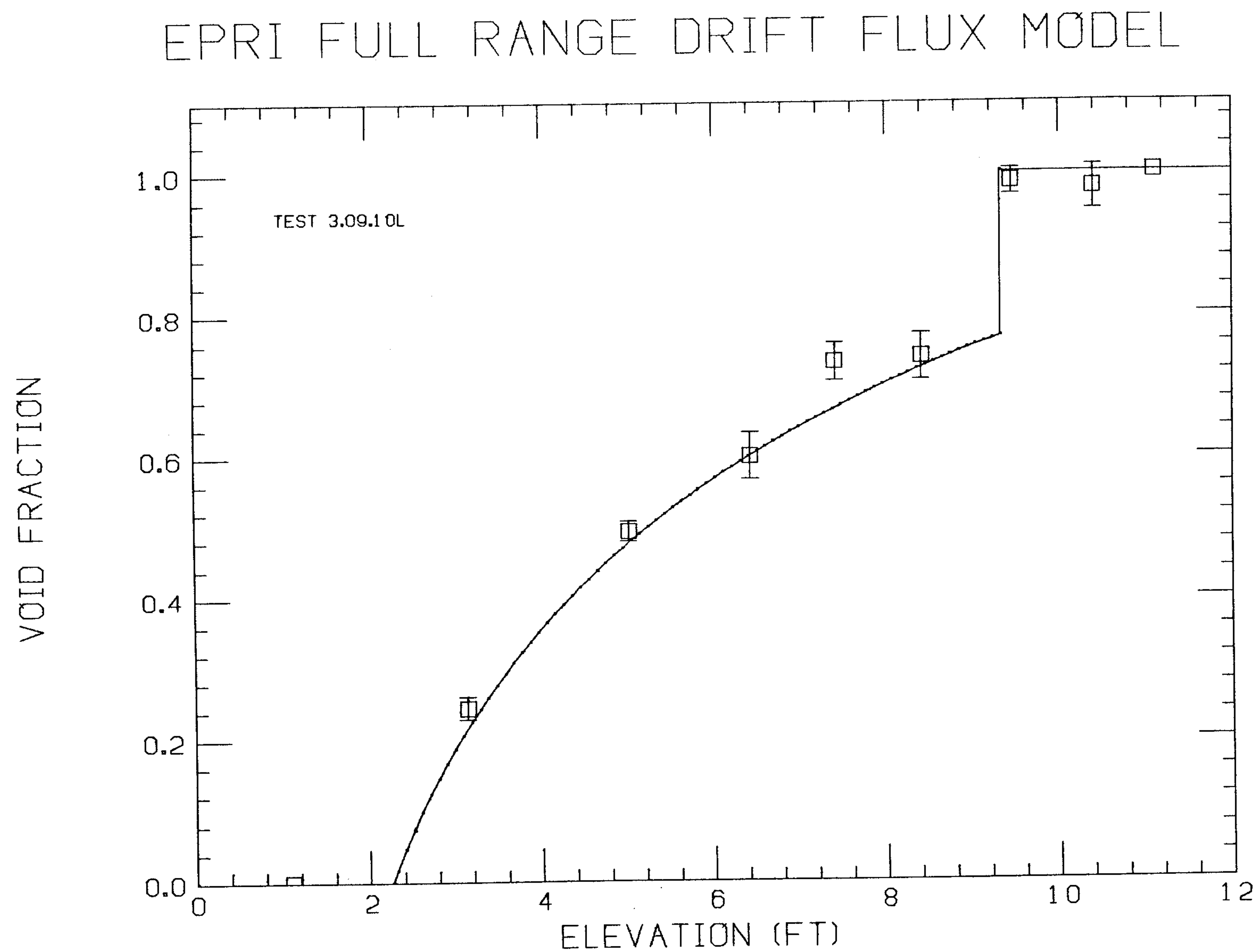

Figure 5-4. Comparison with Anklam et al High Press.-Low Flow Bundle Uncovering Data: Test 3.09.10L

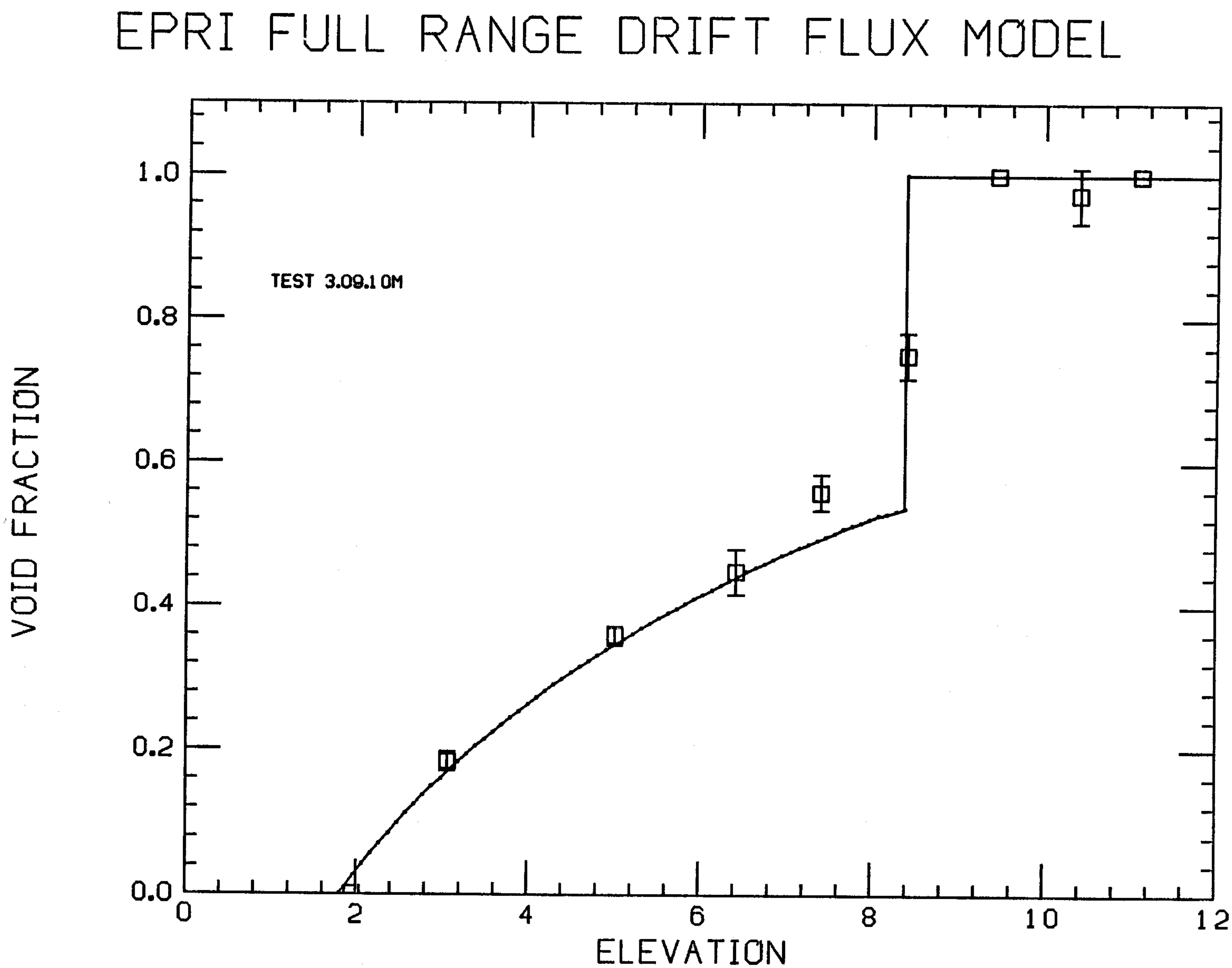

Figure 5-5. Comparison with Anklam et al High Press.-Low Flow Bundle Uncovering Data: Test 3.09.10M

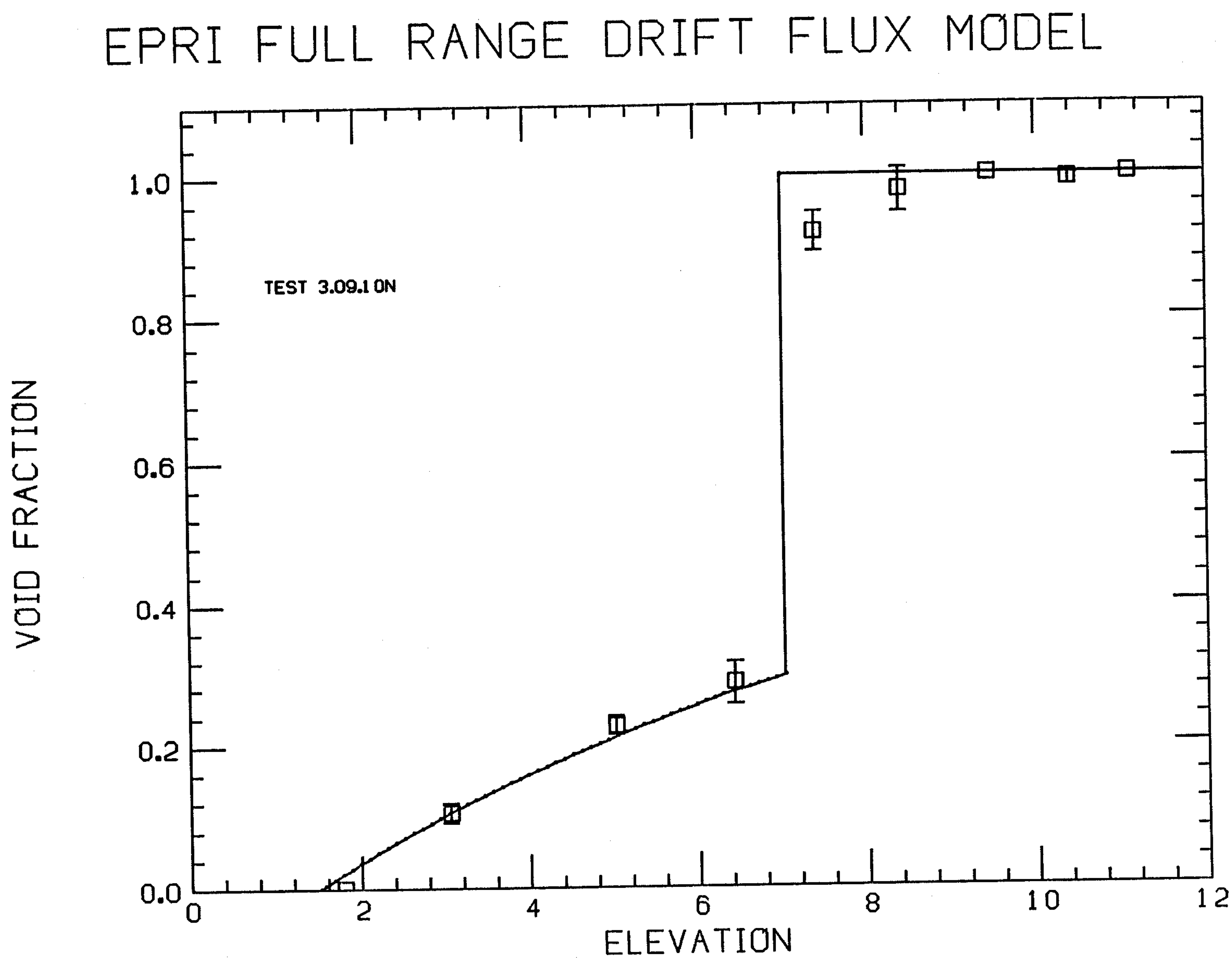

Figure 5-6. Comparison with Anklam et al High Press.-Low Flow Bundle Uncovering Data: Test 3.09.10N

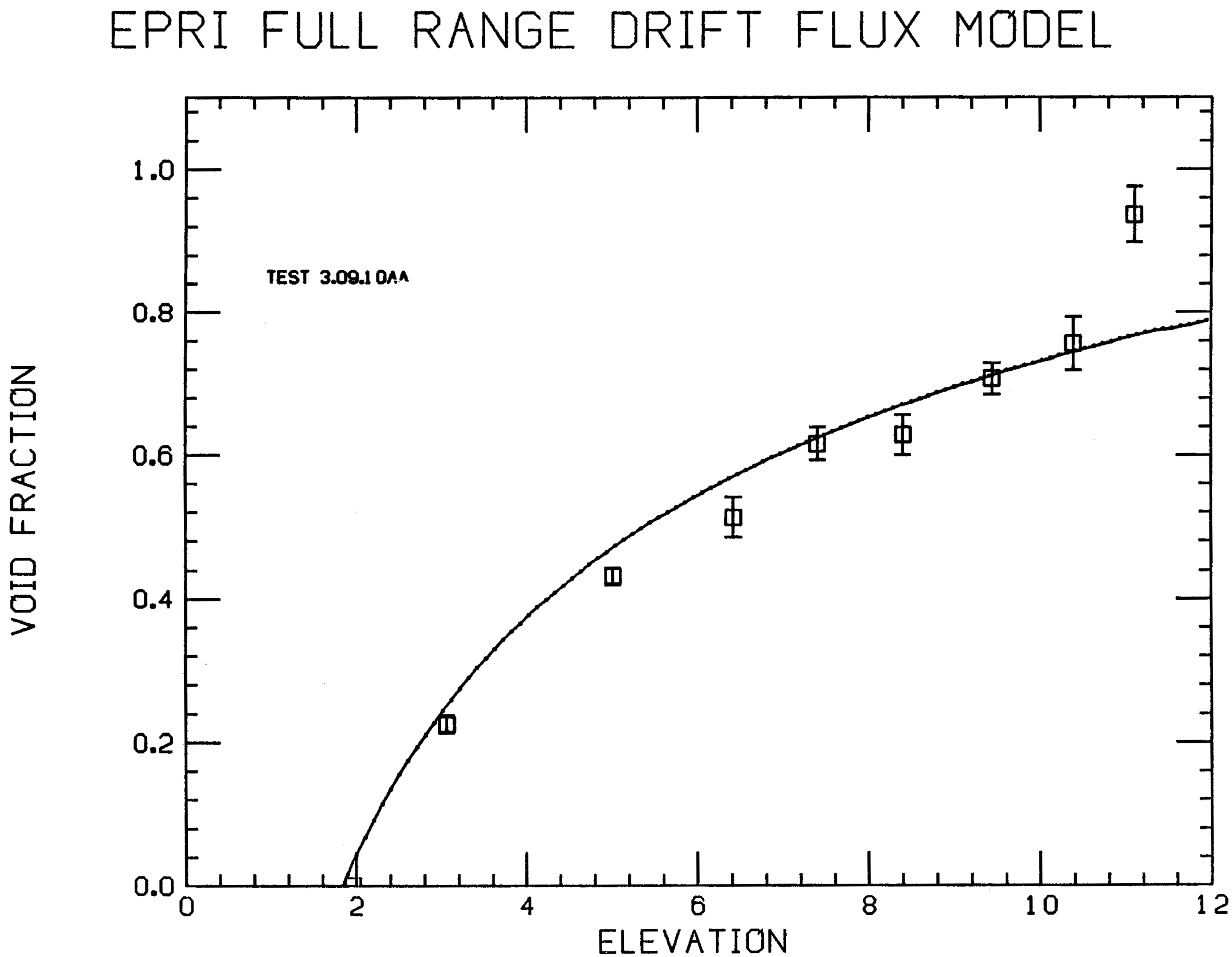

Figure 5-7. Comparison with Anklam et al High Press.-Low Flow Bundle Uncovering Data: Test 3.09.10AA

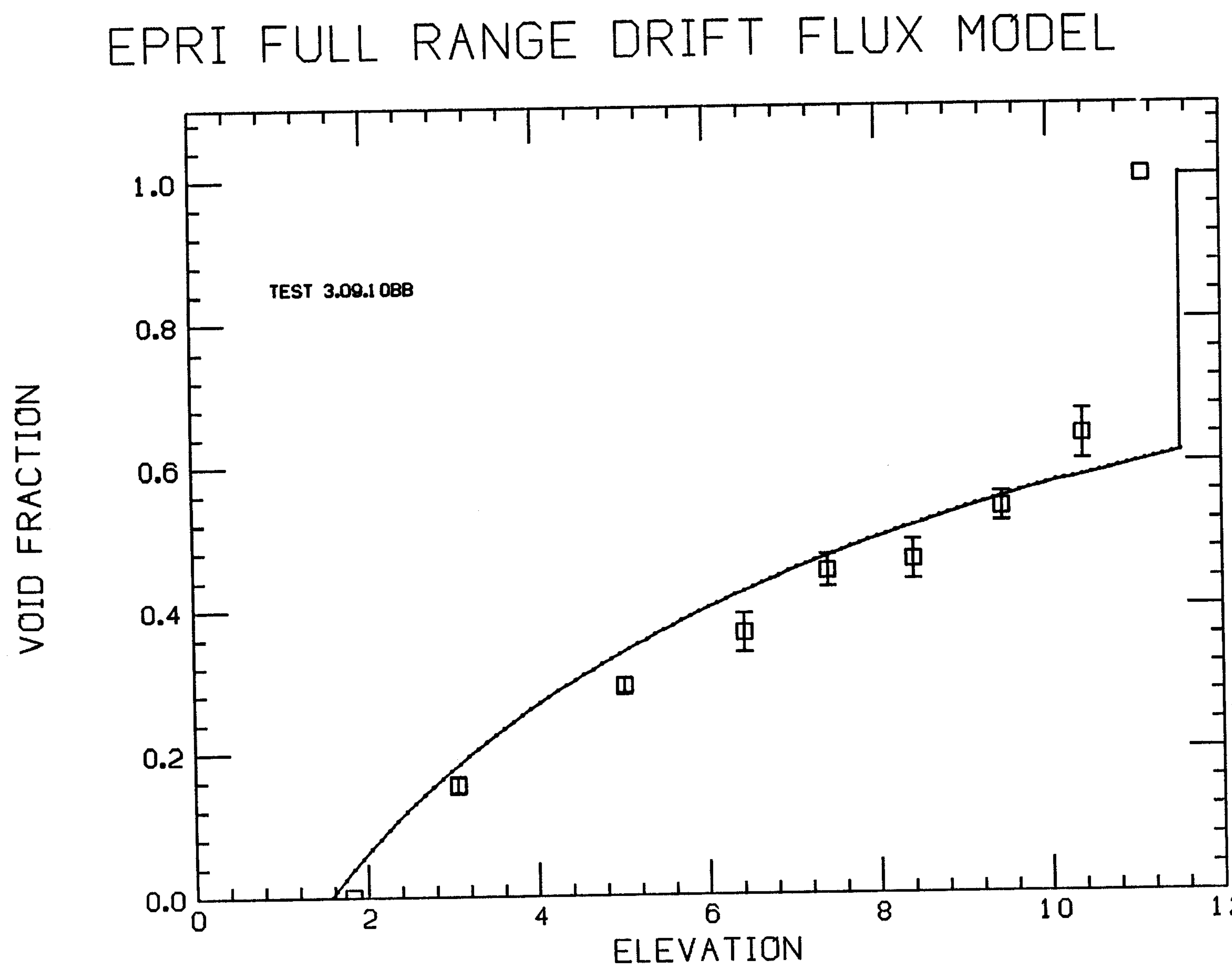

Figure 5-8. Comparison with Anklam et al High Press.-Low Flow Bundle Uncovering Data: Test 3.09.10BB

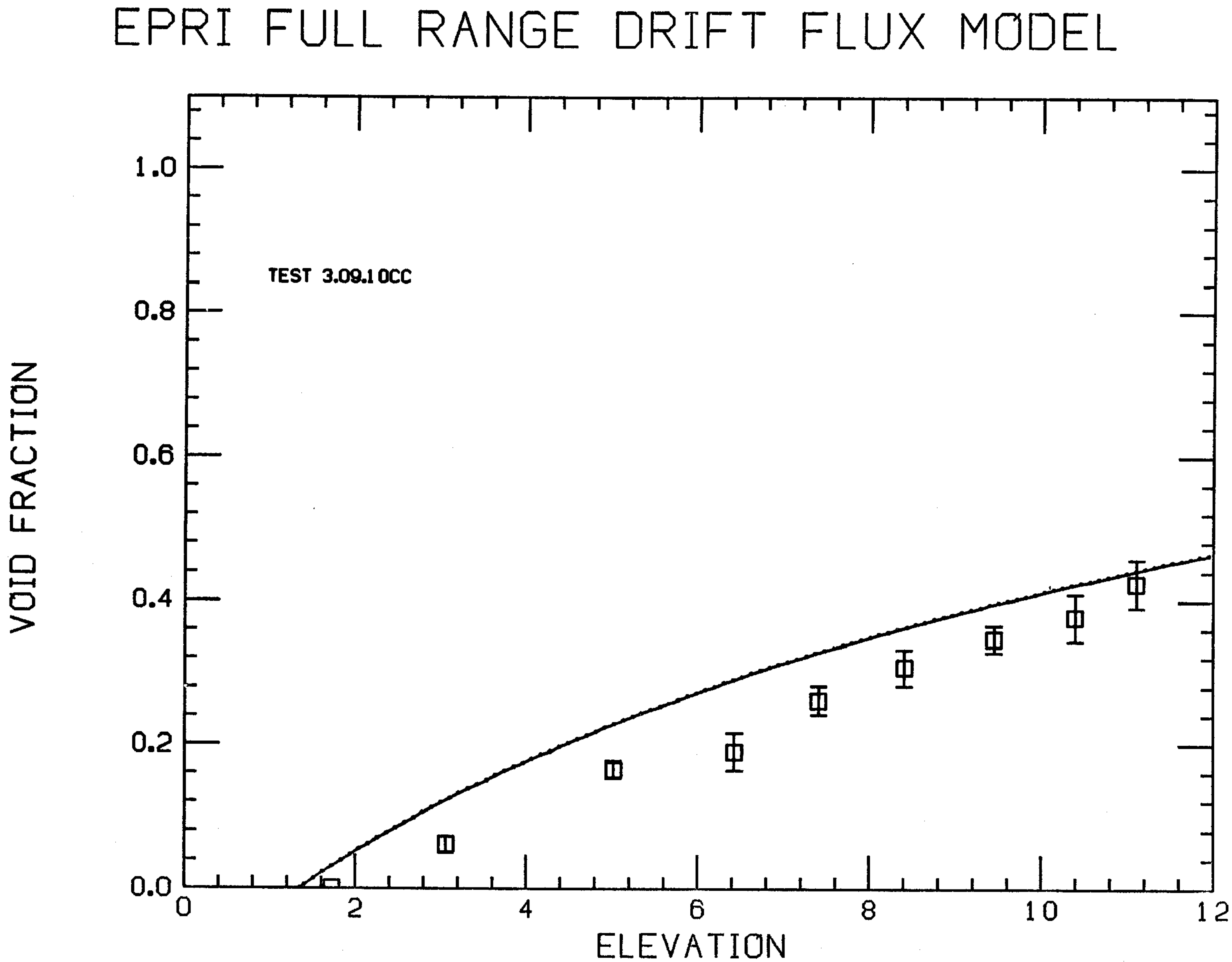

Figure 5-9. Comparison with Anklam et al High Press.-Low Flow Bundle Uncovering Data: Test 3.09.10CC

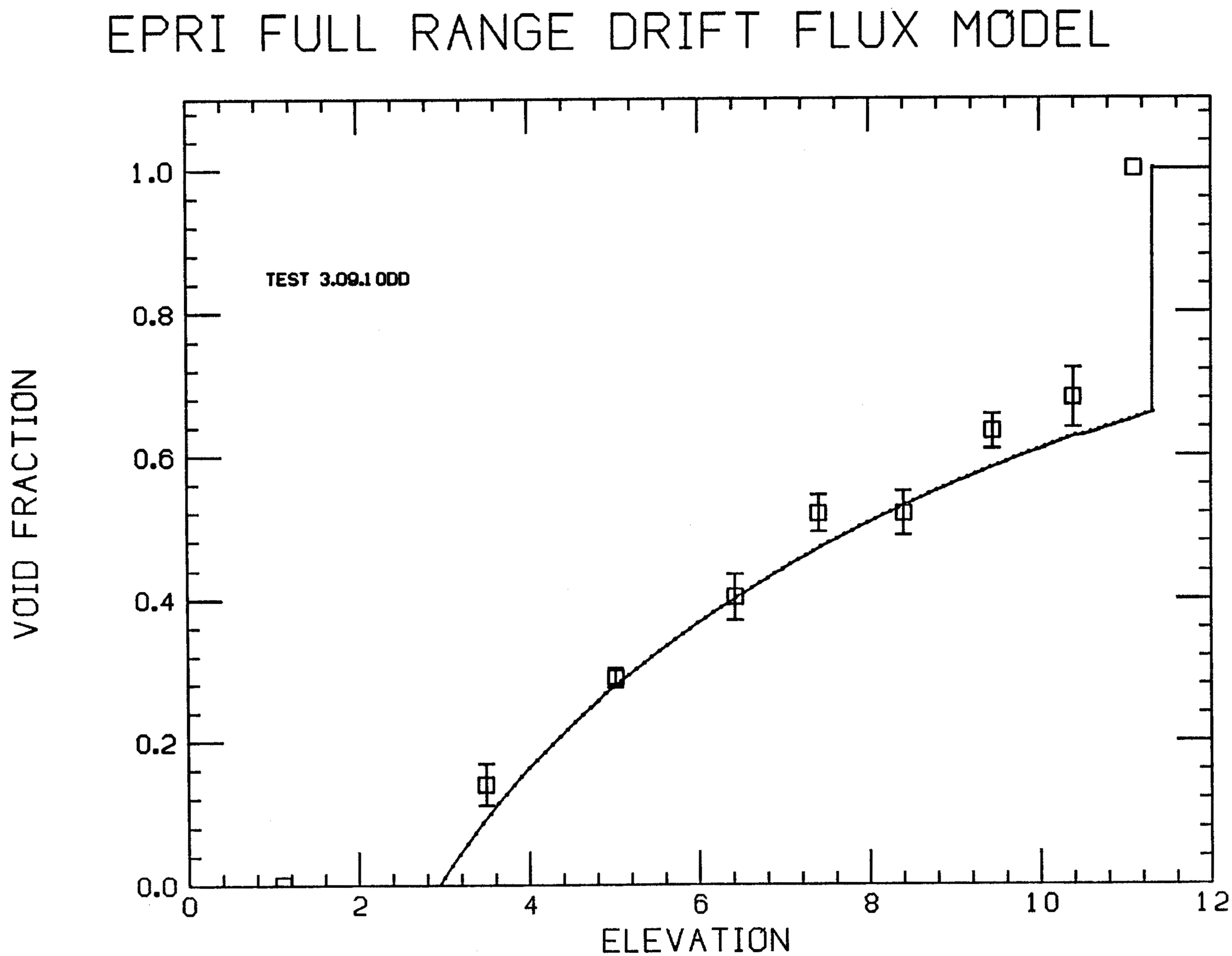

Figure 5-10. Comparison with Anklam et al High Press.-Low Flow Bundle Uncovering Data: Test 3.09.10DD

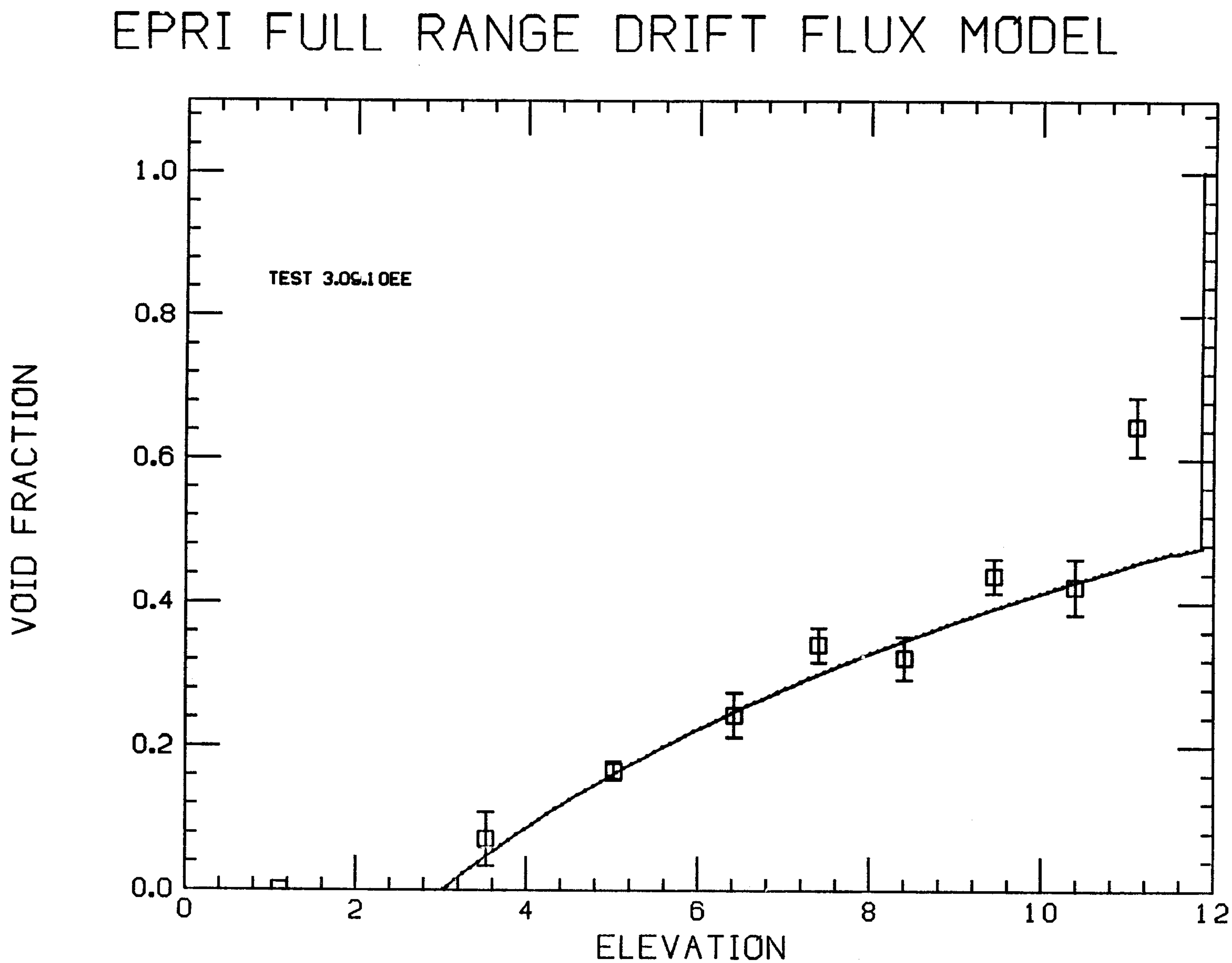

Figure 5-11. Comparison with Anklam et al High Press.-Low Flow Bundle Uncovering Data: Test 3.09.10EE

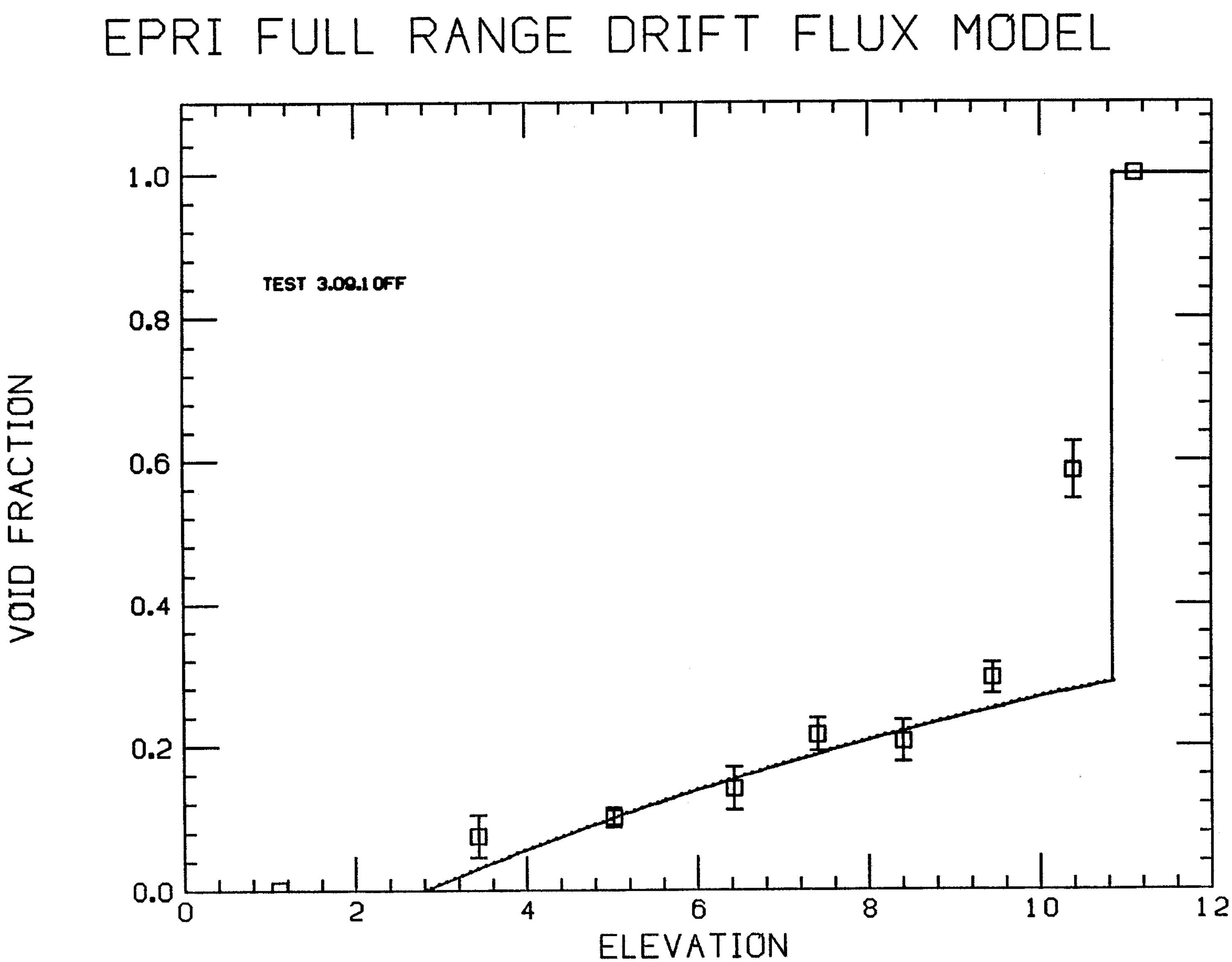

Figure 5-12. Comparison with Anklam et al High Press.-Low Flow Bundle Uncovering Data: Test 3.09.10FF

parameters described in Section 3. The mixture level was predicted by setting experimental collapsed level equal to the calculated collapsed level. The error bars appear on the experimentally derived void fractions.

All experiments and analytical calculations show very low or zero void fraction near the bottom of the heated length due to fluid subcooling. Void fraction then increased with elevation in a relatively linear or slightly parabolic manner. Slope of the void profile varied considerably from test to test with the steepest slopes associated with the highest volumetric vapor generation rate tests. Finally, at a location near the two phase mixture level, a sharp increase in void fraction with elevation occurred. In this region, void fraction rapidly approached 1.0, and dryout occurred. This "transition-to-dryout" region was well defined in the lowest volumetric vapor generation rate tests.

In general, the comparison with the test data is very good.

5.2 COMPARISON WITH TLTA DATA [11]

The General Electric Company conducted a series of transient boil-off tests using constant bundle powers (near decay heat levels) and at constant pressures to determine the effects of power and pressure on BWR 8 x 8 bundle response. The test conditions are shown in Table 5-2.

The primary objective of the low flow, bundle uncovery (boil-off) test series was to obtain data for evaluating heat transfer in a partially uncovered bundle. Boil-off due to decay heat can lead to inventory reduction in the bundle if no makeup emergency core cooling system fluid is made available following a LOCA. Such core inventory reduction can lead to reduced system flow by natural circulation of reactor coolant from the bypass and downcomer regions to the core.

For all tests, the primary measured quantities of interest included system pressure, node differential pressures, fluid temperatures, bundle power, and rod inside cladding temperatures. Local thermohydraulic quantities such as nodal void fraction, average density, and average mass were derived from the pressure drop and temperature measurements.

Table 5-2

SUMMARY OF TLTA TEST CONDITIONS

Test Run	Test Point	System Pressure (psia)	Bundle Power (kW)	Initial Level (2-Phase)
3	5	394±3	400±1	Bundle Top
5	9	195±2	250±1	Bundle Top
6	1	395^{+10}_{-0}	250±2	Bundle Top
7	5	790^{+2}_{-0}	250±1	Bundle Top

The bundle inlet mass flow rate was estimated from a mass balance on the system which included the annulus, guide tube, and lower plenum regions. The fluid mass in each region was derived from nodal pressure drop measurements. The bundle steam generation rate was derived from a bundle mass balance.

Figures 5-13 through 5-16 show the experimentally derived void fraction data at time = 0 second for each test overlaid with void profile computed by using the empirical drift flux correlation parameters described in Section 3. The error bars appear on the experimentally derived void fractions.

In general, the comparison with the test data is very good.

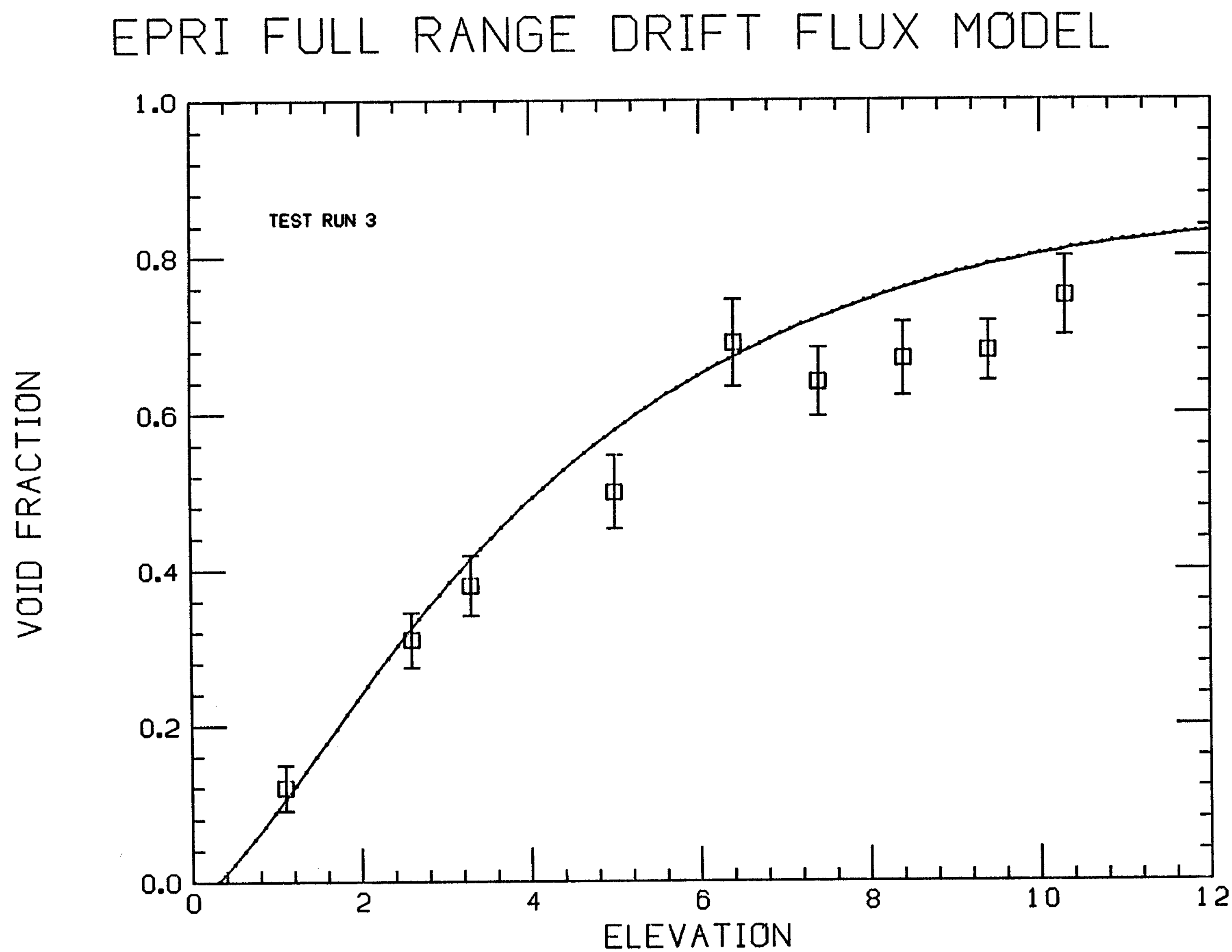

Figure 5-13. Comparison with TLTA BWR High Press.-Low Flow Bundle Uncovery Data: Test Run 3

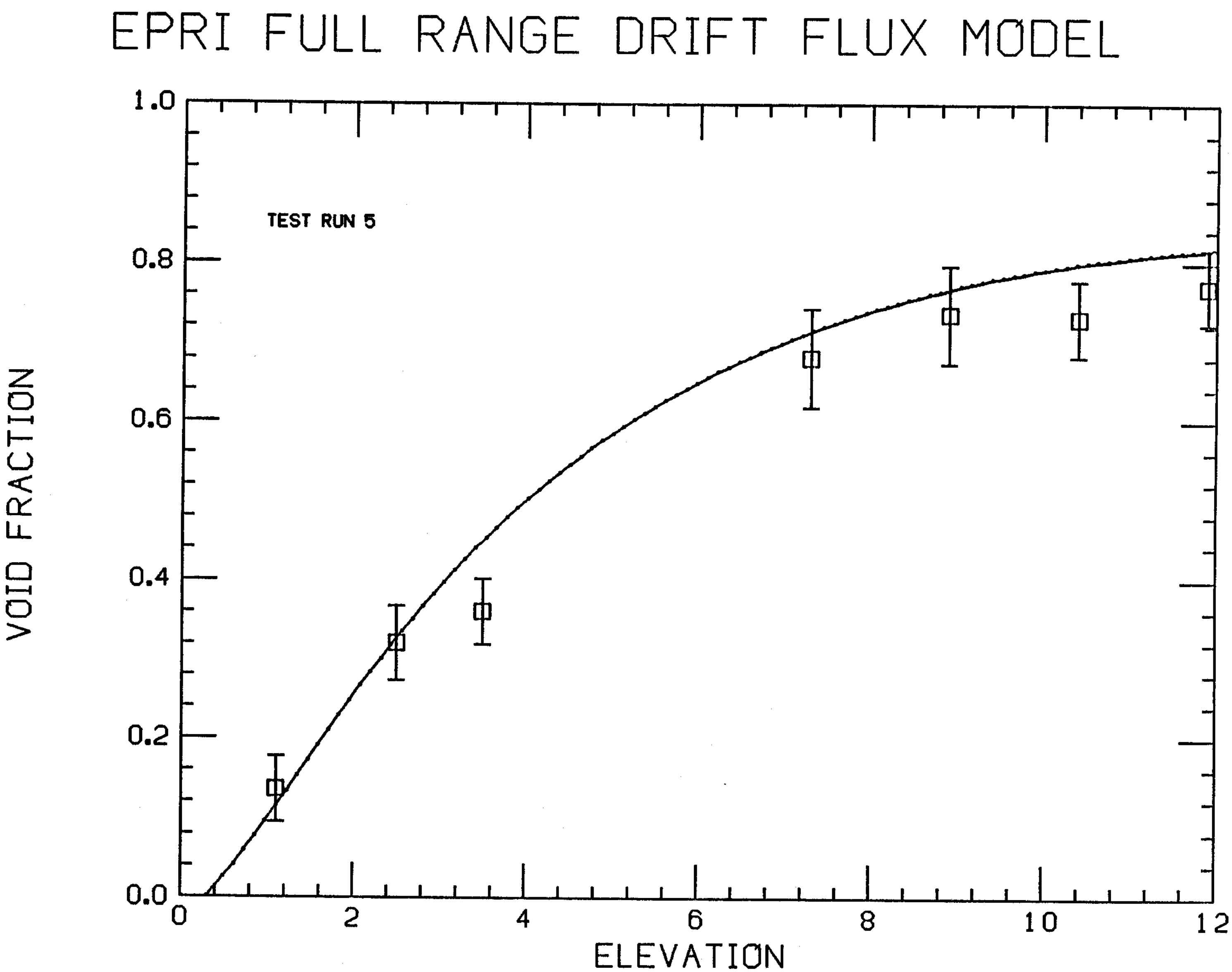

Figure 5-14. Comparison with TLTA BWR High Press.-Low Flow Bundle Uncovery Data: Test Run 5

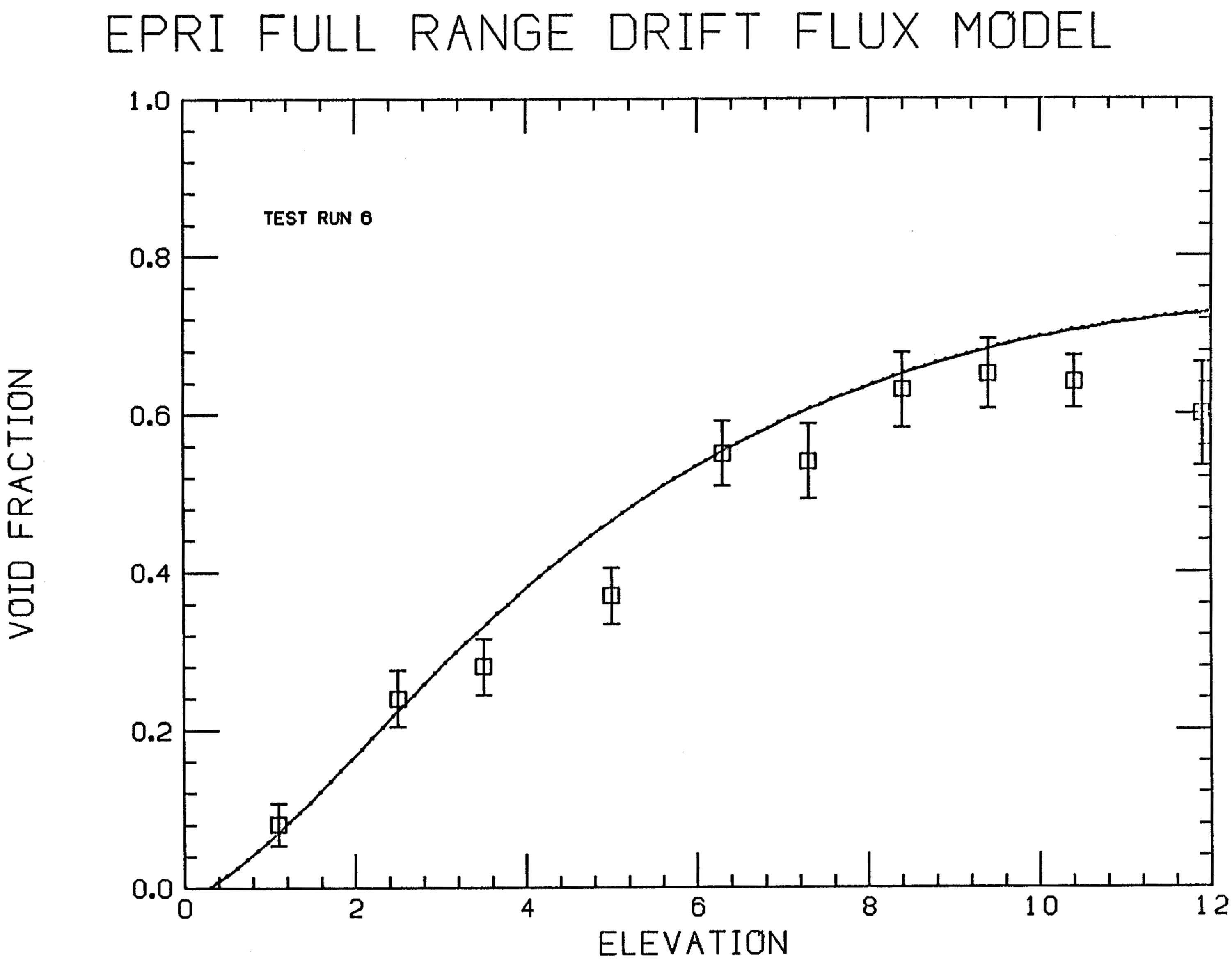

Figure 5-15. Comparison with TLTA BWR High Press.-Low Flow Bundle Uncovery Data: Test Run 6

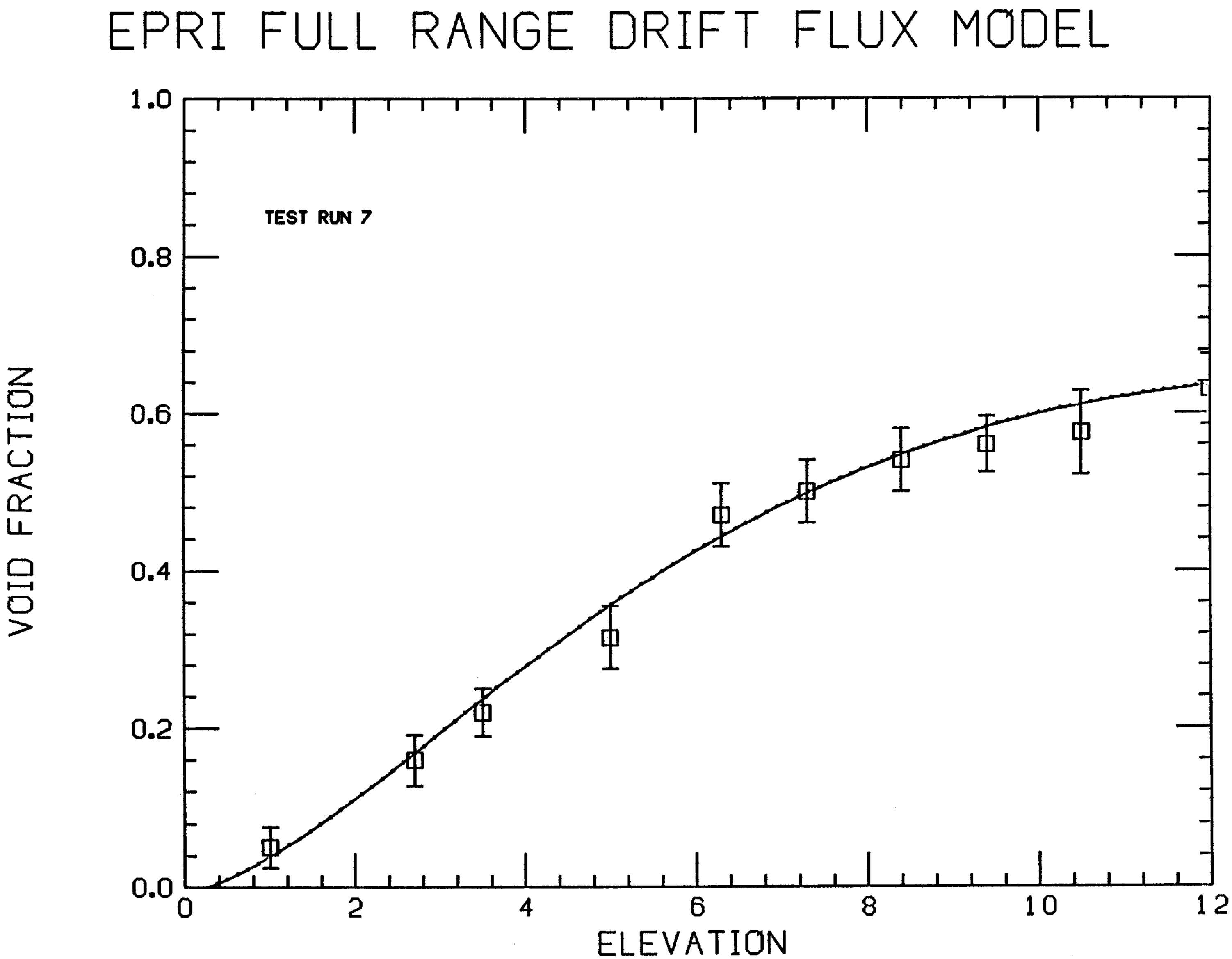

Figure 5-16. Comparison with TLTA BWR High Press.-Low Flow Bundle Uncovery Data: Test Run 7

Section 6

COMPARISON WITH LOW PRESSURE-LOW FLOW DATA

These conditions are typical of a large break LOCA accident and are expected to occur during core uncovering or reflood conditions. The void distribution in the core has a strong effect on core heat transfer, discharge flows during reactor blowdown and influences the progress of the quench front during reflood.

In this section, void fraction predictions using the empirical drift flux correlation are compared with Hall et al [12] data taken at Berkeley Nuclear Laboratories of Central Electricity Generating Board, England; Wong et al [13] data taken at Westinghouse Electric Corporation, and Jowitt [14] data taken at Atomic Energy Establishment, Winfrith of United Kingdom Atomic Energy Authority.

6.1 COMPARISON WITH Hall ET AL Data [12]

A series of tests were conducted in a circular borosilicate glass pipe of 6.5 ft and ~4 inches in diameter. Mounted in the bottom of this vessel was a bundle of 19 x 1 kW electrical heaters with a heated length of 18 inches and diameter of 0.37 inches. The tests were done at a range of steady pressures between 1 and 4 bars.

Rig pressure was measured using a bourdon-tube pressure gauge, and maintained at the required conditions by varying the condenser cooling water flow rate. The electrical power of the bundle was measured using voltmeters and ammeters, to an accuracy of ± 5%, and was varied both by variable transformers and by disconnecting selected heaters from the supply.

Void fraction was inferred from measurements of differential pressure across the heated section of the bundle, and across a 7.1 inch section of the pipe above the bundle. Rosemount oil-filled variable capacitance pressure transducers were used, and their outputs were traced on a U.V. recorder. In addition, a scale was attached to the vessel, for measuring the mixture height.

The vessel was filled to a suitable level with demineralized water, and boiled for ~10 mins to remove dissolved gases. The vessel was then sealed and brought to pressure. The level was reduced to the desired value by venting to atmosphere. The required power was set and when steady conditions had been reached, the output of the differential pressure cells were recorded. The mixture level was also noted. Prior to another test at different conditions, the heaters were switched off in order to check the quiescent water level.

Void fraction data as a function of steam volumetric flux was obtained <u>within the heated bundle</u> as well as <u>above the heated bundle</u> in the unobstructed pipe.

Figure 6-1 compares the experimentally derived void fraction data <u>within</u> the heated bundle with the void fraction computed by using empirical drift flux correlation parameters described in Section 3. Figure 6-2 compares the experimentally derived void fraction data in an open pipe <u>above</u> the heated bundle with the void fraction computed by using empirical drift flux correlation parameters described in Section 3.

In general, the comparison with test data in Figures 6-1 and 6-2 is good and provides confidence in use of the correlation for bundle assemblies as well as open pipes.

6.2 COMPARISON WITH WONG ET AL DATA [13]

Tests were conducted by Wesingthouse Electric Corporation as part of the FLECHT SEASET (Full-Length Emergency Core Cooling Heat Transfer-Separate-Effects Tests and System-Effects Tests) program to address the system and bundle reflood response for a postulated LOCA. The 161-rod test bundle simulates a full-length portion of PWR cores with fuel rod geometry typified by a Westinghouse 17 x 17 assembly design. The experimental steady state void fraction data was deduced from the pressure drop data read at intervals of 12 inch along the entire bundle. The test conditions are given in Table 6-1.

Figures 6-3 through 6-5 show the experimentally derived void fraction data overlaid with void profiles computed by using empirical drift flux correlation parameters described in Section 3.

In general, the comparison with test data is very good.

Table 6-1

SUMMARY OF BOIL-OFF TEST CONDITIONS FOR FLECHT-SEASET DATA

Test Run No.	Pressure (psia)	Axial Power (Kw)	Radial Power Profile	Power Profile
35557	60	460	Cosine	Uniform
35658	40	460	Cosine	Uniform
35759	20	460	Cosine	Uniform

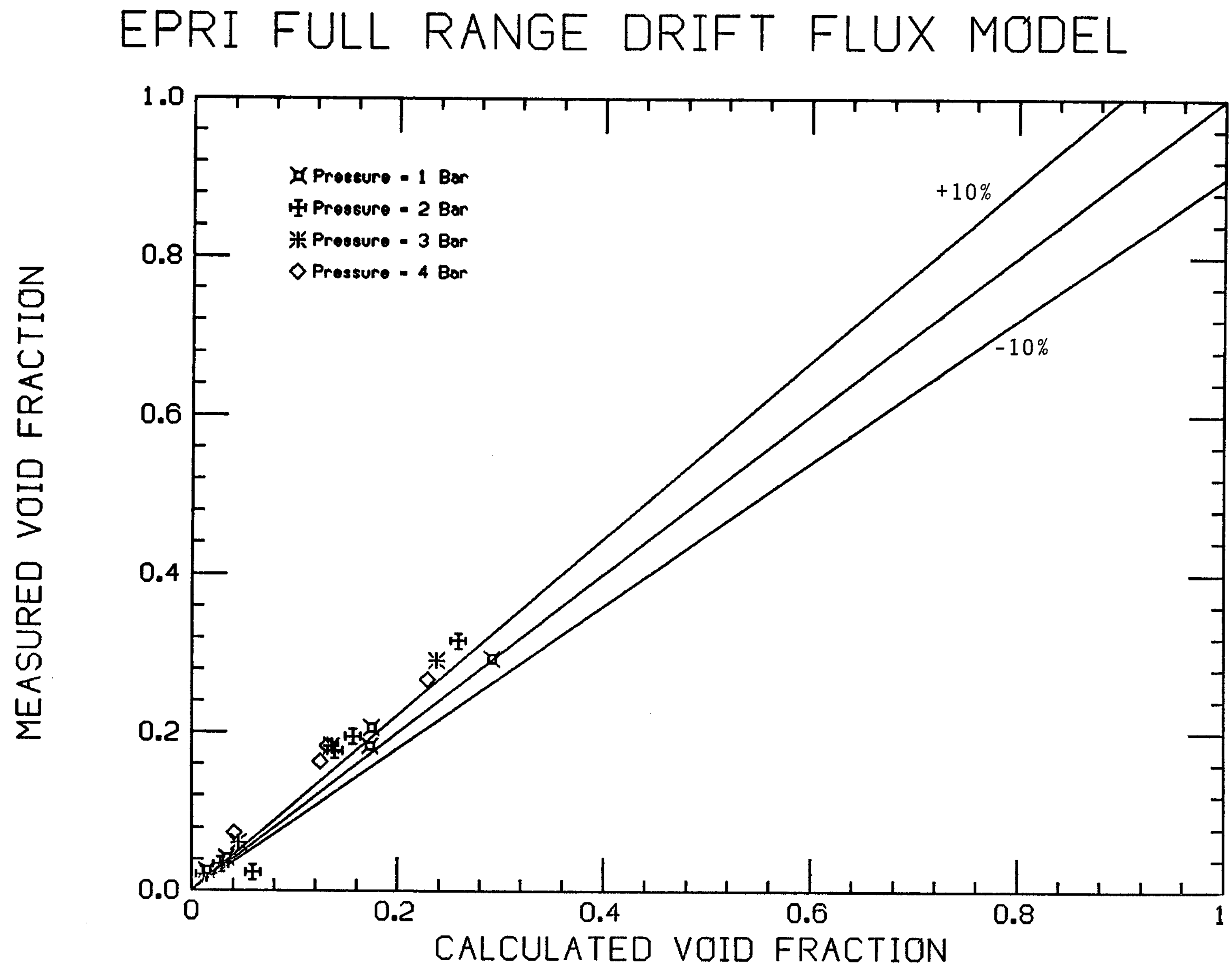

Figure 6-1. Comparison with Hall Data in a Heated Bundle at 1,2,3,4 Bars

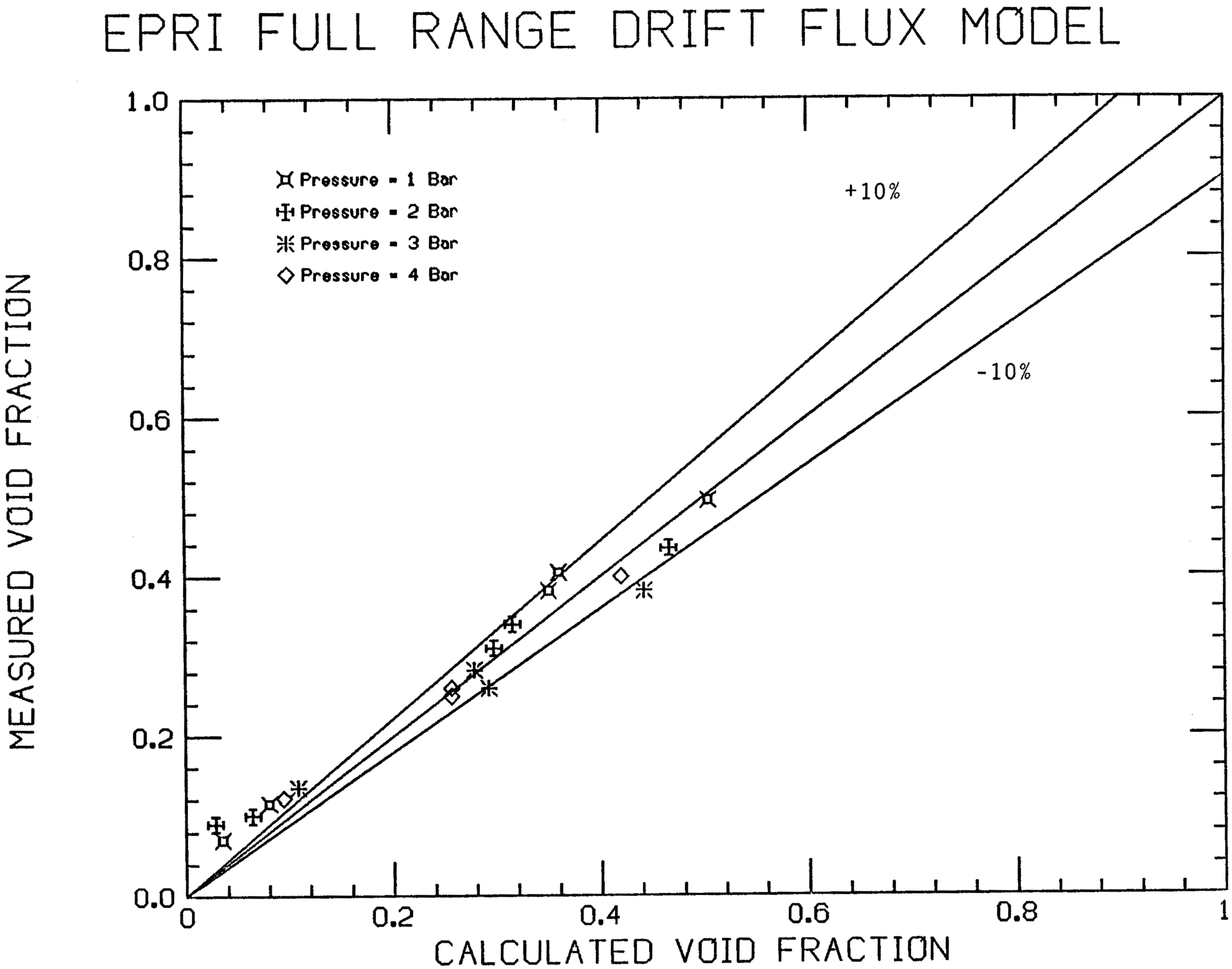

Figure 6-2. Comparison with Hall Data in a 105 MM Pipe at 1,2,3,4 Bars

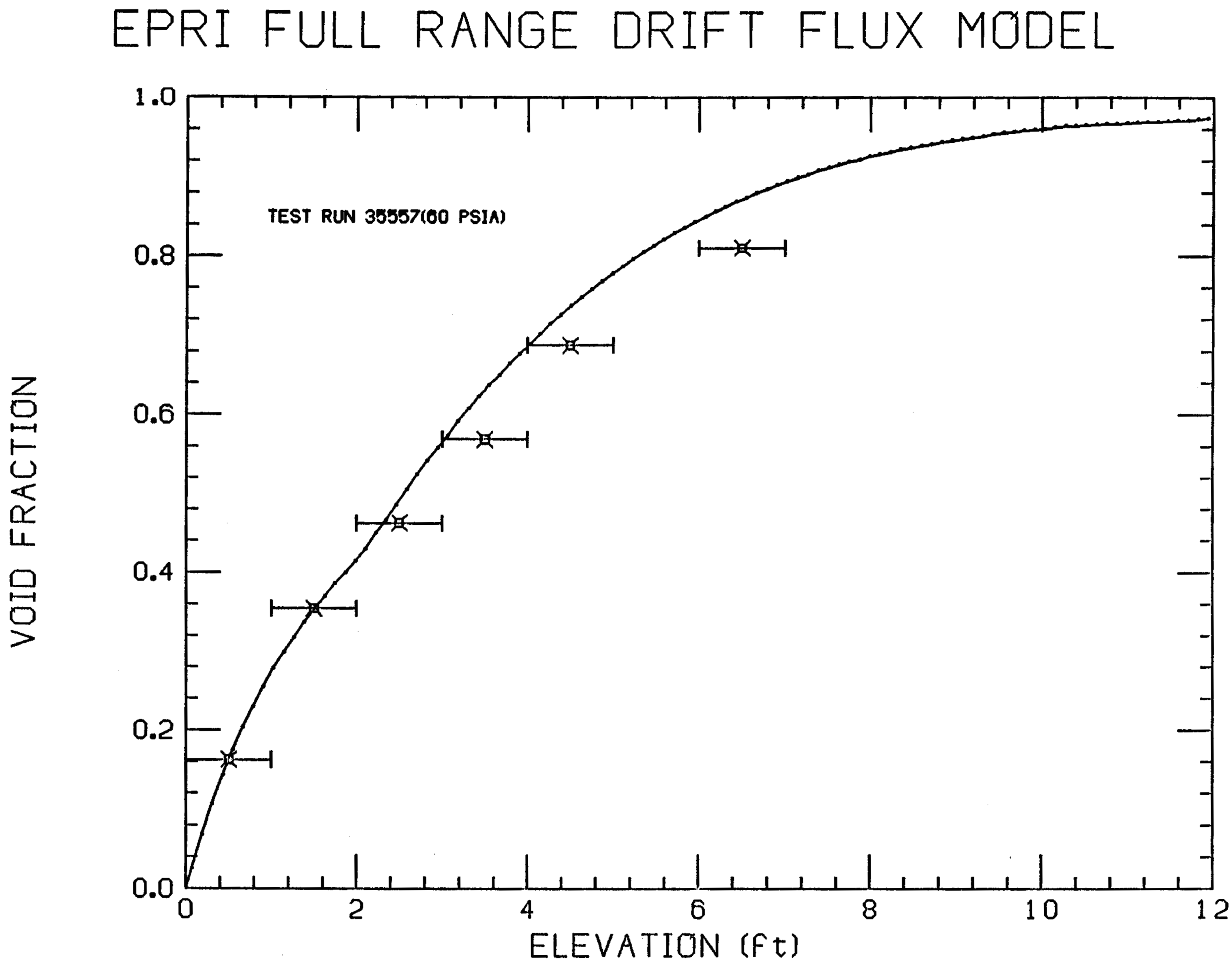

Figure 6-3. Comparison with FLECHT SEASET Low Pres.-Low Bundle Uncovering Data: Test Run 35557

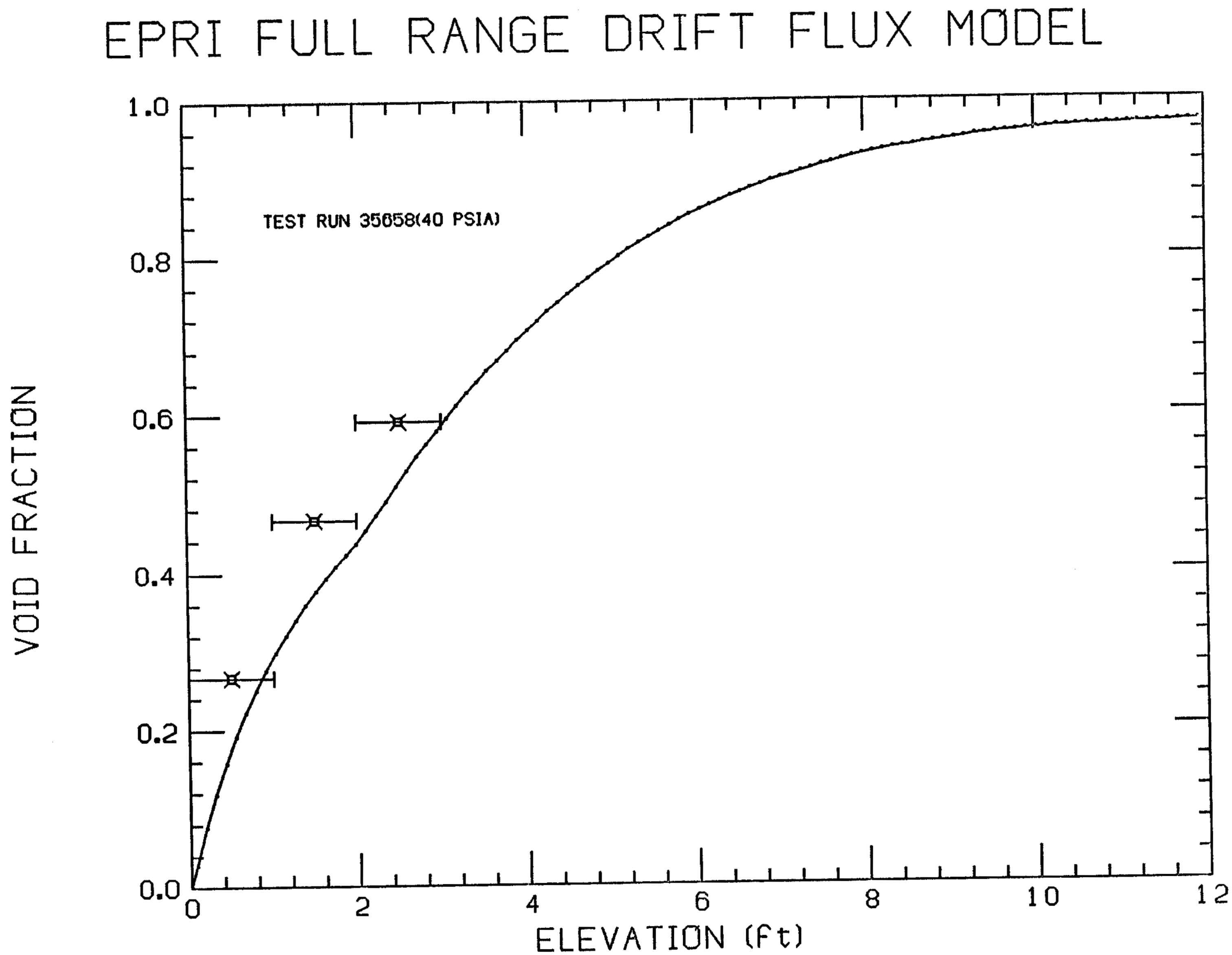

Figure 6-4. Comparison with FLECHT SEASET Low Press.-Low Flow Bundle Uncovering Data: Test Run 35658

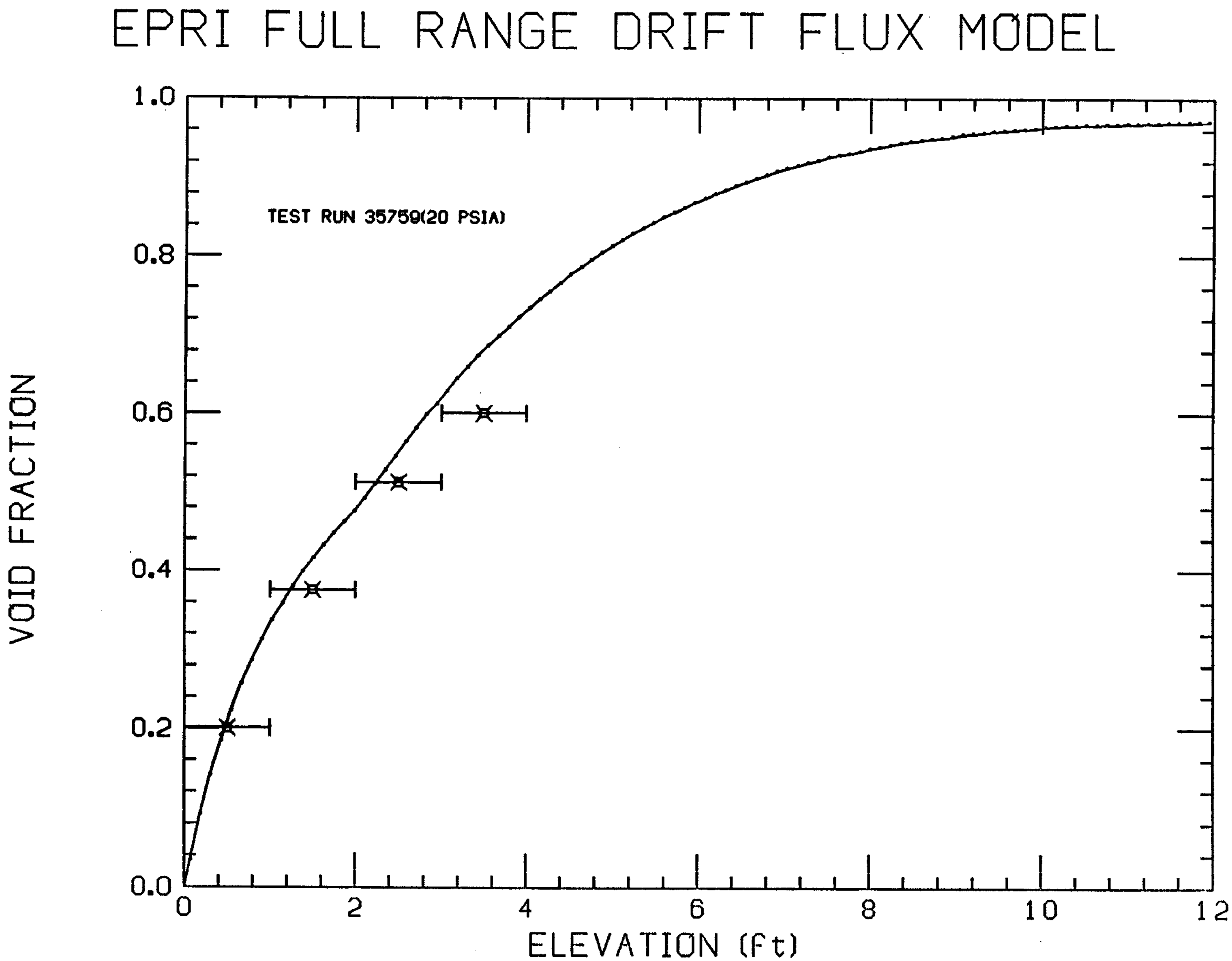

Figure 6-5. Comparison with FLECHT SEASET Low Press.-Low Flow Bundle Uncovering Data: Test Run 35759

6.3 COMPARISON WITH JOWITT DATA [14]

Steady State Level Swell tests were carried out in the THETIS (Thermal Hydraulic Emergency Cooling Test Installation) in a 61 pin cluster at pressures from 2 to 40 bar. The objective was to investigate the thermal hydraulic behavior of partially water filled fuel clusters. The measurements were made at 3 different collapsed liquid levels at each of the 5 pressures (2, 5, 10, 20, 40 bars). The test conditions are shown in Table 6-2.

An experiment began with the system pressure at the desired level, for example 20 bar, the water at saturation and filled to either 50 to 70 percent of the length of the fuel pins. The power applied to the cluster was then increased an increment. As steam formed and flowed out of the pressure vessel, makeup water was introduced at the bottom of the cluster so that the collapsed height remained constant and equal to its original setting, i.e. 50, 60 or 70 percent level. In addition, the system pressure was kept constant via a pressure controlled exhaust. After the two phase mixture level stabilized to its new height for the particular applied power, the power was increased another increment. Adjustments were then again made with the feedwater and pressure exhaust so that the collapsed height and system pressure remained constant. The results of this experiment are the two phase mixture height (level swell) as a function of power with fixed collapsed height for a series of system pressure ranging from 2 to 40 bars.

At low pressures, a high initial liquid level would rapidly swell to fill the whole cluster for only a small increase in power. Consquently, the low pressure experimental runs were made at lower initial liquid levels. Values for the mean density $\overline{\rho}$ and hence for the mean voidage $\overline{\alpha}$ in the boiling region were calculated from the measured swell levels, the measured heights of the sub-cooled region and the measured test section ΔP.

Figure 6-6 compares the experimental mixture level with calculated mixture level at pressures of 2, 5, 10, 10, and 40 bars.

In general, the comparison with test data is very good.

Table 6-2

SUMMARY OF TEST CONDITIONS FOR JOWITT DATA

Collapsed Level (% Full)	Pressure (Bars)				
70				20	40
60			10	20	40
50	2	5	10	20	40
40	2	5	10		
30	2	5			

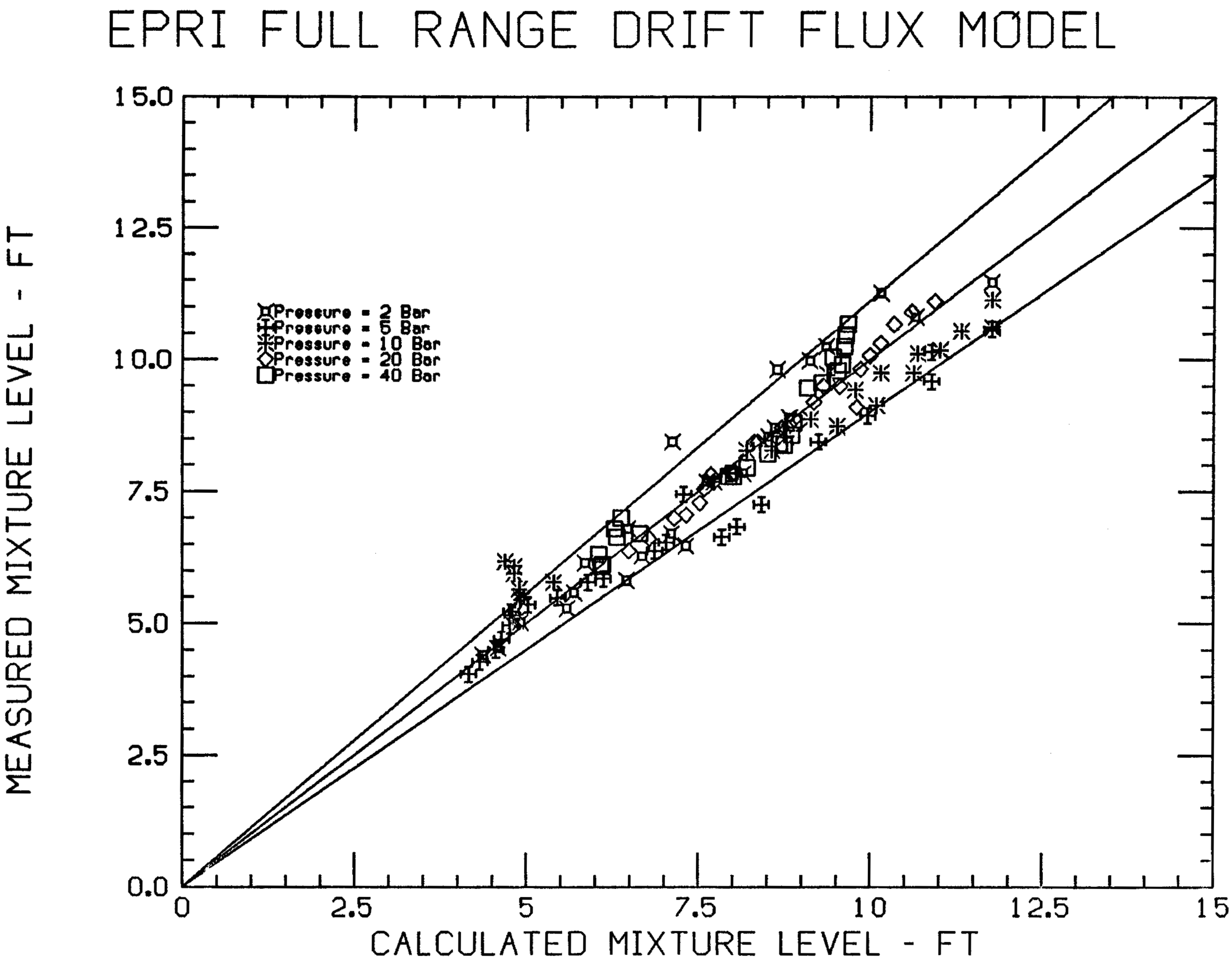

Figure 6-6. Comparison with JOWITT Data in a Heated Bundle at 2,5,10,20,40 Bars

Section 7

COMPARISON WITH COUNTERCURRENT FLOW LIMITATION DATA

Onset of the countercurrent flow limitation (CCFL) or sometimes called flooding limit refers to the limiting condition where the flow rates of neither the gas nor the liquid phase can be increased further without altering the flow pattern. Such a condition occurs in a light water reactor during a LOCA. In a PWR, these conditions are expected to occur at the core/upper plenum interface and in the downcomer where emergency core cooling water is trying to enter the core against the uprising steam. In a BWR, these conditions occur at the core upper tie plates and bottom side-entry orifices. The upper tie plate in a BWR limits the flow entering from the upper plenum into the core and the bottom side entry orifices limit the inventory leaving the core into the lower plenum. Since CCFL restricts the flow entering or leaving the core, its characteristics are important for determination of water inventories and thus the heat transfer in different regions of a light water reactor.

7.1 DEVELOPMENT OF CALCULATIONAL PROCEDURE FOR PREDICTING CCFL

The general drift flux correlation is given by

$$j_g = \frac{\alpha\, C_o}{1-\alpha\, C_o}\, j_f + \frac{\alpha}{1-\alpha\, C_o}\, V_{gj} \tag{7-1}$$

if we let $1-\alpha\, C_o = A_1$, j_g is given by

$$j_g = \frac{\alpha\, C_o}{A_1}\, j_f + \frac{\alpha}{A_1}\, V_{gj} \tag{7-2}$$

On the CCFL line, $\frac{dj_g}{d\alpha} = 0$,

$$\therefore \quad \left.\frac{dj_g}{d\alpha}\right|_{j_f} = 0 = \frac{d}{d\alpha}\left[\frac{\alpha\, C_o}{A_1}\, j_f + \frac{\alpha}{A_1}\, V_{gj}\right] \tag{7-3}$$

Differentiating we obtain j_f and thus j_g that satisfies relationship (7-3) for a given α is

$$-j_f = \frac{V_{gj}\left[1 + \frac{\alpha}{V_{gj}} \cdot \frac{dV_{gj}}{d\alpha} + \alpha A_1 \frac{d\frac{1}{A_1}}{d\alpha}\right]}{C_o\left[1 + \frac{\alpha}{C_o}\frac{dC_o}{d\alpha} + \alpha A_1 \frac{d\frac{1}{A_1}}{d\alpha}\right]} \tag{7-4}$$

Using the empirical drift flux parameters from Section 3, the various terms in eg. (7-3) are given by:

$$V_{gj} = 1.41\left[\frac{(\rho_f - \rho_g)\,\sigma\, g\, g_c}{\rho_f^2}\right]^{1/4} (1 - \alpha)^{K_1}\, C_2\, C_3\, C_4 \tag{7-5}$$

$$\frac{dV_{gj}}{d\alpha} = - K_1 \cdot V_{gj} \cdot (1-\alpha)^{-1} \tag{7-6}$$

$$A_1 = 1 - \alpha C_o \tag{7-7}$$

$$\frac{d\frac{1}{A_1}}{d\alpha} = \frac{C_o + \alpha\frac{dC_o}{d\alpha}}{A_1^2} \tag{7-8}$$

$$C_o = \frac{L(\alpha, P)}{K_o + (1-K_o)\,\alpha^r} \tag{7-9}$$

$$\frac{dC_o}{d\alpha} = C_o\left[\frac{C_1 e^{-C_1\alpha}}{1-e^{-C_1\alpha}} - \frac{(1-K_o)\cdot r\cdot\alpha^{r-1}}{K_o + (1-K_o)\alpha^r}\right] \tag{7-10}$$

K_1, C_2, C_3, L, K_o, and r are defined in Section 3.

Substituting equations (7-5) through (7-10) in equation (7-4); j_f, j_g, and α on CCFL line were determined.

In this section, the CCFL predictions using the empirical drift flux correlation are compared with TLTA side entry orifice steam-water CCFL data by Jones [15] taken at General Electric Company and ORNL PWR core/upper plenum interface steam-water CCFL data by Thomas et al [16] taken at Oak Ridge National Labs.

7.2 COMPARISON WITH TLTA CCFL DATA [15]

A series of tests were conducted to measure the CCFL characteristics of BWR core inlet orifices. Three different orifice sizes were tested. Each orifice was installed in such a way that the steam, which enters the bottom of the zero power loop, must flow through the orifice in order to exit the test section. There is no other passage for steam flow. Similarly, the water enters the test section above the test orifice and must pass through the orifice to reach the lower drain tank, which is the device used to measure the total liquid downflow. All tests were steady state tests conducted by recording data for ~3 minutes for each data point. The liquid flow was held constant while the steam flow was varied for each data point. The initial data point was the highest steam flow; the flow was then decreased in steps down to the minimum flow and then increased in steps back to the maximum flow.

Comparison of predictions from equation (7-4) with test results for three different orifice sizes (diameters of 2.43 in., 1.48 in., and 1.257 in.) on plots of $\sqrt{K_g}$ and $\sqrt{K_f}$ are shown in Figures 7-1 through 7-3, where K_g and K_f are dimensionless volumetric fluxes based on the Kutateladze numbers given by

$$K_g = \frac{j_g \cdot \rho_g^{1/2}}{[g\ g_c\ \sigma\ (\rho_f - \rho_g)]^{1/4}}$$

$$K_f = \frac{j_f\ \rho_f^{1/2}}{[g\ g_c\ \sigma\ (\rho_f - \rho_g)]^{1/4}}$$

In general, the comparison with test data is very good and provides confidence in this drift flux approach for predicting CCFL. Both pressure and diameter effects are accounted for.

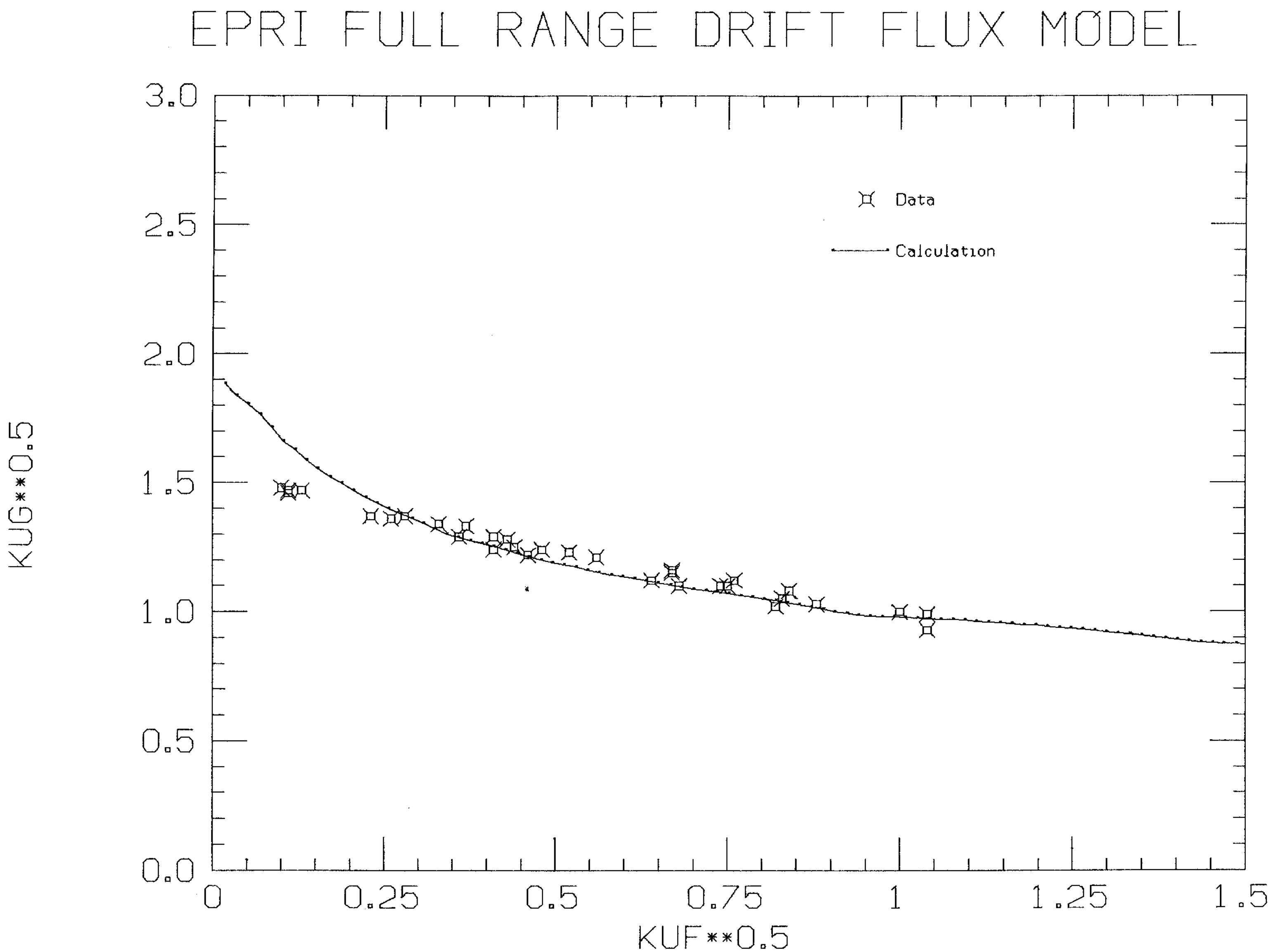

Figure 7-1. Comparison with TLTA Steam-Water CCFL Data for a 2.43 In Orifice at 1 ATM

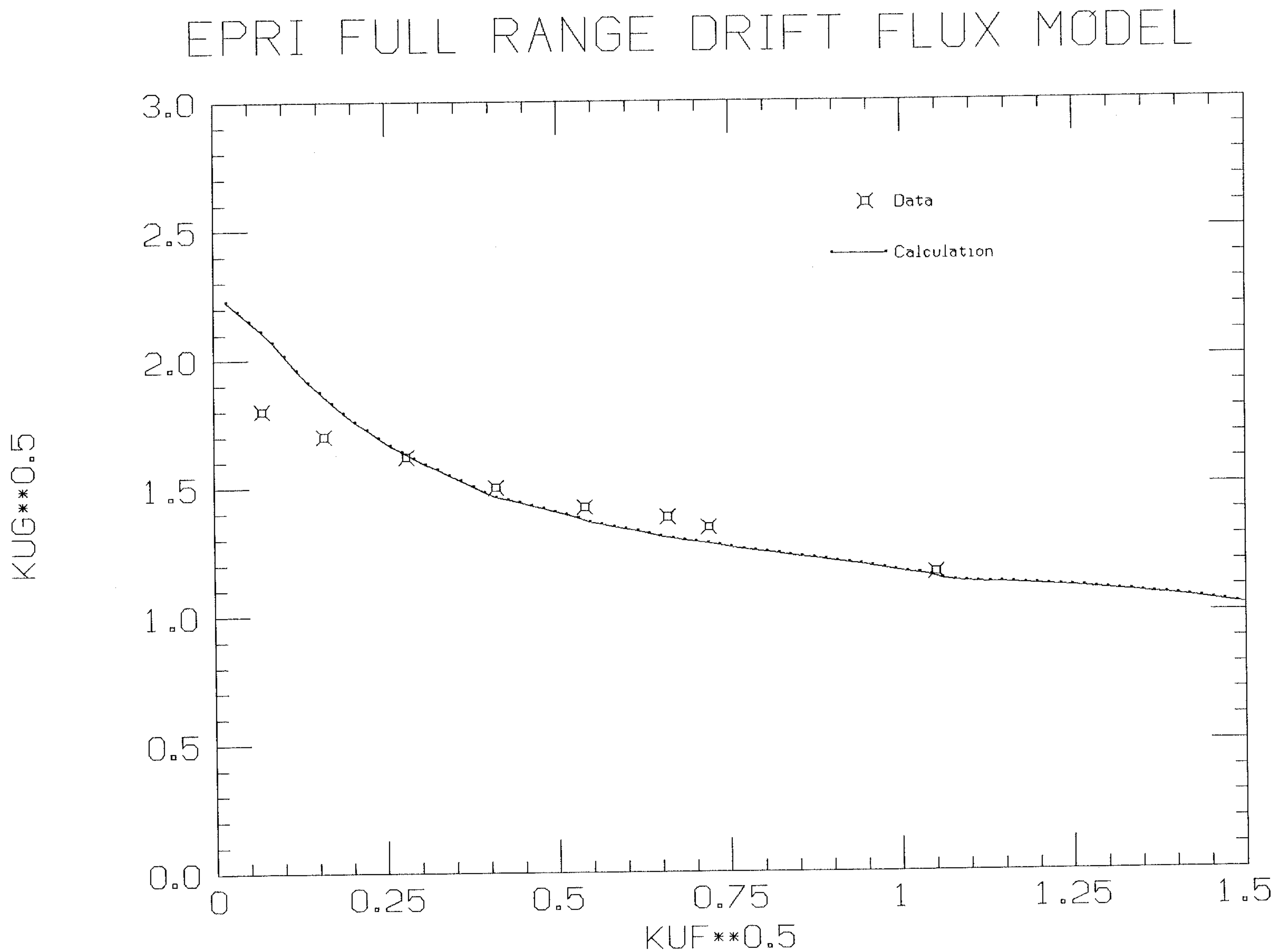

Figure 7-2. Comparison with TLTA Steam-Water CCFL Data for a 1.48 In Orifice at 1 ATM

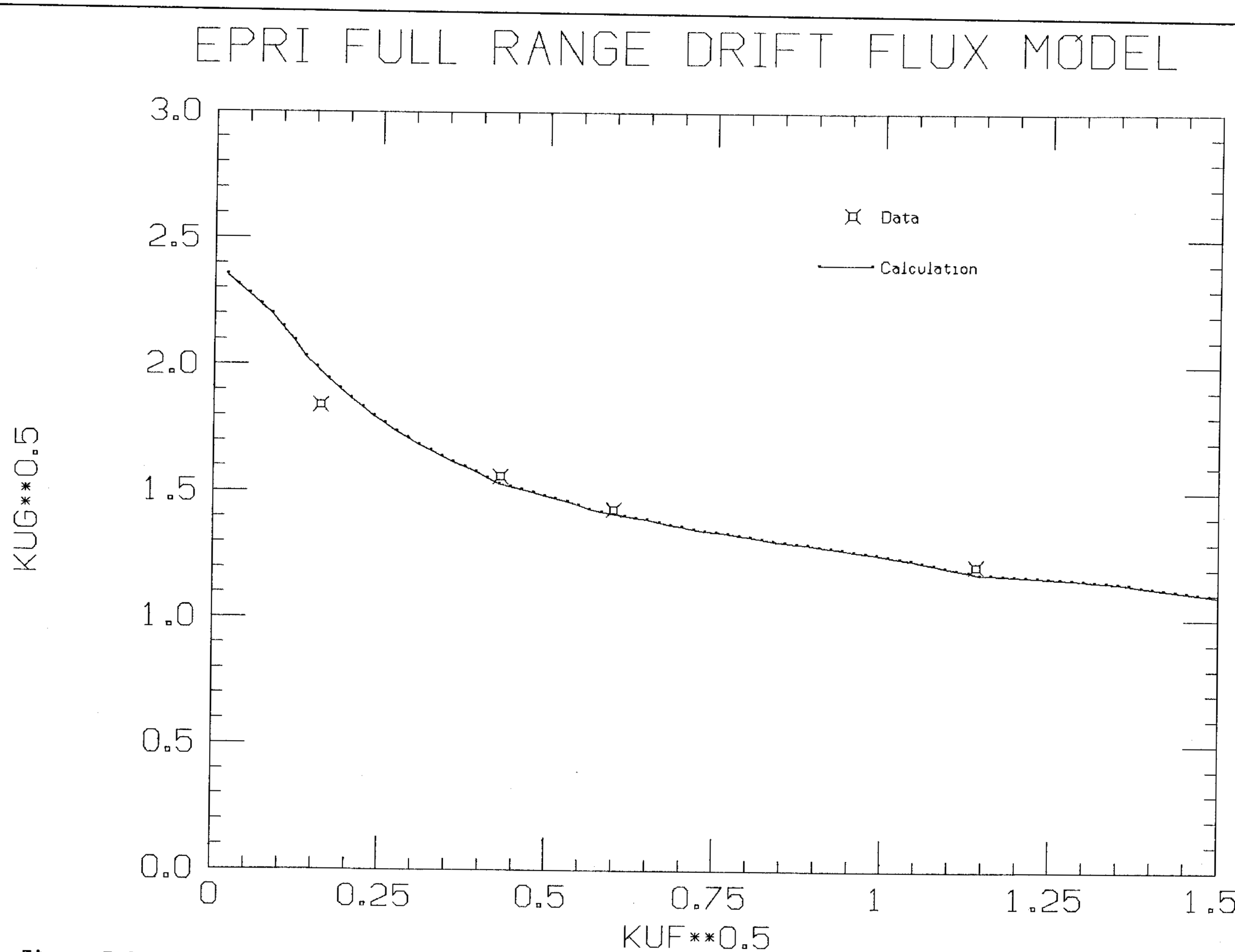

Figure 7-3. Comparison with TLTA Steam-Water CCFL Data for a 1.257 In Orifice at 1 ATM

7.3 COMPARISON WITH ORNL CCFL DATA [16]

A series of tests at pressures up to 100 psia were conducted to measure the CCFL characteristics of PWR core/upper plenum interface. The single-module steam/water facility consisted of a test vessel, core spray and hot leg injection systems, fallback and carryover drains. The stainless steel test vessel was a full-scale representation of a one-bundle section of the upper plenum test facility. The core spray system was designed to mix steam and saturated water in the lower section of the test vessel to simulate the two-phase flow conditions expected during the refill and reflood phases of a 200% cold leg break loss of coolant accident (LOCA). The fallback drain system returns collected water from the lower plenum to the water supply tank where it was recirculated through the core spray. The carryover drain system separated the liquid effluent of the upper plenum from the steam, exhausted the steam to the atmosphere, and returned the liquid to the water supply tank for recirculation. Comparison of predictions using the empirical drift correlation with test data from 45 to 100 psia is shown in Figure 7-4 and Figure 7-5. The data is bounded by the predictions at 45 and 100 psia and the comparison is excellent.

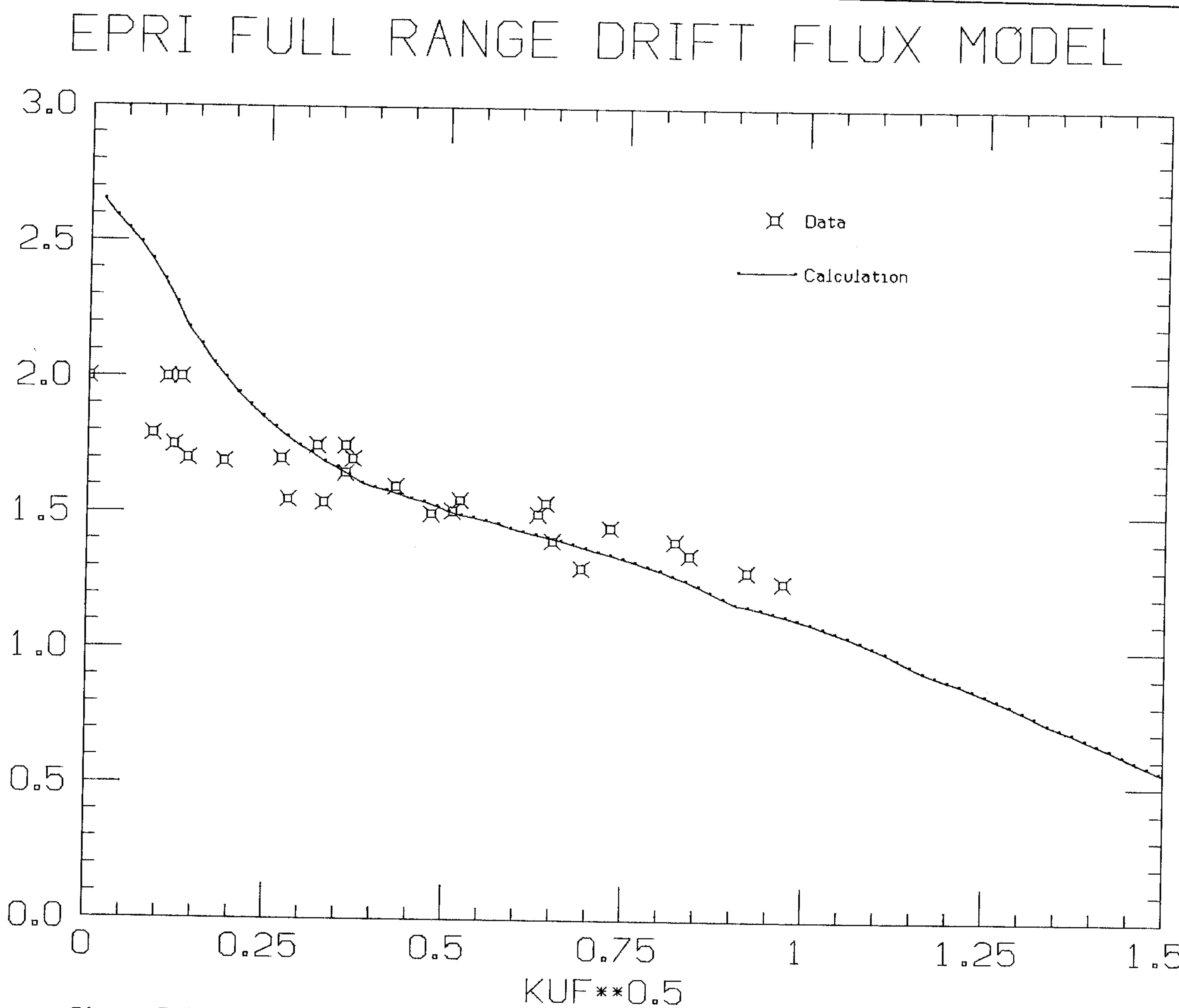

Figure 7-4. Comparison with ORNL Steam - Water CCFL Data - PWR Upper Tie Plate at 65 psia (Hydraulic Diameter=0.0344 ft)

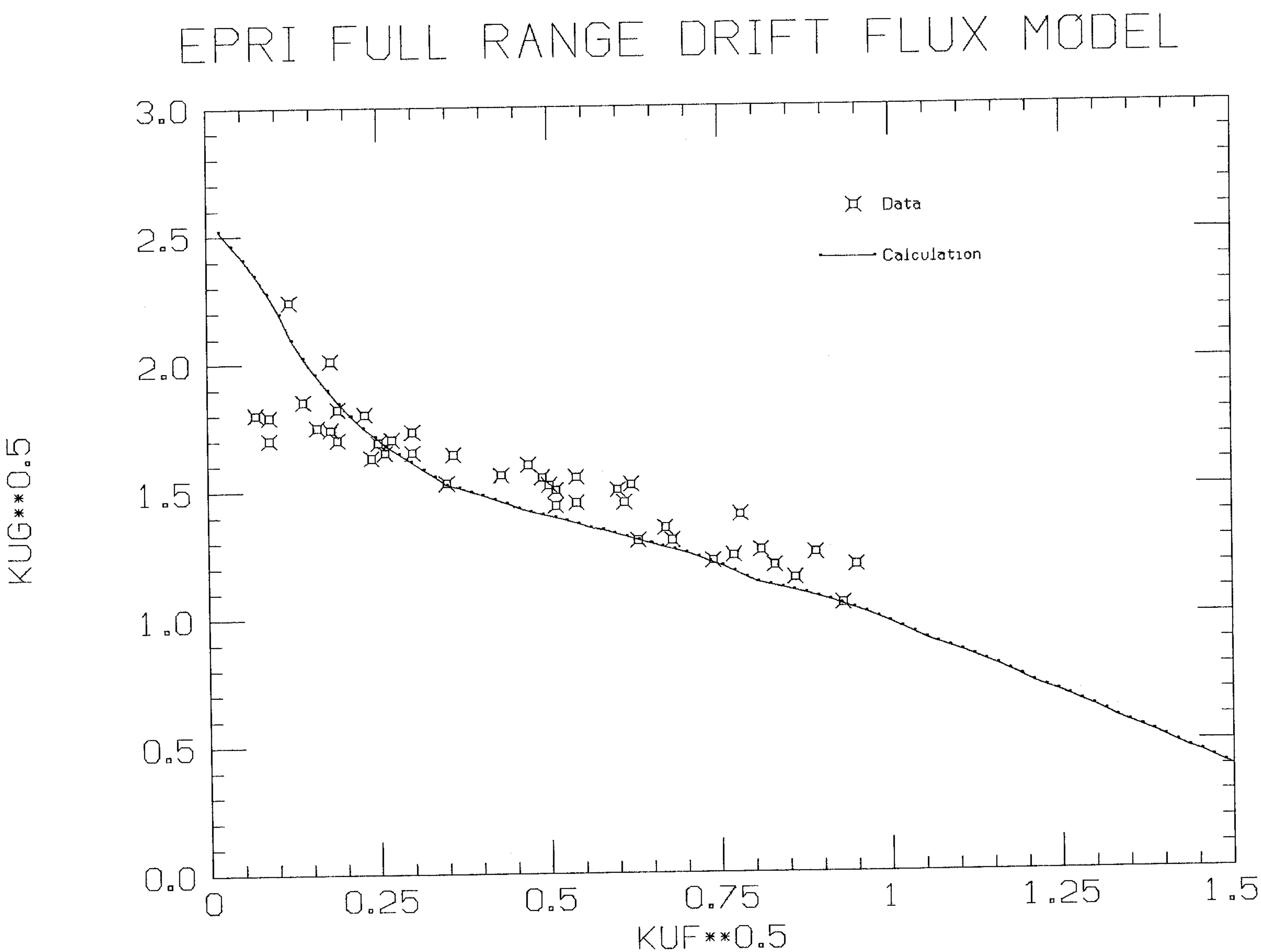

Figure 7-5. Comparison with ORNL Steam Water CCFL Data-
PWR Upper Tie Plate at 100 psia (Hydraulic Diameter=0.0344 ft)

Section 8

COMPARISON WITH NATURAL CIRCULATION FLOW DATA

These conditions are typical of low power reactor operation and also in the event of a small break LOCA this phenomena is important if the operator has turned off the reactor coolant pumps following a reactor trip. The accident at Three Mile Island has shown that natural circulation can be used as an effective method for long-term heat removal from the core. This phenomenon is of particular importance for Boiling Water Reactors (BWRs) where all of them have operated for periods e.g. at the end of a two-pump trip test during start-up.

In this section, the prediction of natural circulation flows using the empirical drift flux correlation are compared with data taken in the FIST (Full Integral Simulation Test) facility [17]. This facility is representative of a BWR/6 and has full BWR height with volume scaling (1/624) to a single BWR fuel bundle. FIST uses a full sized 8 x 8 electrical bundle, prototypical of a BWR.

A series of natural circulation tests were performed with bundle power of 0.1 to 3.0 MW. The system was maintained at a constant pressure of 1040 psia. The downcomer water level was slowly lowered from the normal water level or higher to near the top of the jet pump. Natural circulation data was taken at various power and downcomer water level quasi-steady state conditions.

The BWR natural circulation code, NATBWR [18] was used for performing this analysis. The empirical drift flux correlation given in Section 3 was implemented in the NATBWR code. NATBWR models the fuel channels and bypass region in the reactor core as a series of parallel flow paths. The flow in each of the fuel channels and the bypass is selected so that each fuel channel and the bypass have the same pressure drop from the lower plenum to the upper plenum. Flow out of the fuel channels and bypass mix in the upper plenum and then pass through a simple resistance model for the steam separators.

Outside the core shroud, steam with a saturated liquid carryover fraction is removed, leaving saturated liquid with a saturated vapor carryunder fraction as the recirculation system flow in the downcomer from the water level down to the feedwater inlet. At the feedwater inlet, the feedwater or high pressure coolant injection is added to the recirculation system flow and any heat loss due to the reactor water clean-up system is removed. From here, the recirculation flow is taken down the downcomer, through the jet pumps, and into the lower plenum.

The core flow path can have up to ten parallel paths to represent different fuel channel geometries and power levels. For a given core and recirculation loop hydraulic description, power level, and power distribution, the code iterates on flow and flow distribution to balance pressure drops around the recirculation system.

The flow comparison at various power and downcomer water levels is shown in Figure 8-1. In general, the comparison with test data is quite good.

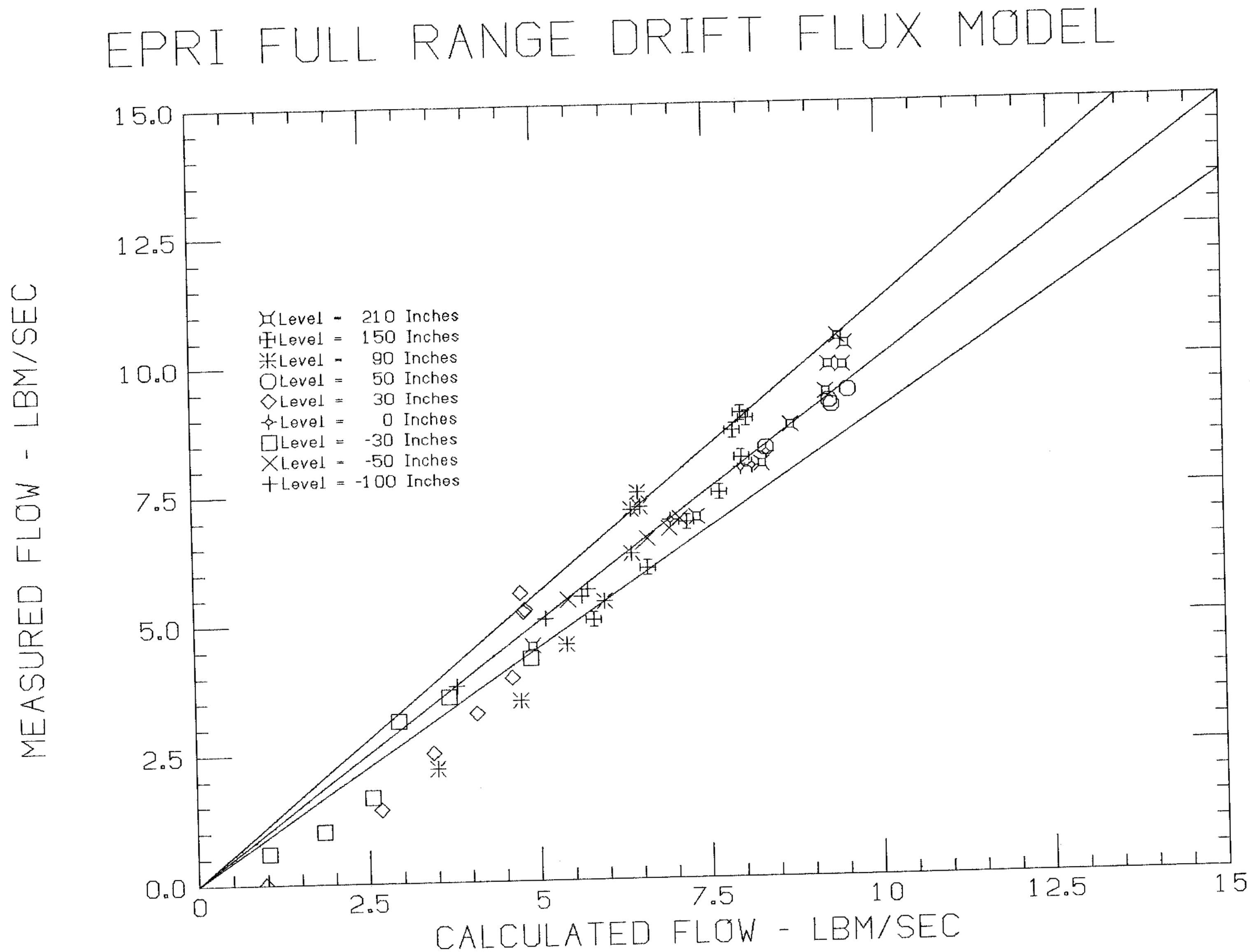

Figure 8-1. Comparison with FIST Natural Circulation Data at Various Downcomer Levels

Section 9

CO-CURRENT DOWN FLOWS

These conditions are typical of a large break LOCA accident in a PWR with upper plenum injection or upper head injection and are expected to occur during reflood conditions. These conditions also occur in the downcomer of a BWR.

In this section, the empirical drift flux correlation void fraction predictions are compared with Petrick Data [19]. The high pressure data were obtained from the 2500-psi Heat Transfer and Fluid Flow Test Facility. A series of tests were made in which data were taken randomly over a velocity range from 0.5 to 5 ft/sec at pressures of 600, 1000, and 1500 psia. The downflow slip ratios were obtained from the adiabatic segment of piping denoted as the downflow test section. The void volume fraction α was determined by 3 methods: namely, by Potter Meter, gamma traversing, and from differential static pressure measurements. The 3 techniques were employed to insure the accuracy of the data. The values of the mean void fraction determined by the 3 methods checked very well. As a result, the differential static pressure-drop-technique was used for determining the steam volume fraction in the majority of runs, since it was the simplest. The measurements were taken in the lower portion of the section to allow the flow to stabilize after completing the 180° turn at the top of the section. The steam weight fractions were determined by a heat balance on the heated test section and checked by a heat balance on the downcomer cooler. The downcomer mixture quality and void fractions were measured, and the slip ratio was calculated from the continuity equation. Figures 9-1 through 9-3 compare the experimental void fraction with calculated void fractions at pressures of 600, 1000 and 1500 psia.

In general, the comparison with test data is very good.

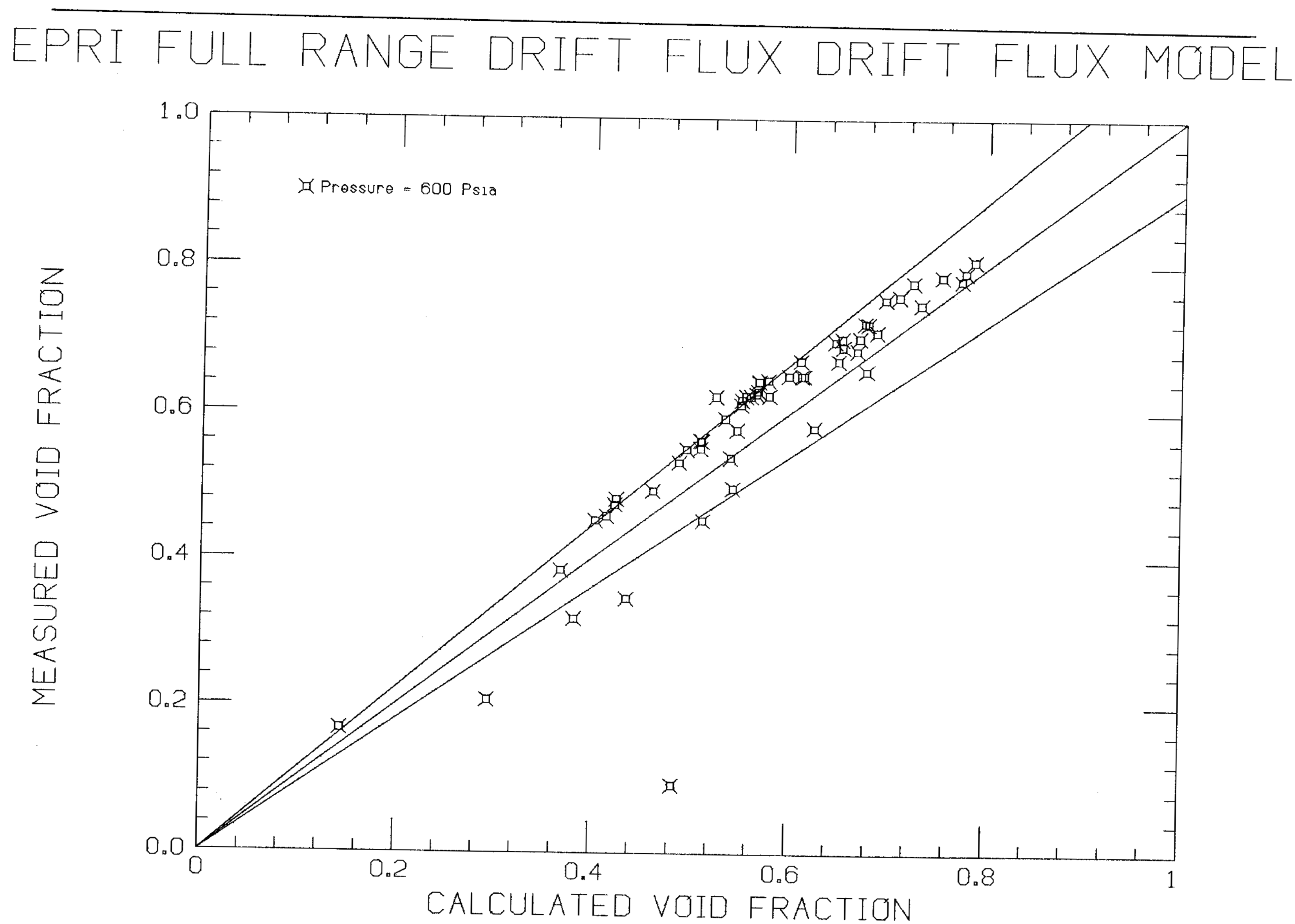

Figure 9-1. Comparison with Petrick's Data in a 1.94 In Pipe at 600 psia

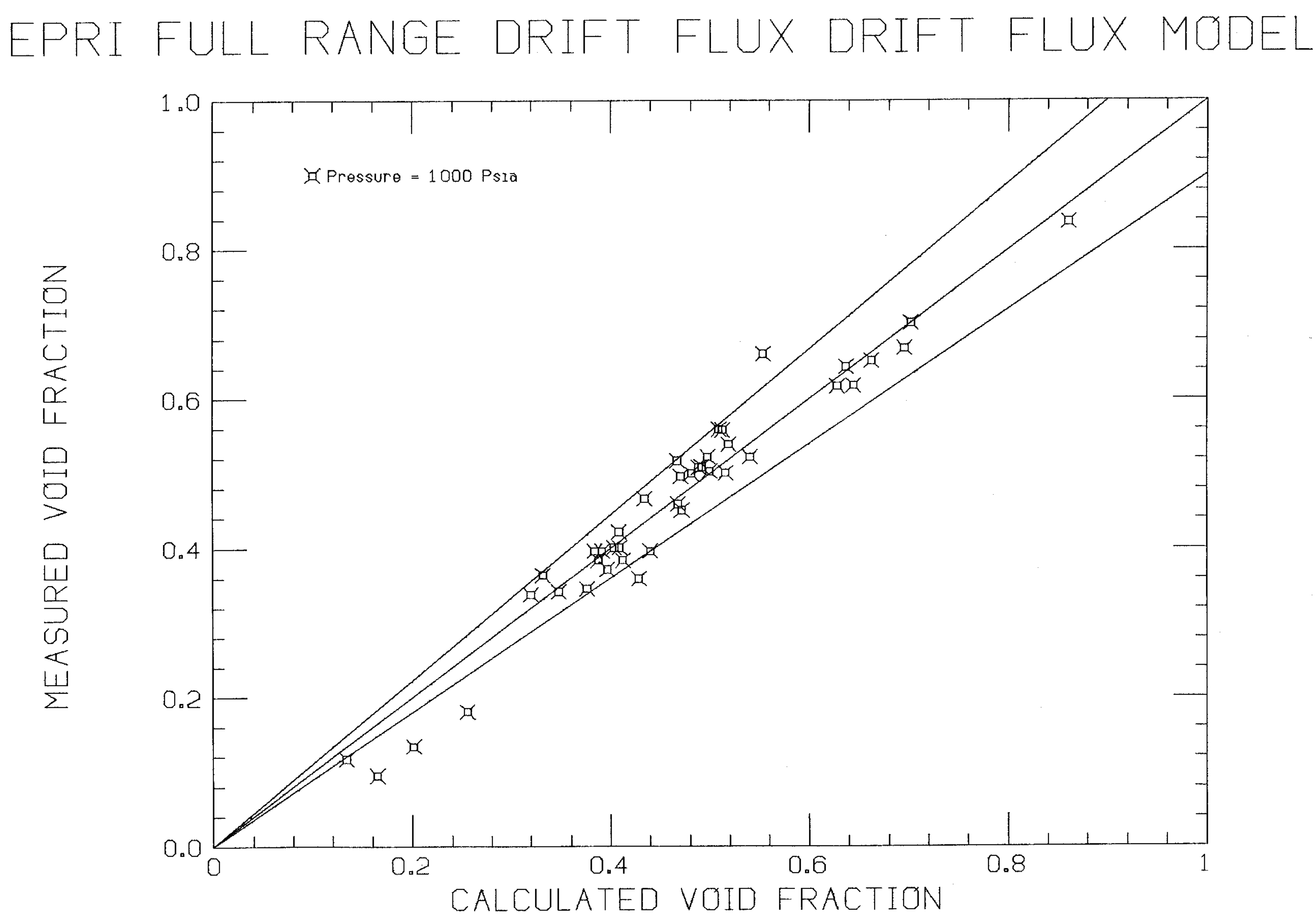

Figure 9-2. Comparison with Petrick's Data in a 1.94 In Pipe at 10000 psia

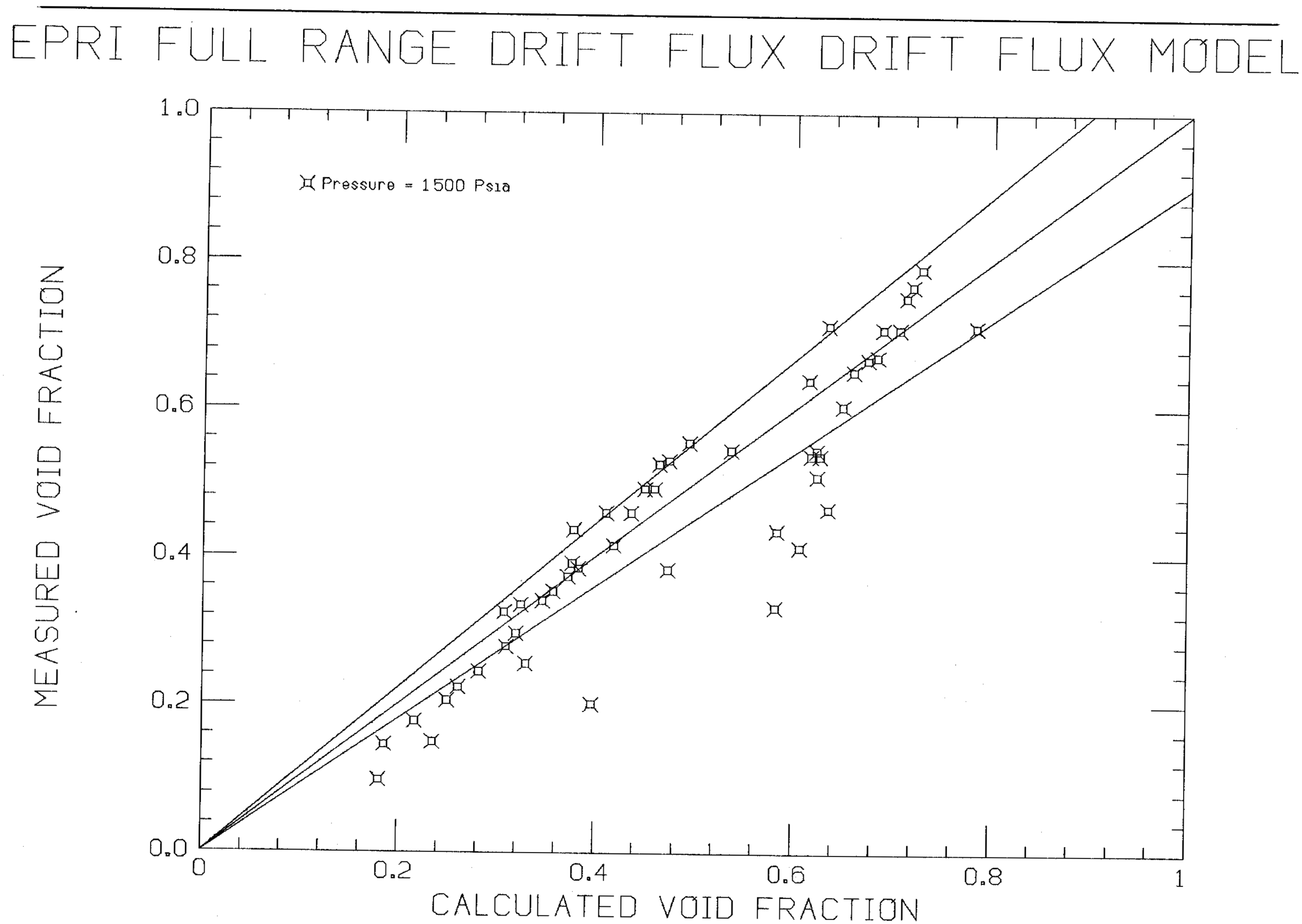

Figure 9-3. Comparison with Petrick's Data in a 1.94 In Pipe at 1500 psia

Section 10

APPLICATION TO LARGE DIAMETER PIPES

Large diameter pipes are typically found in the primary coolant system outside the core region and in the steam generator secondary side above the tube bundle region.

In this section, the empirical drift flux correlation predictions are compared with Hughes data [20] taken at Babock and Wilcox Co. and Carrier data [21] taken at Allis Chalmers.

10.1 COMPARISON WITH HUGHES DATA [20]

The purpose of this experiment was to develop information on mixture density of steam-water mixtures at high pressures and in large diameter vertical tubes. Tests were run on a 6.625 inch ID vertical pipe at pressures of 1200, 1400, 1800 and 2400 psia and steam and water flow rates of 1,000 to 5,880 lb per hour and 20,000 to 60,000 lb per hour, respectively. Water and steam were mixed immediately below the test section and flowed vertically upward. Observations were made at five stations along the length of the test pipe. The observed steam and water flow rates and densitometer measurements through the center of the pipe were used to calculate the per cent steam by weight input, void fraction, slip velocity (difference between steam and water velocities), and the centerline density as measured by the densitometer.

Figure 10-1 compares the experimental void fraction with calculated void fraction at various pressures.

In general the comparison with test data is excellent.

10.2 COMPARISON WITH CARRIER DATA [21]

High pressure tests at pressures of 600, 800, 1000, 1200, 1400 and 2000 psia were done by bubbling steam through a perforated plate into a 456 mm (~18 inch) pipe. The void fraction and steam flow measurements were obtained as steam was passed upwards through stagnant water (liquid level above the plate <3 ft). The void

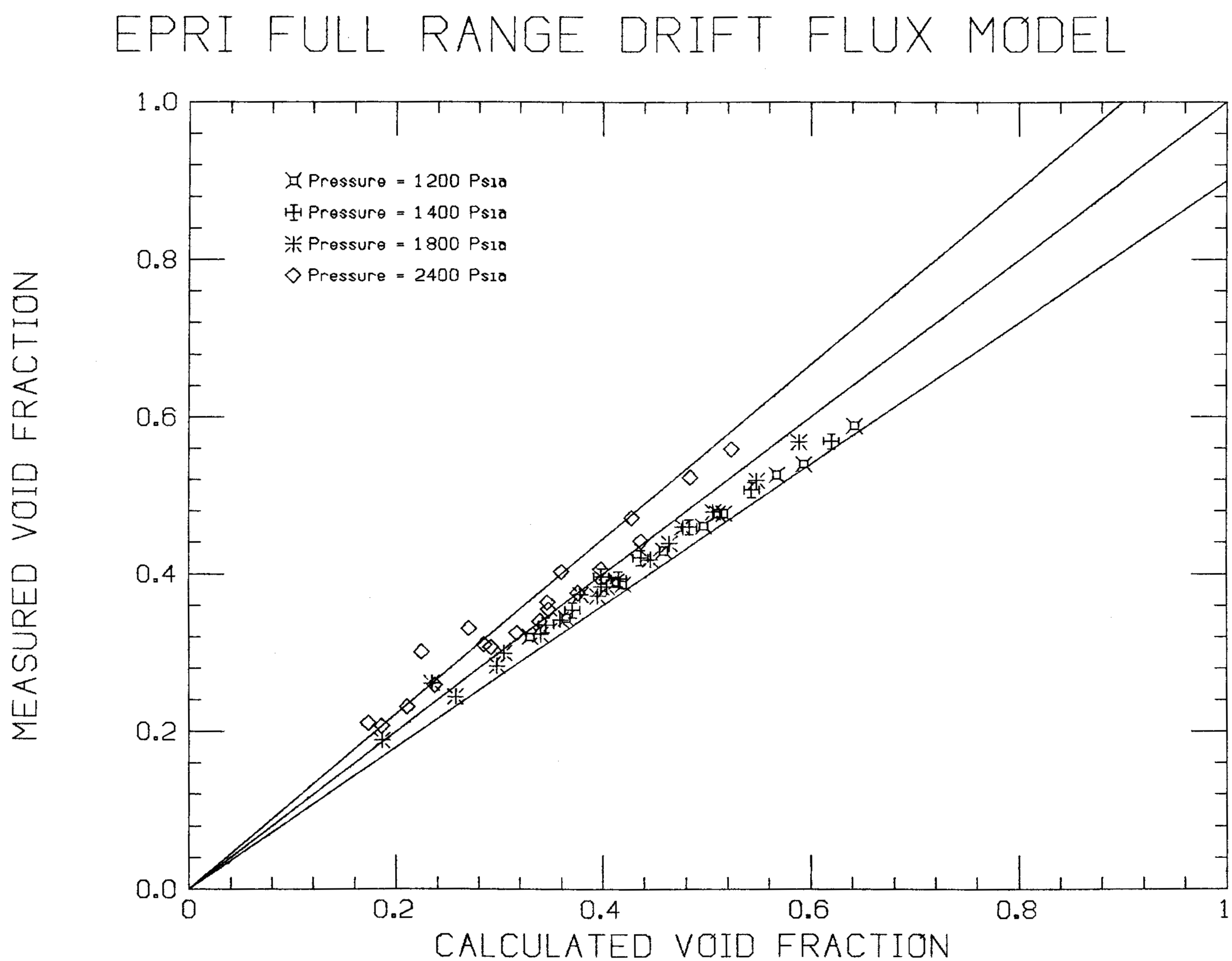

Figure 10-1. Comparison with Hughes Data in a 6.625 Inch Pipe - All Pressures

fraction was obtained from pressure differential measurements taken at three positions within the vessel, and the vertical bars on the data points in Figure 10-2 make the span between the highest and the lowest values of the void fraction.

Comparison of the experimental void fraction with calculated void fraction is shown in Figure 10-2. The comparison ranges from good to excellent. It is likely that under these conditions the flow field is strongly influenced by the boundary condition imposed by the steam jets issuing from the perforations on the plate. This would consist of steam water jet rising in the core above the penetration with a downflow of liquid along the walls of the container [3]. Further, the 3 foot 2 phase level provides an L/D ~2 or less which implies that the entrance effects are significant. The comparison of void fraction data with predictions from empirical drift flux correlation for 18 inch pipe proves the validity of this correlation even for large diameter pipes.

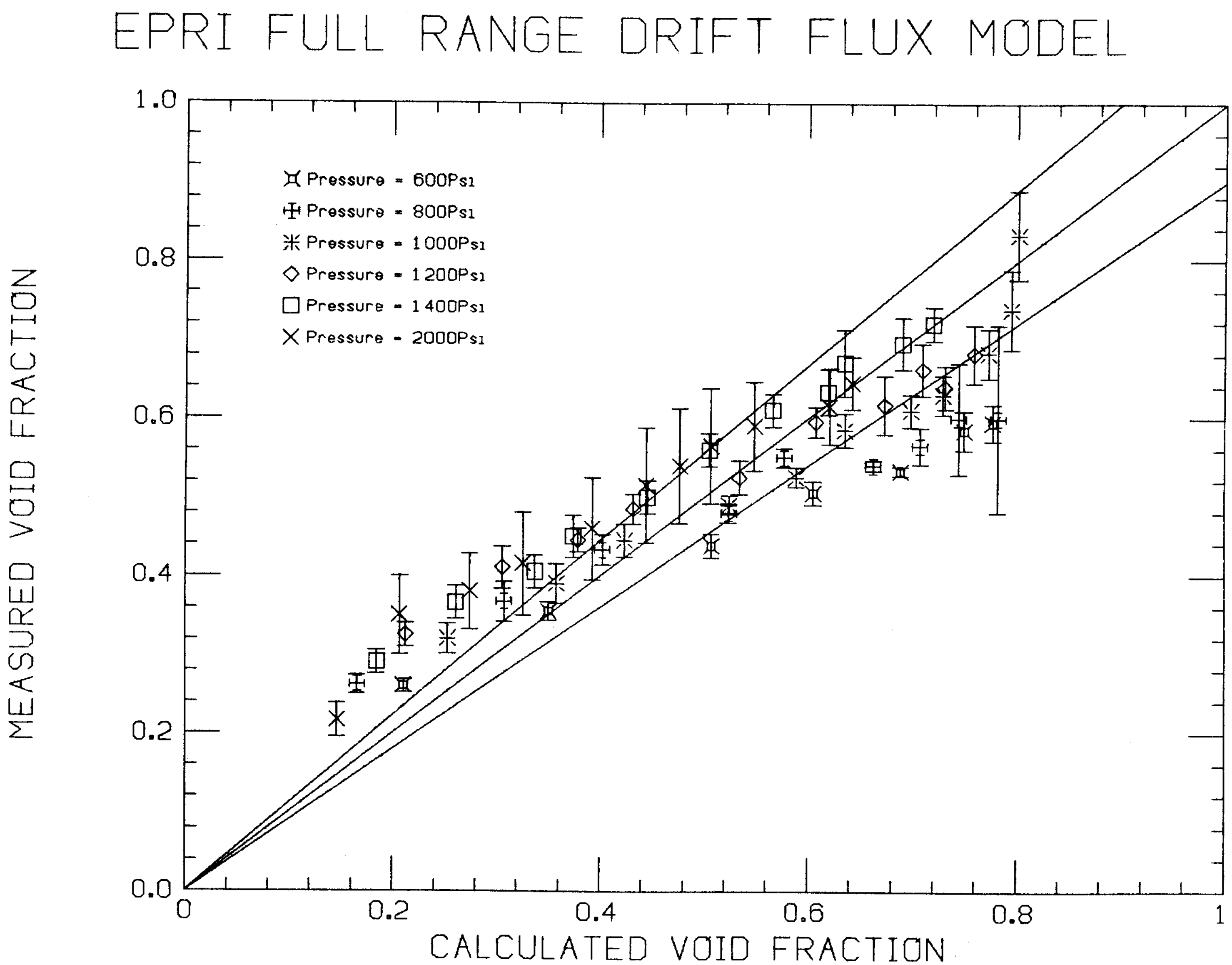

Figure 10-2. Comparison with Carrier Data in a 456 mm Pipe at Several Press

Section 11

REFERENCES

1. Lellouche, G. S. and Zolotar, B. A. Mechanistic Model for Predicting Two-Phase Void Fraction for Water in Vertical Tubes, Channels, and Rod Bundles, EPRI-NP-2246-SR, Special Report, February 1982.

2. Ishii, M. Thermo-Fluid Dynamic Theory of Two-Phase Flow, Chapters IX and X, Eyrolles, Paris, 1975.

3. Zuber, N. and Findlay, J. Average Volumetric Concentration in Two-Phase Flow Systems, J. Heat Transfer 87, 453, 1965.

4. Zuber, N. et al. Steady State and Transient Void Fraction in Two-Phase Flow Systems, General Electric Co. Report GEAP-5417, Vol. 1, 1967.

5. Nylund, O. et al. Measurements of Hydrodynamic Characteristics, Instability Thresholds, and Burnout Limits for 6-Rod Clusters in Natural and Forced Circulation, FRIG Loop Project, FRIGG-1, 1967.

6. Nylund, O. et al. Hydrodynamic and Heat Transfer Measurements on a Full-Scale Simulated 36-Rod Marviken Fuel Element with Uniform Heat Flux Distribution, FRIGG Loop Project, FRIGG-2, 1968.

7. Nylund, O. et al. Hydrodynamic and Heat Transfer Measurements on a Full-Scale Simulated 36-Rod Marviken Fuel Element with Non-uniform Radial Heat Flux Distribution, FRIGG Loop Project, FRIGG-3, 1969.

8. Nylund, O. et al. Hydrodynamic and Heat Transfer Measurements on a Full-Scale Simulated 36-Rod BHWR Fuel Element with Non-Uniform Axial and Radial Heat Flux Distribution, FRIGG-4, 1970.

9. Agostini, G. et al. Density of Steam-Water Mixtures Flowing in 19-Rod Clusters Under Adiabatic and Heated Conditions, CISE-R-309, 1971.

10. Anklam, T. et al. Experimental Investigations of Uncovered-Bundle Heat Transfer and Two-Phase Mixture-Level Swell Under High-Pressure Low Heat-Flux Conditions, NUREG/CR-2456, 1982.

11. Seedy, D. and Muralidhoran. BWR Low-Flow Bundle Uncovery Test and Analysis, EPRI-NP-1781, June 1982.

12. Hall, P. C. and Ardron, K. H. Prediction of Void Fraction in Low Velocity Vertical Bubbling Flows, paper presented at the European Two Phase Flow Group Meeting, Stockholm, Sweden, 1978.

13. Wong, S. and Hochreiter, L. Analysis of the FLECHT SEASET Unblocked Bundle Steam-Cooling and Boiloff Tests, EPRI-NP-1460, 1981.

14. Jowitt, D. A New Voidage Correlation for Level Swell Conditions, AEEW-R-1480, UKAEA Winfrith, 1982.

15. Jones, D. Test Report TLTA Components CCFL Tests, NEDG-NUREG-23732, 1977.

16. Thomas, D, and Combs, S. Measurement of Two-Phase Flow at the Core/Upper Plenum Interface for a PWR Geometry Under Simulated Reflood Conditions, NUREG/CR-3138, 1983.

17. Stephens, A. BWR Full Integral Simulation Test Program, EPRI-NP-2314, 1982.

18. Healzer, J. and Abdollahian, D. NATBWR: A Steady-State Model for Natural Circulation in Boiling Water Reactors, EPRI-NP-2856-CCM, 1983.

19. Petrick, M. A Study of Vapour Carryunder and Associated Problems, ANL-6581, July 1962.

20. Hughes, T. Steam-Water Mixture Density Studies in a Natural Circulation High Pressure System, Babcock and Wilcox, G. Report No. 5435, 1958.

21. Carrier, F. et al. Steam Separation Technology Under the Euratom Program, Allis-Chalmers Atomic Energy Division Report No. ANCP-63021, July 1963

22. Kasai, S. et al. Void Fraction Measurements Under Simulated BWR Thermal-Hydraulic Conditions, Presented at Proceedings of Third International Topical Meeting on Reactor Thermal Hydraulics, Newport, Rhode Island, October 1985.

Appendix A

SAMPLE PROBLEMS

In this section, a total of 12 sample problems are given to help the user to check that the correlation has been correctly programed. The first eight cover the pressure effect, diameter effect and the flow direction effect and are shown in Table A-1. In each case, the C_o, V_{gj} and a values are obtained by solving the following equation:

$$a\ (C_o\ j + V_{gj}) - j_g = 0$$

The last four cases present the points on the CCFL line for a typical pressure and hydraulic diameter. These are shown in Table A-2.

TABLE A-1

SAMPLE RESULTS

Case No.	Input: P	D	j_f	j_g	Results: Re_f	Re_g	C_o	V_{gj}	α
1	14.7	0.05	5	10	78,684	2,297	1.2037	0.5979	0.5361
2	1000	0.05	5	10	184,219	87,257	1.1116	0.1410	0.5947
3	1000	1.0	5	10	3,684,867	1,745,362	1.1119	0.2234	0.5914
4	14.7	1.0	5	10	1,573,883	45,947	1.1922	0.9054	0.5323
5	14.7	1.0	-5	-10	-1,573,883	-45,947	1.0400	5.1172	0.9538
6	1000	1.0	-5	-10	-3,684,867	-1,745,362	1.0498	4.8444	0.9171
7	1000	0.05	-5	-10	-184,219	-87,257	1.2948	1.8775	0.5700
8	14.7	0.05	-5	-10	-78,684	-2,297	1.3036	4.6590	0.6714

P = Pressure, psia

D = Diameter, ft

j_f = Superficial liquid velocity, ft/sec

j_g = Superficial vapor velocity, ft/sec

Re_f = Liquid Reynolds Number

Re_g = Vapor Reynolds Number

C_o = Drift Flux Parameter

V_{gj} = Drift Flux Parameter, ft/sec

α = Void Fraction

TABLE A-2

SAMPLE CCFL RESULTS

Case No.	Input			Output		
	P	D	j_f	j_g	Ku_f	Ku_g
9	14.7	0.0833	-0.0024	120.756	.0684	2.4237
10	14.7	0.0833	-0.2400	46.199	.6835	1.4491
11	14.7	0.0833	-0.9699	31.295	1.3670	1.2321
12	14.7	0.0833	-1.5000	23.175	1.7087	1.0618

P = Pressure, psia
D = Diameter, ft
j_f = Superficial liquid velocity at CCFL, ft/sec
j_g = Superficial vapor velocity at CCFL, ft/sec
Ku_f = Liquid Kutateladze Number
Ku_g = Vapor Kutateladze Number